N° Ordre...../ FT / UEHL / 2022

REPUBLIQUE ALGERIENNE DEMOCRATIQUE ET POPULAIRE
MINISTERE DE L'ENSEIGNEMENT SUPERIEUR ET DE LA RECHERCHE SCIENTIFIQUE
UNIVERSITE ECHAHID HAMMA LAKHDAR D'EL OUED

Faculté de Technologie

Laboratoire de Théorie des Opérateurs et EDP (Fondements et Applications) -LABTHOP

Thèse de Doctorat

Présentée par :

Nassima BEKHOUCHA

En vue de l'obtention du diplôme de **DOCTORAT LMD** en **:**

Option : Optimisation et Gestion d'Énergie

Contribution à la Commande Prédictive des Convertisseurs Statiques Associés à un Système de Production d'Énergie Renouvelable

Thèse soutenue publiquement le **03 Janvier 2022**, devant le jury composé de :

BEKAKRA Youcef	Professeur	UEHL-El Oued	*Président*
MESBAHI Nadhir	Professeur	UEHL-El Oued	*Directeur de thèse*
MEKHILEF Saad	Professeur	Université de Swinburne	*Co-Directeur de thèse*
KERMADI Mostefa	Docteur	Université de Malaya	*Co-Directeur de thèse*
SERHOUD Hicham	MCA	UEHL-El Oued	*Examinateur*
LAMMOUCHI Zakaria	MCA	UEHL-El Oued	*Examinateur*
BOUZIDI Mansour	MCA	UKM-Ouargla	*Examinateur*
BOUKADOUM Aziz	MCA	ULT-Tébessa	*Examinateur*
OUARI Ahmed	Professeur	UBM-Annaba	*Invité*
OMEIRI Amar	Professeur	UBM-Annaba	*Invité*

N° Ordre...../ FT / UEHL / 2022

PEOPLE'S DEMOCRATIC REPUBLIC OF ALGERIA
MINISTRY OF HIGHER EDUCATION AND SCIENTIFIC RESEARCH
UNIVERSITY OF ECHAHID HAMMA LAKHDAR EL OUED

جامعة الشهيد حمه لخضر - الوادي
Université Echahid Hamma Lakhdar - El-Oued

Faculty of Technology

Laboratory of Operator Theory and PDEs: Foundations and Applications (LABTHOP)

Doctoral Thesis

Presented by:

Nassima BEKHOUCHA

With a view to obtaining the **LMD DOCTORATE** diploma in:

Specialty: Energy management and optimization

Contributions to Predictive Control of Static Converters Associated with a Renewable Energy Production System

Thesis publicly defended on **January 03, 2022**

Dissertation Committee:

BEKAKRA Youcef	*Professor*	UEHL-El Oued	*President*
MESBAHI Nadhir	*Professor*	UEHL-El Oued	*Supervisor*
MEKHILEF Saad	*Professor*	University of Swinburne	*Co-supervisor*
KERMADI Mostefa	*Doctor*	University of Malaya	*Co-supervisor*
SERHOUD Hicham	*MCA*	UEHL-El Oued	*Examiner*
LAMMOUCHI Zakaria	*MCA*	UEHL-El Oued	*Examiner*
BOUZIDI Mansour	*MCA*	UKM-Ouargla	*Examiner*
BOUKADOUM Aziz	*MCA*	ULT-Tébessa	*Examiner*
OUARI Ahmed	*Professor*	UBM-Annaba	*Guest*
OMEIRI Amar	*Professor*	UBM-Annaba	*Guest*

Dedication

I dedicate this work to

My mother and my father

My sisters and my brothers

And all my family

Acknowledgments

In the name of Allah, the Most Gracious and the Most Merciful

Alhamdulillah, all praises to Allah for the strengths and His blessing in completing this thesis.

I would like to thank my PhD supervisor, full Prof. MESBAHI Nadhir, Professeur at El Oued University for his guidance, encouragement, and continuous support throughout my PhD period.

I would like to thank my co-supervisor Prof. MEKHILEF Saad, The dean of the Faculty of Engineering, University of Malaya. I am grateful for his suggestion and invaluable supports during my internship, and for giving me the opportunity to work in the Power Electronics and Renewable Energy Research Laboratory.

Special appreciation goes to Dr. KERMADI Mostefa, Post-doctoral Research at University of Malaya, for his constant support, his invaluable help, and his constructive comments and suggestions. He helped me in experimental setup and control algorithm implementation.

I would like to thank the Algeria Ministry of Higher Education and Scientific Research for giving me the opportunity to study abroad by granting me a scholarship. Also, thanks to the University of El Oued for the support during all these years.

I thank all members of the jury who agree to judge my work and for the interest they have shown in this last.

List of Publications

Publications in refereed journals

1. **N. Bekhoucha**, M. Kermadi, N. Mesbahi, and S. Mekhilef, "Performance Investigation of Deadbeat Predictive Controllers for Three-Level Neutral Point Clamped Inverter," *IEEE J. Emerg. Sel. Top. Power Electron.*, vol. 10, no. 1, pp. 1165–1177, 2022.

Publications in refereed conferences

1. **N. Bekhoucha**, N. Mesbahi, and S. Ouchen,''Predictive Current Control of Three Level Neutral Point Clamped Grid Connected Inverter in Photovoltaic Generation Systems,'' IEEE International Conference on Electrical Sciences and Technologies in Maghreb (CISTEM), 2018.
2. **N. Bekhoucha**, N. Mesbahi, ''Model Predictive control of Shunt Active Power Filter Connected to a Photovoltaic System,'' International Symposium on Mechatronics & Renewable Energies (ISMRE'2018).
3. **N. Bekhoucha**, N. Mesbahi, ''Finite-Set Model Predictive control of Three-Level NPC Shunt Active Power Filter Using High Selectivity 'HSF' Filter based Reference Current'' International Conference on Communications and Electronical Engineering (ICCEE18).

Abstract

The use of multilevel inverters in industrial installations has been motivated by energy benefits, such as reducing the total harmonic distortion of current and voltage. This thesis aims to develop new control algorithms for a three-phase three-level neutral point clamped (NPC) inverter based on predictive control. In this research, two control strategies have been proposed:

The first strategy is deadbeat predictive control (DBPC). The experimental validation of this method made it possible to test its performance, approve its feasibility and underline its original approach in comparison with the conventional model predictive control (MPC). Furthermore, balances the dc-link capacitor voltages without using the weighting factor, reduces the total harmonic distortion of output currents, reduces computation burden, and minimizes power losses.

The second strategy is modulated predictive control (M²PC). This approach relies on the use of space vector modulation (SVM) for the selection of the optimal control vector and allows to control of the switches of 3L NPC with a constant switching frequency.

Last study is focused on the performance evaluation of proposed control strategies (MPC, DBPC, and M²PC) for a three-level NPC inverter grid-connected photovoltaic generation system. The comparative study made it possible to justify the choice of the proposed control strategies.

Keywords: Three-level neutral point clamped (NPC) inverter, Model predictive control (MPC), Deadbeat predictive control (DBPC), Modulated model predictive control (M²PC), Total harmonic distortion (THD), Computational burden, Power losses.

Résumé

L'utilisation des onduleurs multiniveaux dans les installations industrielles a été motivée par des avantages énergétiques, notamment la réduction du taux de distorsion harmonique totale de la tension et du courant. Le travail de recherche développé par cette thèse a pour objectif le développement de nouveaux algorithmes de commande d'un onduleur triphasé à trois niveaux (NPC). Pour ce faire, deux stratégies de contrôle du courant, basées sur les lois de commande prédictives sont proposées :

La première est basée sur le principe de la commande à réponse pile "Deadbeat predictive control (DBPC) ". Sa validation expérimentale a permis de tester sa performance, d'agréer sa faisabilité et de souligner son approche originale en comparaison avec la commande prédictive à modèle (MPC). En outre, elle permet aussi d'équilibrer les tensions du bus continu sans utiliser le facteur de pondération, de réduire le taux de distorsion harmonique du courant, de réduire considérablement le temps de calcul et de minimiser les pertes par commutation.

La seconde est établie sur la technique de commande prédictive modulée (M²PC). Cette approche repose sur l'utilisation de la modulation vectorielle spatiale (SVM) pour la sélection du vecteur de commande optimal et permet de commander les interrupteurs de l'onduleur 3L-NPC avec une fréquence de commutation constante.

L'onduleur 3L-NPC, reliant le système photovoltaïque PV au réseau électrique, a été étudié. Trois stratégies (MPC, DBPC et M²PC) ont été appliquées et évaluées pour différents critères. Une étude comparative a permis de justifier le choix des stratégies de commande proposées.

Mots Clés : Onduleur NPC à trois niveaux (NPC), Commande prédictive à modèle (MPC), Commande à réponse pile "Deadbeat predictive control (DBPC) ", Commande prédictive modulée (M²PC), Taux de distorsion harmonique totale (THD), Temps de calcul, Pertes de puissance.

Abstract (in Arabic)

الملخص

ان الدافع وراء استخدام المموج متعدد المستويات في المنشآت الصناعية هو الاستفادة من مزايا الطاقة، على سبيل المثال تقليل التشوه التوافقي الكلي للجهد والتيار. يهدف العمل البحثي الذي قدم في هذه الأطروحة إلى تطوير خوارزميات تحكم جديدة للمموج ثلاثي المستويات (NPC)، بحيث تم اقتراح تقنيتين للتحكم ترتكز على قوانين الرقابة التنبؤية:

التقنية الأولى تعتمد على مبدأ التحكم التنبؤي المحكم (DBPC). حيث أتاح التحقق التجريبي لها إمكانية اختبار أدائها والموافقة على جدواها والتأكيد على نهجها الأصلي مقارنةً بالتحكم التنبؤي (MPC). بالإضافة إلى ذلك، تحقيق توازن جهد المكثفتان بدون استخدام عامل الترجيح، التقليل من معدل تشويه التيار التوافقي، التقليل بشكل كبير من العبئ الحسابي، والتقليل من الضياعات.

التقنية الثانية تعتمد على تقنية التحكم التنبؤي المعدل (M^2PC) اذ تعتمد هذه الاخيرة على استخدام تقنية التعديل الشعاعي (SVM) لاختيار شعاع التحكم الأمثل والذي يسمح بالتحكم في المموج 3L-NPC بتردد تبديل ثابت.

لتقييم فوائد تقنيات التحكم الثلاث المقترحة (MPC، DBPC، وM^2PC) تم اجراء دراسة مفصلة على المموج ثلاثي المستويات NPC المتصل بنظام توليد الطاقة الكهروضوئية والمتصل بشبكة وفقا لمعايير مختلفة. تؤكد النتائج المتحصل عليها مدى فعالية التقنيات المقترحة.

الكلمات المفتاحية : المموج ثلاثي المستويات (NPC)، التحكم التنبؤي (MPC)، التحكم التنبؤي المحكم (DBPC)، تحكم تنبؤي المعدل (M^2PC)،معامل التشوه التوافقي الكلي(THD)، العبئ الحسابي، ضياع الطاقة.

Contents

List of Figures

List of Tables

Acronyms and Symbols

Acronyms

AC	Alternating current
ANN	Artificial neural network
CHB	Cascaded H-bridge
CSI	Current source inverter
DBPC	Deadbeat predictive control
DC	Direct current
DPC	Direct power control
FLC	Fuzzy logic control
GPC	Generalized predictive control
LUT	Lookup table
MPPT	Maximum power point tracking
MPC	Model predictive control
M²PC	Modulated model predictive control
NF	Neural fuzzy
NP	Neutral-point
P&O	Perturb & Observe
PV	Photovoltaic
PI	Proportional-integral
PR	Proportional resonant
PWM	Pulse width modulation
RMS	Root mean square
SMC	Sliding mode control
SVM	Space vector modulation

3L-NPC	Three-level neutral point clamped
THD	Total harmonic distortion
VOC	Voltage-oriented control
VSI	Voltage source inverter

Symbols

[P], [O], [N]	Switching states of three-level neutral-point clamped inverter
i_a, i_b, i_c	Three-phase output currents.
V_{an}, V_{bn}, V_{cn}	Three-phase output voltage inverter
S_a, S_b, S_c	Switching states
V_{dc}	DC-link voltage
i_{C1}, i_{C2}	DC-link capacitors currents
V_P, V_N	DC-link capacitor voltages of inverter
R	Load resistance
L	Load inductance
C	DC-link capacitor
T_s	Controller sampling time
g	Cost function
$V_{\alpha n}^*, V_{\beta n}^*$	Reference voltages
θ	The position of the reference voltage vector
S_n	Sector number
m_a	Modulation index
λ_{dc1}	Weighting factor
f_{sw}	Average switching frequency
n_{sw}	Total number of switching cycles
RMS_i	RMS current error
d_a, d_b, d_c	Dwell time applications
ΔV	Balancing factor
V_{gabc}	Three-phase grid voltages
i_{gabc}	Three-phase grid currents
R_f, L_f	Filter resistance and inductance

I_{PV}	The light generated current
I_{ph}	Photovoltaic current
I_D	Diode current
I_{sh}	Short circuit current
I_0	Saturation current
D	Diode
P^*	Active power reference
Q^*	Reactive power reference
$i^*_{g\alpha}$ & $i^*_{g\beta}$	Reference current
Pd_con	DIODE conduction losses
Ps_con	MOSFET conduction losses
Pd_sw	DIODE switching losses
Ps_sw	MOSFET switching losses

Superscripts

~	Error value
^	Estimated value
P	Predictive value
*	Reference value

Subscripts

α,β	α,β axis
d,q	d,q axis

Résumé en Français

1. Généralités sur les convertisseurs statiques

L'électronique de puissance, dans le domaine de l'électricité, joue un rôle vital dans le fonctionnement de diverses activités tel que la gestion du réseau électrique, le transport, les énergies renouvelables et l'industrie[1][2]. Actuellement, l'énergie électrique est l'élément prépondérant dans la vie quotidienne de l'homme. Ainsi, il est nécessaire d'améliorer les performances des dispositifs de l'électronique de puissance pour contribuer à la bonification du signal électrique.

Les convertisseurs électriques sont des dispositifs composés de semi-conducteurs, d'éléments passifs (résistances), de condensateurs et d'inductances. La combinaison de ces éléments permet de convertir la forme de signal électrique (tension ou courant) en une autre forme adaptable à une utilisation efficiente dans les activités industrielles. Il existe quatre types de convertisseur [3]:

- **Type 1 :** les convertisseurs continu-continu (les hacheurs). Ces convertisseurs DC/DC sont utilisés pour une exploitation rationnelle (maximale) de la puissance fournie par le générateur PV et aussi parfois pour l'adaptation de la tension continue du générateur à la charge.
- **Type 2 :** les convertisseurs continu-alternatif (les onduleurs). Ces convertisseurs DC/AC sont utilisés pour une conversion de la tension continue fournie par le GPV en une tension alternative et aussi parfois ils font fonction d'adaptation de la charge de manière rationnelle à la puissance fournie.
- **Type 3 :** les convertisseurs alternatif-continu (les redresseurs). Ces convertisseurs AC/DC sont utilisés pour l'alimentation des moteurs à courant continu et le chargement des batteries.
- **Type 4 :** les convertisseurs alternatif-alternatif. ces convertisseurs AC/AC sont utilisés seulement lorsque la valeur efficace de la tension alternative est modifiée. Ils sont utilisés pour la générations des vitesses variables en alternatif (levage, machine-outil).

Ces dernières années, des convertisseurs statiques sont de plus en plus employés dans de diverses applications. Certaines d'entre elles exigent une alimentation électrique haute tension facilement réglable et ayant de bonnes performances spectrales[4]. De nouvelles techniques dites multiniveaux et de nouvelles topologies des convertisseurs ont été développées. Celles-ci permettent de générer plusieurs niveaux de tension à la sortie du convertisseur[5]. Le nombre de semi-conducteurs nécessaire à la réalisation de ces topologies augmente avec le nombre de niveaux désiré. Un convertisseur statique est dit « multiniveaux » lorsqu'il génère une tension découpée de sortie composée d'au moins trois niveaux. Ce type de convertisseur présente essentiellement deux avantages. D'une part, les structures multi-niveaux permettent de limiter les contraintes en tension subies par les interrupteurs de puissance : chaque composant, lorsqu'il est à l'état bloqué, supporte une fraction d'autant plus faible de la pleine tension de bus continu que le nombre de niveaux est élevé. D'autre part, la tension de sortie délivrée par les convertisseurs multiniveaux présente d'intéressantes qualités spectrales. Le fait de multiplier le nombre de niveaux intermédiaires permet de réduire l'amplitude de chaque front montant ou descendant de la tension de sortie. Ainsi, l'amplitude des raies harmoniques est par conséquent moins élevée. Dans le cas de modulation de largeur d'impulsion, le recours à un convertisseur multi-niveaux associé à une commande judicieuse des composants de puissance permet en outre de supprimer certaines familles de raies harmoniques[6].

Ayant les capacités pour fournir un niveau de tension élevé et une puissance élevée tout en maintenant une faible tension en mode commun, les convertisseurs multiniveaux s'affirment comme une solution idoine dans les systèmes éoliens.

En général, trois différentes topologies sont proposées: le convertisseur clampé par le neutre (NPC), le condensateur volant (FC) et cascade en pont H (CHB)[7]–[9]. Actuellement, les onduleurs à trois niveaux à structure NPC sont les convertisseurs de puissance DC/AC les plus utilisés. Ils présentent plusieurs avantages : coût réduit, faible poids et taille compacte. La première topologie pratique d'onduleur de tension multiniveaux est le NPC (neutral point clamped). Celle-ci a été initialement proposée par A.Nabac en 1981 pour la génération de N niveaux de tension. Dans le bus continu de l'onduleur à trois niveaux à structure NPC, le condensateur est divisé en deux, ce qui offre un point neutre. Les diodes connectées au point neutre se référant à diodes flottantes. Elles connectent les bras de l'onduleur au point neutre, ce qui réduit la tension inverse de non-conduction de chaque interrupteur à $V_{dc}/2$. Chaque bras de l'onduleur peut prendre trois valeurs de tension : 0, $V_{dc}/2$ ou $-V_{dc}/2$, ce qui permet d'approximer au mieux la tension de sortie à la sinusoïde, et d'avoir une meilleur qualité d'énergie[10][9]. Par conséquent, le convertisseur à trois niveaux clampé par le neutre (NPC) est considéré

comme étant une bonne solution pour les systèmes de conversion de l'énergie du système photovoltaïque te ce grâce à ses avantages en termes d'économie, de complexité de la commande et de performance. En effet, cette topologie est très commercialisée et disponible sur le marché.

Dans ce travail, la structure de l'onduleur à trois niveaux 'NPC', son principe de fonctionnement, sa modélisation et en particulier sa commande prédictive sont abordés.

2. Types de commande des convertisseurs statiques

Plusieurs méthodes sont proposées pour contrôler le convertisseur statique. La commande des convertisseurs statiques peut être divisée en deux types principaux : le premier type commande linéaire, et le second commande non linéaire comme - commande à hystérésis[11], commande mode de glissement[12], commande intelligente et commande prédictive[13]. Récemment, des commandes basées l'hystérésis, notamment la commande directe de la puissance (DPC) sont proposées pour améliorer les performances de l'asservissement[14]. Ces méthodes permettent de sélectionner les états de commutation de l'onduleur à partir d'une table de commutation (LUT). La sélection s'effectue sur la base des erreurs numérisées, entre les références des puissances active et réactive. Ainsi, ces méthodes n'ont pas besoin des boucles de commande actuelles et de modulation vectorielle[15]. En comparaison avec le contrôleur linéaire PI[16], ces méthodes ont une réponse dynamique rapide, aucune exigence de découplage entre la commande des composantes active et réactive, et conduit à une meilleure dynamique. Néanmoins, l'inconvénient de LUT est qu'il présente une grande ondulation de puissances active et réactive et la variation de la fréquence de commutation. Pour surmonter ce problème, une modulation vectorielle est introduite dans la structure DPC. Par ailleurs, une fréquence d'échantillonnage élevée est utilisée dans ce type de commande pour garantir des performances stables, dynamiques et acceptables. Avec des techniques de contrôle linéaire et d'hystérésis, il n'est pas facile d'inclure les contraintes du système et les exigences techniques tel que le courant maximal, la distorsion harmonique totale, la tension en mode commun et la fréquence de commutation.

Ces derniers temps, la commande prédictive s'est imposée comme étant une technique de commande majeure qui s'applique aux convertisseurs de statiques. La commande prédictive à modèle (MPC) est une commande avancée, appliquée pour la commande de différents systèmes linéaires ou non linéaires [17][18]. L'idée principale de la commande prédictive repose sur l'utilisation d'un modèle du système à commander pour prédire sa sortie (le comportement futur du processus) sur un certain horizon fini, appelé horizon de prédiction. La décision de

commande est prise en fonction de la référence, la sortie actuelle, la sortie précédente, et parfois les contraintes. La décision optimale est prise en minimisant les coûts. La procédure se répète pour la période suivante en appliquant à chaque période d'échantillonnage uniquement la composante qui correspond à la valeur minimale de la fonction objective parmi les différentes combinaisons qui puissent avoir lieu. Le principe de fonctionnement de MPC est basé sur l'utilisation du modèle mathématique pour prédire le comportement du système, puis minimiser la fonction de coût prédéfinie pour atteindre les objectifs de commande spécifiés. Elle est puissante et donne de bons résultats lorsque la trajectoire de sortie est prédéfinie[3][19][20].Les principaux avantages de la commande prédictive sont:

- L'idée générale est intuitive et facile à comprendre.
- Elle permet de respecter les contraintes sur les variables commandées et manipulées.
- Haute précision, flexibilité stabilité.
- Elle présente un outil très puissant pour affronter les restrictions.
- Simple à implémenter.
- Elle autorise l'adaptation automatique du système en cas de perturbations mesurables.
- Bonne poursuite de référence surtout pour les systèmes lents.
- Elle donne de meilleures performances si le système réagit avec un retard.
- Elle donne des meilleures performances si les consignes du système sont connues d'avance.
- Elle prend en compte la nature discrète du système à commander.
- Simple à appliquer dans les systèmes multi variables, systèmes linéaires est non linéaires.
- Les différentes contraintes du système peuvent être incorporées dans le contrôleur.
- Nombre fini d'optimisation durant une période échantillonnage.

Mais possède trois cruciaux inconvénients :

- Temps de calcul élevé en particulier pour un nombre élevé d'états de commutation et de longs horizons de prédiction pour certains convertisseurs.
- Les performances dépendent essentiellement de l'écart entre le modèle du système et le système réel à commander.
- Sélection heuristique des facteurs de pondération.

3. Classification de la commande prédictive

La commande prédictive est considérée comme étant une excellente solution qui répond aux exigences de contrôle d'un onduleur NPC à trois niveaux. De plus, il s'agit d'une approche de contrôle alternative intéressante pour différents onduleurs multiniveaux en raison de sa haute précision, de sa réponse transitoire rapide et de sa nature discrète inhérente. Les techniques de la commande prédictive peuvent être classées en tenant compte de la présence de modulation :

- **Type1 :** Commande prédictive sans modulateur (fréquence de commutation variable (VSF-MPC)).
- **Type 2 :** Commande prédictive avec un modulateur (fréquence de commutation constante (FSF-MPC)).

Parmi ces deux stratégies existent quatre types [3][21]:

- **Type 1 :** Commande prédictive à réponse pile "deadbeat control". Cette technique utilise un modèle du système de calcul de la tension de référence requise pour atteindre la valeur de référence. Cette tension est appliquée aux convertisseurs via un modulateur à l'instant suivant d'échantillonnage.
- **Type2 :** Commande prédictive basée sur des comparateurs à hystérésis. Dans cette technique la variable à commander est mise dans une bande d'hystérésis. Cette méthode n'exige pas un bloc intermédiaire de modulation, mais les signaux de commande sont envoyés directement au convertisseur.
- **Type 3 :** Commande prédictive basée sur la poursuite d'une trajectoire de référence. Dans cette technique les variables à commander sont forcées par la trajectoire précalculée. Elle n'exige pas de bloc intermédiaire de modulation où les signaux de commande sont envoyés directement au convertisseur.
- **Type 4 :** Commande prédictive à base de modèle (MPC). Grâce à ses avantages, elle est reconnue comme étant une stratégie de contrôle simple et puissante pour la commande des convertisseurs de puissance et les moteurs électriques. Le MPC s'applique aux convertisseurs de puissance et peut être classé en deux groupes principaux :
    - la commande prédictive à ensemble de commande continue MPC (CCS-MPC)
    - la commande prédictive à ensemble de commande finie (FCS-MPC).

4. Principe de fonctionnement d'un FCS-MPC

Cette stratégie est basée sur la recherche de l'optimum d'une fonction de performance (fonction de coût) permettant de déterminer le vecteur de commande optimal, parmi l'ensemble des vecteurs possibles, à appliquer à l'entrée du redresseur durant chaque période de commutation. Elle consiste donc à appliquer un seul vecteur de commande durant cette période. Ainsi, les interrupteurs du pont triphasé sont commandés avec une fréquence de commutation variable[22][23].

La conception MPC est réalisée selon les étapes suivantes[24][25]:

- Obtenir les signaux de retour requis pour le modèle prédictif ou le calcul de la référence.
- Calculer la variable de référence en fonction de l'application spécifique, puis obtenir les valeurs futures de la référence en utilisant l'extrapolation.
- La modélisation du système s'effectue en dérivant des équations qui décrivent le comportement dynamique des variables contrôlées généralement basées sur un modèle linéaire comme suit :

  $$\frac{dx}{dt} = Ax + Bu$$

  Où x représente la variable à contrôler (tension, courant, flux, puissance) et u est l'entrée de contrôle (tension de réseau, état de commutation, tension continue).

  Pour discrétiser l'équation précédente la méthode d'Euler a été utilisée et donne la formule suivante:

  $$\frac{dx}{dt} = \frac{x(k-1) - x(k)}{T_s}$$

  Où $x(k+1)$ et $x(k)$ représente la variable de sortie à l'instant suivant et l'instant actuel respectivement, et T_s représente la période d'échantillonnage.
- Prédire la valeur future des variables de commande basées sur les modèles à temps discret, les valeurs mesurées et tous les états possibles de commutation du convertisseur.
- L'étape finale est de minimiser la fonction de coût. La fonction de coût contient des termes principaux (l'objectif de contrôle qui doit être atteint afin de fournir un bon comportement du système) et d'autres secondaires (les exigences qui devraient être remplies pour améliorer les performances du système). Ceci conduit à l'intégration

des coefficients de pondération. La valeur du facteur de pondération reflète l'importance de terme inclus dans la fonction du coût.

$$g = \left| x^{*}\left(k+1\right) - x_i^{P}\left(k+1\right) \right| + \lambda_{dc} \left| y_1(k+1) - y_2(k+1) \right|, i = 1,....,n$$

La commande prédictive conventionnelle nécessite d'évaluer la fonction de coût pour tous les états de commutation de l'onduleur NPC à trois niveaux. La sélection heuristique du facteur de pondération requis pour maintenir l'importance relative de ces objectifs de contrôle multiples entre le suivi de courant et l'équilibrage de tension NP est une tâche complexe. Ce qui nécessite un temps plus long pour le processus d'exécution, ce qui implique une charge de calcul élevée consommant beaucoup de ressources de calcul et augmentant ainsi le coût de mise en œuvre. Par conséquent, la charge de calcul élevée et le contrôle multi-objectifs sont devenus un défi pour la mise en œuvre pratique de MPC pour les topologies d'onduleurs à multiniveaux. Pour réduire le temps du calcul, une nouvelle commande prédictive basée sur le sur la réponse pile 'deadbeat' sans facteur de pondération est proposée et adopté à la place du contrôle actuel[22][26][27]. Pour l'équilibrage de tension des condensateurs NP, les petits vecteurs de tension redondants sont utilisés [28]–[30].

5. Commande prédictive modulée M²PC

Cette technique est un schéma de modulation intrinsèque approprié pour l'algorithme MPC combinant à la fois les algorithmes MPC [3]et SVM[5]qui y sont introduits. Cette méthode a été proposée par ''Tarisciotti''[31]–[33]. Cette méthode vise à améliorer la qualité de la puissance électrique de sortie du système avec un modulateur intrinsèque tout en préservant les avantages du MPC. L'utilisation d'un modulateur permet une meilleure sortie de l'état de commutation qui ressemble à la référence d'entrée. Un modèle SVM symétrique avec des états adjacents a été préféré pour réduire les harmoniques de courant de sortie et l'ondulation de tension NP. La majorité des schémas d'équilibrage de tension NP utilisés dans SVM reposent sur une certaine forme de manipulation de petits vecteurs redondants, où la durée relative des petits vecteurs positifs et négatifs est généralement ajustée afin de compenser l'erreur de tension NP.

6. Objectifs

L'objectif de ce travail de thèse est d'élaborer de nouvelles stratégies de commande basées sur la commande prédictive pour l'onduleur NPC à trois niveaux et sa mise en œuvre pour

l'amélioration de ses performances en termes de temps du calcul, de réponse dynamique, d'efficacité, et de pertes de puissance de l'onduleur a trois niveaux.

Ainsi, les axes de recherche tiennent compte des objectifs suivants :

- Développement original d'une commande prédictive à réponse pile 'deadbeat control' associée à l'onduleur NPC à trois niveaux, constituant notre contribution dans le domaine de la commande prédictive.
- Description détaillée du schéma de commande prédictive modulée (M²PC) pour contrôler l'onduleur NPC à trois niveaux.
- Proposition deux types de commutation pour la commande prédictive modulée (M²PC).

7. Résumé de la thèse

L'introduction générale présente les différents types de convertisseurs statiques et leurs applications et le développement historique de la commande prédictive pour les onduleurs à trois niveaux.

La thèse est organisée comme suit :

Chapitre II : Commande prédictive basé sur la réponse pile 'deadbeat' pour l'onduleur NPC à trois niveaux

Ce chapitre est consacré à la présentation générale de la commande prédictive basée sur le modèle (MPC). Il commence par une description de la commande prédictive. Puis, il aborde le principe de fonctionnement et l'objectif principal des différents contrôleurs prédictifs basés sur la réponse pile 'deadbeat' pour l'onduleur NPC à trois niveaux. L'effet du nombre de vecteurs actifs pour l'évaluation de la fonction de coût a été étudié pour les performances en régime permanent et dynamique. Pour ce faire, une comparaison entre les trois types de commande prédictive basé sue la réponse pile 'deadbeat' avec différents nombres des vecteurs (19,6, et 3) avec la commande prédictive conventionnelle a été effectuée. La tension du point neutre est équilibrée à l'aide des vecteurs redondants. Les résultats de la simulation et les résultats expérimentaux montrent que les techniques de commande prédictive basées sur le deadbeat présentent de bonnes performances et robustesses en terme d'erreur d'équilibrage de la tension au point neutre (NP), de distorsion harmonique totale (THD), de charge de calcul, de fréquence de commutation moyenne, de pertes de puissance et de sensibilité à l'inadéquation des paramètres par rapport la commande prédictive conventionnelle (C-MPC).

Chapitre III : Commande prédictive modulée (M²PC) pour l'onduleur NPC à trois niveaux

Ce chapitre est consacré à la présentation du modèle de la commande prédictive modulée M²PC pour l'onduleur NPC à trois niveaux. Et ce afin de surmonter l'inconvénient de l'approche de la commande prédictive conventionnelle (MPC) qui est caractérisée par une fréquence de commutation variable, une grande ondulation du courant de sortie, un temps de calcul lourd, et une fréquence de commutation moyenne plus élevée. Dans ce chapitre, une commande prédictive modulée (M²PC) base sur une nouvelle forme de modèle de commutation est proposée. Cette méthode répond à l'exigence d'un onduleur haute performance, d'une fréquence de commutation constante, de ce fait résoudre les inconvénients du C-MPC conventionnel. Dans ce travail, l'effet du nombre des segments du modèle de commutation est évalué expérimentalement et comparé au nouveau modèle de commutation à cinq et neuf segments. De plus, la régulation de la tension du bus continu sera assurée grâce à des stratégies proposées. Ce chapitre se termine par les résultats de simulations et expérimentaux obtenus qui indique clairement l'avantage de l'augmentation de nombre de segments de commutation pour la commande M²PC.

Chapitre IV : Etude comparative entre les commandes prédictives développées pour un onduleur NPC à trois niveaux associé à un système photovoltaïque

Le quatrième chapitre sera dédié à l'étude comparative entre les commandes prédictives développées pour un onduleur 3L-NPC associé à un système photovoltaïque. On commencera par la modélisation du système PV connecté au réseau électrique avec un algorithme MPPT de type "Perturbation & Observation (P&O)" via un convertisseur DC-DC. Ensuite, on présentera les résultats des simulations qui permettront d'évaluer les performances des stratégies proposées. Ce chapitre est clôturé par une étude comparative entre les commandes prédictives proposées : DBPC, M²PC et MPC conventionnelle.

Conclusions

Un résumé des résultats obtenus des travaux de recherche effectués durant la thèse et d'éventuelles contributions et/ou innovations futures sont présentés dans ce chapitre.

8. Références

[1] K. Bimal, "Energy, Rnvironment and Improtance of Power Electronics," *Recent Res.*

Environ. Geol. Sci., vol. 9, no. 1, pp. 13–28, 2010.

[2] N. Mohan, T. M. Undeland, and W. P. Robbins, *Power Electronics: Converters, Applications, and Design, 3rd Edition*, 3rd ed. John Wiley & Sons, Inc., 2003.

[3] J. Rodriguez and P. Cortes, *Predictive Control of Power Converters and Electrical Drives*. New York, NY, USA: Wiley–IEEE Press, 2012.

[4] R. Teodorescu, M. Liserre, and P. Rodriguez, *Grid Converters for Photovoltaic and Wind Power Systems*, Wiley–IEEE. New York, NY, USA, 2011.

[5] B. Wu, *High-Power Converters and AC Drives*. Wiley–IEEE. New York, NY, USA, 2006.

[6] J. Rodríguez, J. S. Lai, and F. Z. Pen, "Multilevel Inverters : A Survey of Topologies, Controls, and Applications," *IEEE Trans. Ind. Electron.*, vol. 49, no. 4, pp. 724–738, 2002.

[7] S. Daher, J. Schmid, and F. L. M. Antunes, "Multilevel Inverter Topologies for Stand-Alone PV Systems," *IEEE Trans. Ind. Electron.*, vol. 55, no. 7, pp. 2703–2712, 2008.

[8] K. K. Gupta, A. Ranjan, P. Bhatnagar, L. K. Sahu, and S. Jain, "Multilevel Inverter Topologies with Reduced Device Count: A Review," *IEEE Trans. Power Electron.*, vol. 31, no. 1, pp. 135–151, 2016.

[9] H. Du Toit Mouton, "A new Nonlinear PI / PID Controller for Quadrotor Posture Regulation," *IEEE Trans. Ind. Electron.*, vol. 49, no. 5, pp. 1017–1025, 2002.

[10] T. Brückner and D. G. Holmes, "Optimal Pulse-Width Modulation for Three-Level Inverters," *IEEE Trans. Power Electron.*, vol. 20, no. 1, pp. 82–89, 2005.

[11] K. K. Leung and H. S. Chung, "Dynamic Hysteresis Band Control of the Buck Converter With Fast Transient Response," *IEEE Trans. Circuits Syst.*, vol. 52, no. 7, pp. 398–402, 2005.

[12] K. D. Young, V. I. Utkin, and Umit Ozguner, "A Control Engineer 's Guide to Sliding Mode Control," *IEEE Trans. Syst. Technol.*, vol. 7, no. 3, pp. 328–342, 1999.

[13] Carlos E. Garcia, David M. Prett, and Morari Morar, "Model Predictive Control : Theory

and Practice a Survey," *Automatica*, vol. 25, no. 3, pp. 335–348, 1989.

[14] Y. Zhang, J. Gao, and C. Qu, "Relationship Between Two Direct Power Control Methods for PWM Rectifiers Under Unbalanced Network," *IEEE Trans. Power Electron.*, vol. 32, no. 5, pp. 4084–4094, 2017.

[15] M. Malinowski, M. Jasin, and M. P. Kazmierkowski, "Simple Direct Power Control of Three-Phase PWM Rectifier Using Space-Vector Modulation (DPC-SVM)," *IEEE Trans. Ind. Electron.*, vol. 51, no. 2, pp. 447–454, 2004.

[16] S. Gonz, J. Moreno-valenzuela, and B. C. Tijuana, "A New Nonlinear PI / PID Controller for Quadrotor Posture Regulation," *Electron. Robot. Automot. Mech. Conf.*, pp. 642–647, 2010.

[17] P. Cortes, A. Wilson, S. Kouro, J. Rodriguez, and H. Abu-Rub, "Model Predictive Control of Multilevel Cascaded H-Bridge Inverters," *IEEE Trans. Ind. Electron.*, vol. 57, no. 8, pp. 2691–2699, 2010.

[18] P. Wipasuramonton, Z. Q. Zhu, and D. Howe, "Predictive Current Control with Current Error Correction for PM Brushless AC Drives," *IEEE Trans. Ind. Appl.*, vol. 42, no. 4, pp. 558–564, 2006.

[19] J. D. Barros and J. F. Silva, "Optimal Predictive Control of Three-Phase NPC Multilevel Converter for Power Quality Applications," *IEEE Trans. Ind. Electron.*, vol. 55, no. 10, pp. 3670–3681, 2008.

[20] P. Cortés, M. P. Kazmierkowski, R. M. Kennel, D. E. Quevedo, and J. Rodríguez, "Predictive Control in Power Electronics and Drives," *IEEE Trans. Ind. Electron.*, vol. 55, no. 12, pp. 4312–4324, 2008.

[21] V. Yaramasu and B. Wu, *Model Predictive Control of Wind Energy Conversion Systems*. New York, NY, USA: Wiley–IEEE Press, 2017.

[22] C. Xia, T. Liu, T. Shi, and Z. Song, "A Simplied Finite-Control-Set Model-Predictive Control for Power Converters," *IEEE Trans. Ind. Informatics*, vol. 10, no. 2, pp. 991–1002, 2014.

[23] Y. Yang, H. Wen, M. Fan, M. Xie, and R. Chen, "Fast Finite-Switching-State Model

Predictive Control Method Without Weighting Factors for T-Type Three-Level Three-Phase Inverters," *IEEE Trans. Ind. Informatics*, vol. 15, no. 3, pp. 1298–1310, 2019.

[24] J. Rodr, J. Pontt, P. Cort, R. Vargas, and S. Mar, "Predictive Control of a Three-Phase Neutral Point Clamped Inverter," *2005 IEEE 36th Power Electron. Spec. Conf.*, no. 4, pp. 1364–1369, 2005.

[25] A. Calle-Prado, S. Alepuz, J. Bordonau, J. Nicolas-Apruzzese, P. Cortés, and J. Rodriguez, "Model Predictive Current Control of Grid- Connected Neutral-Point Clamped Converters to Meet Low Voltage Ride-Through Requirements," *IEEE Trans. Ind. Electron.*, vol. 62, no. 3, pp. 1503–1514, 2015.

[26] J. D. Barros, J. F. A. Silva, and É. G. A. Jesus, "Fast-Predictive Optimal Control of NPC Multilevel Converters," *IEEE Trans. Ind. Electron.*, vol. 60, no. 2, pp. 619–627, 2013.

[27] Y. He, J. Liu, J. Tang, Z. Wang, and Y. Zou, "An Novel Deadbeat Control Method for Active Power Filters with Three-Level NPC Inverter," *2008 IEEE Power Electron. Spec. Conf.*, pp. 661–665, 2008.

[28] Y. Jiao, F. C. Lee, and S. Lu, "Space Vector Modulation for Three-Level NPC Converter With Neutral Point Voltage Balance and Switching Loss Reduction," *IEEE Trans. Power Electron.*, vol. 29, no. 10, pp. 5579–5591, 2014.

[29] F. Wang, Z. Li, and Z. Liu, "Model Predictive Control Methods for Three-level Sparse Neutral Point Clamped Inverter," *IEEE J. Emerg. Sel. Top. Power Electron.*, vol. 8, no. 4, pp. 4355–4366, 2020.

[30] X. Xing, X. Li, F. Gao, C. Qin, and C. Zhang, "Improved Space Vector Modulation Technique for Neutral-Point Voltage Oscillation and Common-Mode Voltage Reduction in Three-Level Inverter," *IEEE Trans. Power Electron.*, vol. 34, no. 9, pp. 8697–8714, 2019.

[31] L. Tarisciotti, P. Zanchetta, A. Watson, S. Bifaretti, and J. C. Clare, "Modulated Model Predictive Control for a Seven-Level Cascaded H-Bridge Back-to-Back Converter," *IEEE Trans. Ind. Electron.*, vol. 61, no. 10, pp. 5375–5383, 2014.

[32] L. Tarisciotti, P. Zanchetta, A. Watson, J. Clare, M. Degano, and S. Bifaretti, "Modulated

Model Predictive Control for a Three-Phase Active Rectifier," *IEEE Trans. Ind. Appl.*, vol. 51, no. 2, pp. 1610–1620, 2015.

[33] L. Tarisciotti, P. Zanchetta, A. Watson, P. Wheeler, and S. Bifaretti, "Multiobjective Modulated Model Predictive Control for a Multilevel Solid-State Transformer," *IEEE Trans. Ind. Appl.*, vol. 51, no. 5, pp. 4051–4060, 2015.

Chapter I

Introduction

I.1 Overview of power converter system

Power converters are electronic circuits associated to the conversion, control, and conditioning of electric power. It have become an enabling technology in most areas of life, such as: industrial and household applications, renewable energies, flexible AC transmission systems and micro grids, as well as automotive and transport applications [1][2]. Newer applications in transportation can be found in electric and hybrid vehicles, and in aircraft. Conversion and control of electrical energy using power electronics is a very important topic today, considering the increasing energy demands and new requirements in terms of power quality and efficiency. In order to fulfill these demands new semiconductor devices, topologies, and control schemes are being developed. The use of power converters can help to improve the quality and stability of the grid. Power electronic converters have been used in many industrial applications for efficient power conversion and energy conservation, some examples in power systems are active filters, converters for distributed generation, energy storage systems and others [3]. Especially, the use of power converters in renewable energy conversion systems has been constantly increasing in recent years, mainly due to growing energy demands and environmental concerns. Among the different renewable energy sources, photovoltaic (PV) generation systems are a very interesting example of power converter applications because it is not possible to deliver power from the PV panel to the grid without a converter [4][3].

This chapter presents a basic introduction and useful references of power converters especially the multilevel converters, and their applications. The most common applications that involve the use of power converters are presented, and a general scheme for a drive system is explained. The power converter topologies found in the industry are introduced according to a simple classification. A brief introduction to control schemes for power converters, specially, the basic principles of predictive control, are discussed.

I.2 Classification of power converters

Power electronic converters have been used in many industrial applications for efficient power conversion and energy conservation. Depending on the type of electric power conversion and the electric power flow, the power converters can be divided into the following four categories:

- AC-DC rectifiers: Convert a single-phase or three-phase AC voltage to DC is used as front-end in variable-speed motor drives and wind energy conversion systems.
- DC-DC converters: Convert a DC voltage from one level and a certain polarity to a DC voltage of another level and in some applications to another polarity.
- DC-AC inverters: Conversion from DC to variable-voltage and variable-frequency AC is used invariable-speed motor drives. Conversion of unregulated or regulated DC to fixed AC is used in grid-connection of renewable energy sources.
- AC-AC cycloconverters: Convert an AC voltage of one level, frequency and number of phases to an AC voltage of a different level, frequency, and in some applications to different number of phases.

The voltage source inverters (VSIs) are a matured technology that uses a DC capacitor as a storage element in the DC-link. Over the past decade, VSIs exhibited higher market penetration and more development that is evident compared to current source inverters (CSIs) and matrix inverters. Furthermore, they are widely used in many power conversion applications, e.g., electrical drives, renewable energy systems, and flexible alternating current transmission systems [5]. The most prominent developments in VSIs are shown in Figure I.1. The three-phase two-level inverter is limited to low voltage and low-power applications, also it suffers from high electrical stress and harmonics, especially for medium or high voltage applications [6]. For that, it requires either devices in parallel to carry high current at low-voltage operation or devices in series to reach medium-voltage operation with low current-carrying capacity. The parallel and series connections of devices do not introduce any additional bene test in the improvement of power quality (reduction of voltage and current harmonic distortion) and dv/dt reduction. Power losses and voltage blocking are uneven in series-connected devices. Thus, two-level converters are not very popular for high-power applications, which motivated the researchers to develop new topologies to mitigate these problems, such as multilevel power converters [6]–[8]. Many topologies have been suggested for high power applications, among them neutral point clamped (NPC) inverter, cascaded H-bridge (CHB) inverter, and flying capacitor inverter [9]–[11].

A multilevel converter is structured to synthesize a voltage from several levels of voltages, which are a result of capacitor voltages. A multilevel converter starts with three levels and consists of a neutral tap between the capacitors in most cases. Clamping of these converters with different diodes and different topologies generates more levels. The clamping also affects the output waveforms; it increases the steps in output waveforms. The increase in the levels mean that higher voltages can be handled by the converters [12][13]. However, the voltage levels are limited in any multilevel converter due to voltage balancing between the capacitors. Recently, a three-level neutral point clamped inverter is one of the most widely used and commercially accepted multilevel inverters due to low voltage harmonic distortion (THD), near-sinusoidal currents, smaller size of input and output filters, high-efficiency, low common-mode voltage, and possible fault-tolerant operation in certain cases [11][14].

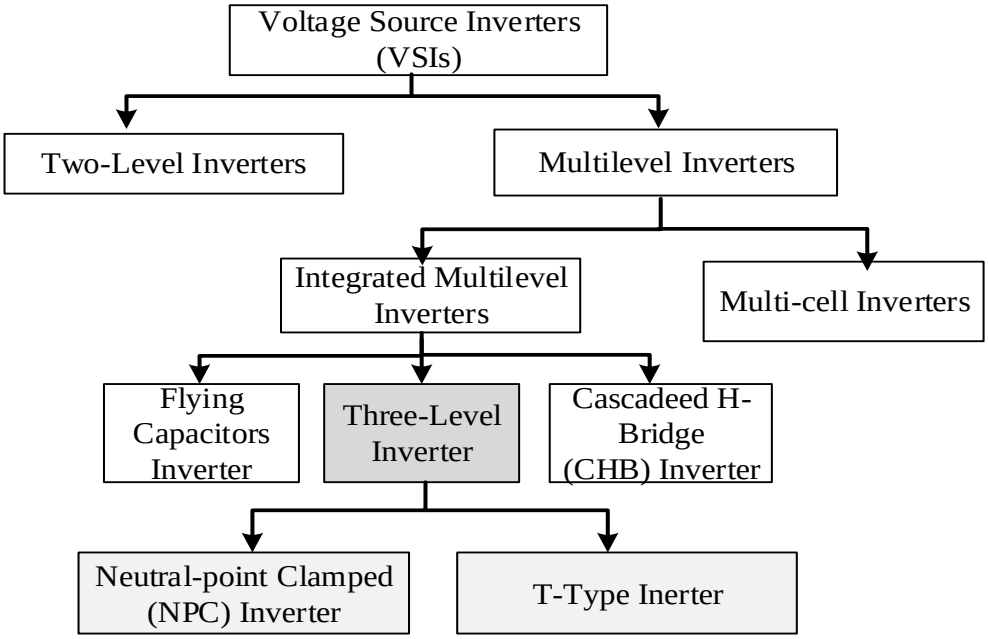

Figure I.1 : Voltage source inverter types.

I.3 Literature review and statement of the problem

I.3.1 Existing classical control strategies

Many control methods have been proposed over the last few years to control multilevel voltage source inverters. Among them, linear control techniques [15]. The main idea of linear control is to assume that the linearized system model is valid at a small range of operation. This

limitation is exposed once a large operation range is the case. Operating a linear controller at a wider range could lead to instability or at most, poor performance. Assuming the model is fully linearizable is another problem associated with linear controllers. This is due to the fact that there are hard nonlinearities, which cannot be linearized due to their discontinuous nature. Model uncertainties contribute significantly to the deterioration of the linear controller's performance. Finally, linear control typically exhibits a complex control design due to the need for a modulation stage and signal transformations. These control strategies have some unsatisfactory characteristics, such as erratic switching frequency, unconditional reliability, and poor dynamic response; also, they require a complex modulation system to balance the capacitor voltages [16].

The second control method is non-linear control such as: Hysteresis control [17], which includes direct power control (DPC) [18], has been deployed on multiple power electronic applications. These methods used hysteresis control and inverter-switching states, selected from a lookup table (LUT) based on errors between the reference and the estimated values of active and reactive power. In comparison with the PI linear controller [17], these methods have a fast dynamic response, no requirement for decoupling between the control of the active and reactive components, and leads to better dynamics. However, the downside of LUT is that it exhibits a large ripple of active and reactive power and variation in switching frequency. To overcome this problem, vector modulation has been introduced into the DPC structure. However, it suffers from the variable switching frequency, which may lead to resonance problems. In addition, in order to improve the output waveform quality, hysteresis control has to be operated using high sampling time such that the controlled signal can always be within the defined hysteresis bands. With linear control and hysteresis techniques, it is not easy to include system constraints and technical requirements such as maximum current, total harmonic distortion, common mode voltage, and switching frequency.

Scientists have resorted to new complex and intelligent nonlinear controls to overcome these problems. Among them: sliding mode control, intelligent control (fuzzy logic control (FLC), artificial neural network control (ANN), neuro-fuzzy (NF)) [19], and predictive control (PC) [20][21]. These nonlinear control strategies have shown considerable improvement in the system operation, where the fast-dynamic response and the certainty against parameter changes are desirable. Shown in Figure I.2 is a chart that categorizes and demonstrates the different types of control methods used for three-level NPC inverter.

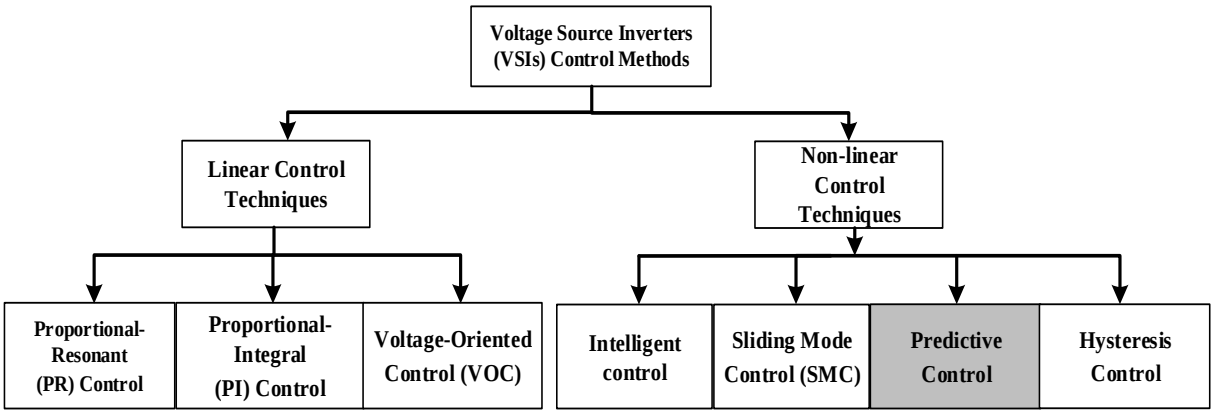

Figure I.2: Classification of control techniques used in voltage source converters.

I.3.2 Model predictive control (MPC)

In recent years, with the technological advancements in digital signal processors, the model predictive control (MPC) strategy has emerged as a simple and promising digital control tool in power electronics, variable-speed motor drives, and energy conversion systems; also, it has become popular for different industrial applications [22]. The predictive is a nonlinear control method and provides an approach that is better suited for controlling power converters [23][24]. This method also mitigates several technical and operational disadvantages associated with classical control techniques, particularly during the low-switching frequency operation needed by the megawatt level energy conversion systems. The predictive control is attractive for controlling fast varying electrical variables because of its simple and intuitive concept, digital controller friendliness, finite number of optimizations, elimination of proportional-integral (PI) controllers, pulse-width modulator-free structure, fast dynamic response, good steady-state performance during all operating conditions, capability to compensate perturbations and dead times of power conversion system, ease in incorporating nonlinearities and limitations in the design, and improved treatment of multivariable control problems with decoupling [25]. The predictive control uses the system model to predict the future behavior of the process for a specific control variable and then obtain the optimal actuation based on the predefined optimization criteria. The MPC techniques applied to power electronics have been classified into four groups as shown in Figure I.3: deadbeat control, hysteresis based control, trajectory based control, and model predictive control (MPC) [26][27].

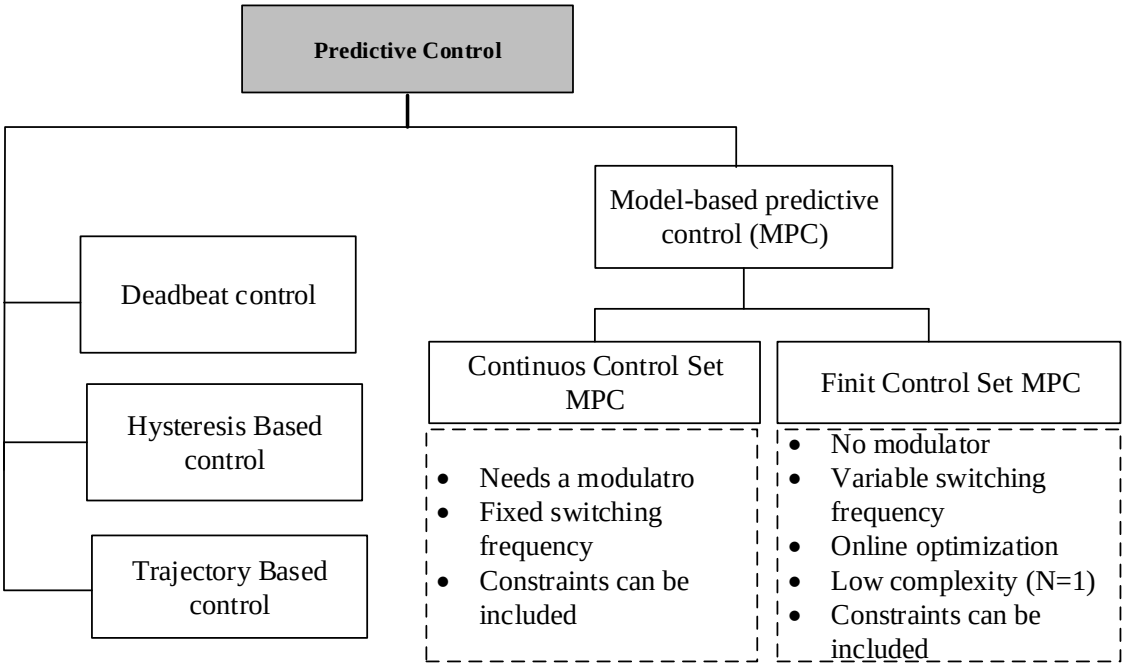

Figure I.3: Classifications of predictive control methods.

The optimization criterion in the hysteresis-based predictive control is to keep the controlled variable within the boundaries of a hysteresis area, while in the trajectory based, the variables are forced to follow a predefined trajectory. In deadbeat control, the optimal actuation is the one that makes the error equal to zero in the next sampling instant. A more flexible criterion is used in MPC, expressed as a cost function to be minimized. Model predictive control (MPC) is recognized as a simple and powerful control strategy to control power converters and electrical drivers thanks to its advantages such as simple to apply in multivariable systems and considering nonlinearities and constraints in the control system and presenting a fast dynamic response compared to the other predictive methods. The working principle of MPC is based on using the mathematical model to predict the system behavior and then minimize the cost function predefined to fulfill the control objectives. There are two main categories comprising the MPC techniques applied to power electronics [28][29]:

- The first type is continuous control set MPC (CCS-MPC). In this technique, the control variables are continuous. The CCS-MPC (Figure I.4 (a) uses of an average model of the converter to perform an optimization that minimizes the error between the reference and the future state. In this case, the controller output is the duty cycle reference applied to the modulator, which then generates the proper switch positions. On this basis, due to the use of a modulator, the converter presents a fixed switching frequency.

- The second type is finite control set MPC (FCS-MPC). This method (Figure I.4 (b) makes use of the discrete nature of power converters to select the optimal switch positions. This control method evaluates all the possible switching states and selects the one, which minimizes the designed cost function.

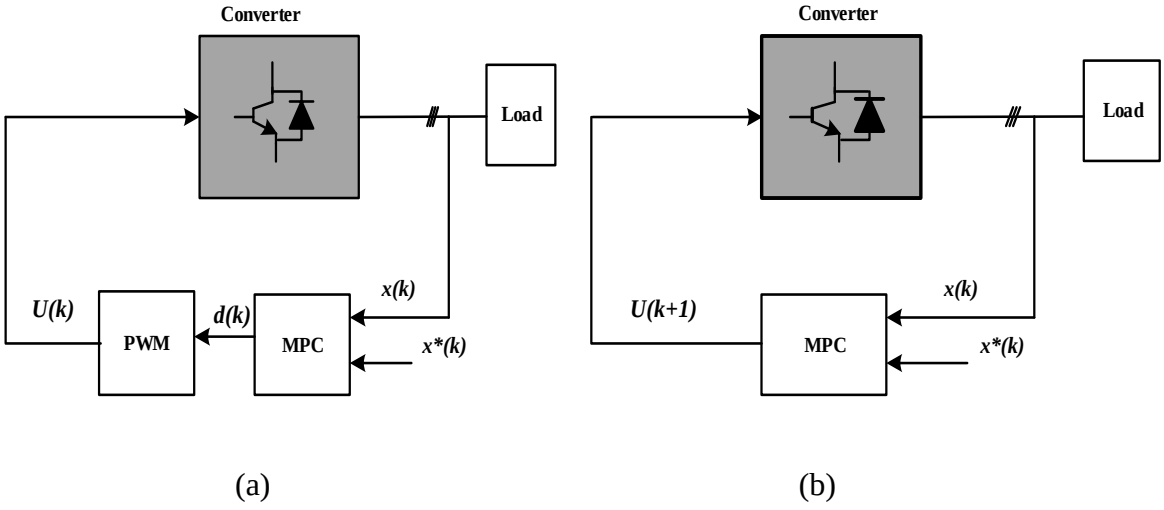

(a) (b)

Figure I.4: (a) Continuous Control Set MPC (CCS-MPC). (b) Finite Control Set MPC (FCS-MPC).

I.3.3 Principle and basic structure of MPC

Model predictive control is considered an excellent solution that fulfills the control requirements of a three-level NPC inverter. In addition, it is an attractive alternative control approach for different multilevel inverters due to its high accuracy, fast transient response, and inherent discrete nature. The basic concept of this strategy is based on the discrete-time model of the system to predict the future behavior of the control variables using the available switching states [14][24][25]. The working principle of MPC is summarized in Figure I.5. The future values of the states of the system are predicted until a predefined horizon in time k+ *N* using the system model and the available information (measurements) until time *k*. The sequence of optimal actuations is calculated by minimizing the cost function and the first element of this sequence is applied. This whole process is repeated again for each sampling instant considering the new measured data.

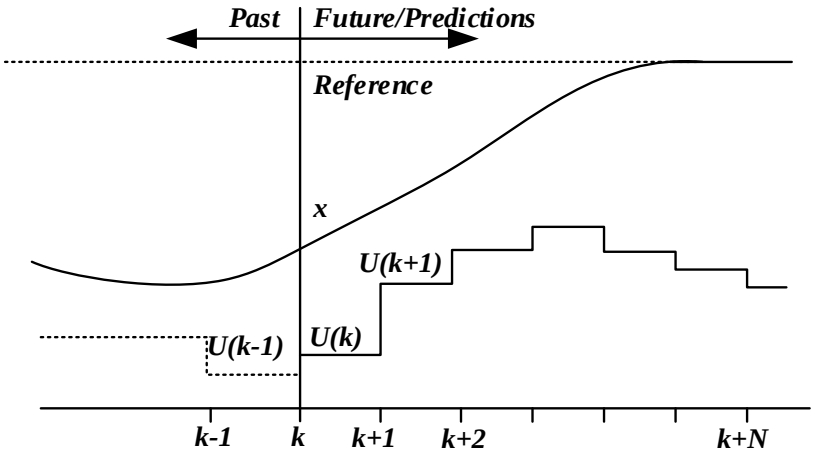

Figure I.5: Working principle of MPC.

The block diagram of a general MPC control scheme is shown in Figure I.6. In summary, the MPC design is performed according to the following steps:

- Obtain the required feedback signals for predictive model or reference calculation.
- Calculate the reference control variable according to the specific application, and then obtain the future values of the reference by using the extrapolation.
- The modelling system is accomplished by deriving equations that describe the dynamic behaviour of the controlled variables generally based on a linear model as:

$$\frac{dx}{dt} = Ax + Bu \tag{I.1}$$

where x represents the variable to be controlled (voltage, current, flux, power) and u is control input (grid voltage, switching state, DC voltage).

- A discrete-time model of the system is required to predict the behavior of the variables evaluated by the cost function. In order to discretize the system model, the first-order forward Euler method is used due to its simplicity. It also gives acceptable accuracy that is necessary for good performance. According to this approach, we have the discrete-time form of the system as follows:

$$\frac{dx}{dt} \simeq \frac{x(k+1) - x(k)}{T_s} \tag{I.2}$$

where T_s is the sampling time, $x(k + 1)$ and $x(k)$ are the value of the controlled variable in the next sampling time and at the current state, respectively.

- Final step is minimization cost function, all values of predicted variables x^{p}_{i} (k + 1) are compared with their reference $x^{*}(k+1)$ using a cost function g as follows:

$$g = \left| x^{*}\left(k+1\right) - x_{i}^{P}\left(k+1\right) \right|, i = 1,....,n \tag{I.3}$$

The goal of cost function optimization is to select the cost value g as close as possible to zero. The optimal switching state which minimizes the cost function is chosen and then applied to the converter at the next sampling instant. Therefore, this method does not require a modulation block, which simplifies the system design.

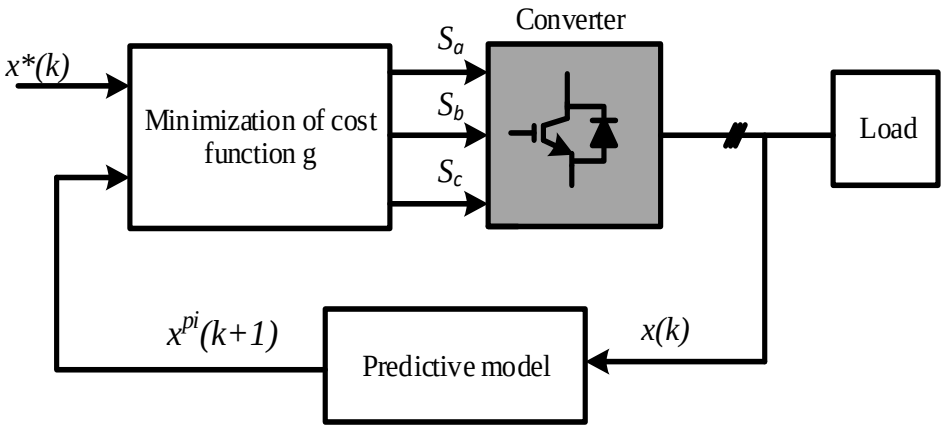

Figure I.6: Model predictive control scheme for power converters.

I.4 Implementation challenges of MPC

Researchers have been focused on improving the performance of MPC over the last years to reduce the computational burden. In [31][32], a new predictive control based on voltage vector saves more running time in the prediction and cost function processes. On the other hand, the three-level NPC inverter suffers from a basic issue that is represented in how to balance the capacitor voltages. In other words, how to keep the neutral-point (NP) potential stable and the ripple supposed [33][34]. If the NP voltage is not effectively controlled, many problems appear; among them: the deviation of the inverter output voltage from its reference, the increase of the voltage THD due to the mismatch between the capacitor voltages, which in turn, leads to the degradation of the inverter performance. Hence, this inverter requires a closed-loop control for currents and DC-link capacitor voltage balancing. Due to its capability to handle multi-objective control problems, MPC is considered an excellent solution that fulfills the control requirements of a three-level NPC inverter. In addition, it is an attractive alternative control

approach for different multilevel inverters due to its high accuracy, fast transient response, and inherent discrete nature. The basic concept of this strategy is based on the discrete-time model of the system to predict the future behavior of the control variables using the available switching states [30]. This strategy relies on the cost function, which embeds the current tracking and the dc-link capacitor voltages error. The optimal switching state that minimizes the cost function is selected and applied to the inverter in the next sampling instant [16][25]. Conventional MPC requires evaluating the cost function for all the switching states of the inverter also the weighting factor must be well-tuned to balance the NP voltage effectively, thus requiring a longer time for the execution process. This, in turn, imposes a high computational burden that consumes a lot of the calculations resources [35], increasing the cost of implementation. Therefore, the high computational burden and multi-objective control have become a challenge for the practical implementation of MPC for multilevel inverter topologies. Authors in [36]–[38] proposed MPC algorithms without weighting factor. The NP voltage balancing is obtained by specialized selective the redundant small voltage vectors and inverter current directions, which saved the computational time compared to the conventional MPC. In all these papers, the MPC algorithms utilize only one switching state corresponding to one voltage vector in every control period, which leads to the variable switching frequency and relatively large ripple in the inverter output current. To solve the issue of variable switching frequency for the MPC method, several strategies have been proposed in the literature to maintain the switching frequency fixed or inside a narrow range. Several modulation strategies, e.g., space vector modulation (SVM) and level-shifted pulse width modulation (PWM), have been reported in the literature [39][40]. The SVM method has more control freedom because the vector selection and pulse generation can be flexibly configured. Considering the extra control flexibility and freedom, SVM is used for the high-frequency inverter to yield a better performance [41]. Furthermore, it has the advantage of allowing simple identification of the redundant states, which can be used to balance the dc-link capacitor voltages [33].

Overall, model predictive control was considered a promising non-linear controller due to its advantages of eliminating PWM block, multi-objective control, and fast dynamic response. However, the variable switching frequency issue was another consideration factor. Furthermore, it suffers from heavy computational burden and cumbersome weighting factors tuning. To suppress these issues, a variant of the MPC method was introduced with an intrinsic modulation scheme named modulated model predictive Control (M^2PC) with the aim of improving the performance of conventional MPC. This method was first proposed by Tarisciotti et al [42]–[44]. Generally, M^2PC has the same prediction and optimization pattern as MPC with

the fixed switching frequency. Many new modulated predictive controls has been presented and applied to several power converter. In [45] and [46], a M^2PC method is proposed for indirect matrix converters and direct matrix converter, respectively, which is capable to produce fixed switching frequency, and improved waveform quality. This technique retains the benefits of the conventional MPC while obtaining minimized current ripples and steady-state error by modulation the switching signals, to improve the quality of current a different number of segments switching pattern is proposed and compared between the conventional MPC.

I.5 Thesis objectives

The aim of this thesis is to elaborate new control strategies based on model predictive control philosophy for three-level NPC inverter. We will illustrate how to implement the model predictive control to improve the performance in terms of power quality, dynamic response, and efficiency of power converters. Thus, the research directions for this thesis consider the following objectives:

- A detail description of the model predictive power control scheme is presented for control three-level NPC inverter.
- Development of model predictive control based on deadbeat control and the selected prediction vectors to reduce the number of prediction vectors and hence the computational burden.
- Development of a second control modulated model predictive control M²PC of the three-level NPC inverter with optimized segment switching pattern. This proposed method fulfills the requirement of a high-performance inverter, constant switching frequency, and enhanced load voltage tracking at a lower sampling rate and, thus, solves the drawbacks of the conventional MPC.
- Finally, the proposed deadbeat predictive and M²PC methods have been applied successfully for the three-level NPC grid-connected photovoltaic generation system.

I.6 Thesis outline

The general introduction of the present chapter discussed power converters types and their applications, and the historical development of model predictive control for power converters. The remaining of the thesis is organized as follows:

- **Chapter II: Deadbeat predictive control for three-level neutral point clamped inverter**

This chapter aims to improve the performance of deadbeat (DB) predictive controller for a three-level neutral point clamped (NPC) inverter. The effect of the number of effective vectors considered for the cost function evaluation on steady-state and dynamic performance is investigated. To do that, three DB predictive controllers with different numbers of effective vectors, namely, 19 vectors-based, 6 vectors-based, and 3 vectors-based DB, are compared beside the conventional current-based model predictive control (MPC). The neutral-point voltage is balanced using the redundant vectors. Simulations and experimental tests are performed to evaluate the performance of the competing MPC algorithms in terms of four main criteria, namely: neutral-point (NP) voltage balancing error, total harmonic distortion (THD), the computational effort required, average switching frequency, power losses, and sensitivity to parameters mismatch.

- **Chapter III: Modulated model predictive control of three-level neutral point clamped inverter**

This chapter presents the modulated model predictive control for three-level NPC inverter, to overcome the disadvantage of the conventional predictive control (C-MPC) approach is typically characterized by a variable switching frequency, a large ripple in the output current, a heavy computational time, and a higher average switching frequency, especially in a three-level neutral point clamped (NPC) inverter. In this chapter, a novel modulated predictive control (M²PC) method is introduced, named higher-segments based M²PC. This proposed method fulfills the requirement of a high-performance inverter, constant switching frequency, and enhanced load voltage tracking at a lower sampling rate and, thus, solves the drawbacks of the conventional MPC. In this chapter, simulations and experimental tests are performed to evaluate the effect of the number of segment switching patterns is experimentally evaluated and compared. Moreover, in these proposed M²PC methods, the redundant positive and negative small voltage vectors are employed in each control cycle with adjusted dwell time calculation to eliminate the imbalance of the neutral-point (NP) voltage.

- **Chapter IV: Comparative study of proposed MPC strategies for three-level NPC grid-connected photovoltaic system**

This chapter presents a comparative study between the predictive controls developed for a 3L-NPC inverter associated with a photovoltaic system. The chapter begins with the modeling of a photovoltaic generator, followed by the application of the Perturb & Observe (P&O) MPPT algorithms, via a DC-DC boost type converter. The performance of the proposed predictive controls 'DBPC, M²PC and conventional MPC' are evaluated based on simulation results.

- **Chapter V: Conclusion and Future Work**

A summary of the contributions of this thesis and the possible future extensions of the research are presented in this chapter.

I.7 Chapter references

[1] K. Bimal, "Energy, Rnvironment and Improtance of Power Electronics," *Recent Res. Environ. Geol. Sci.*, vol. 9, no. 1, pp. 13–28, 2010.

[2] N. Mohan, T. M. Undeland, and W. P. Robbins, *Power Electronics: Converters, Applications, and Design, 3rd Edition*, 3rd ed. John Wiley & Sons, Inc., 2003.

[3] S.N. Manias, *Power Electronics and Motor Drive Systems*. Joe Hayton, 2017.

[4] F. Blaabjerg, Z. Chen, and S. B. Kjaer, "Power Electronics as Efficient Interface in Dispersed Power Generation Systems," *IEEE Trans. Power Electron.*, vol. 19, no. 5, pp. 1184–1194, 2004.

[5] R. Teodorescu, M. Liserre, and P. Rodriguez, *Grid Converters for Photovoltaic and Wind Power Systems*, Wiley–IEEE. New York, NY, USA, 2011.

[6] J. Rodríguez, J. Lai, and F. Z. Peng, "Multilevel Inverters : A Survey of Topologies , Controls , and Applications," *IEEE Trans. Ind. Electron.*, vol. 49, no. 4, pp. 724–738, 2002.

[7] A. Nabae, I. Takahashi, and H. Akagi, "A New Neutral-Point-Clamped PWM Inverter," *IEEE Trans. Ind. Appl.*, vol. IA-17, no. 5, pp. 225–230, 1981.

[8] J. Rodríguez, J. S. Lai, and F. Z. Pen, "Multilevel Inverters : A Survey of Topologies, Controls, and Applications," *IEEE Trans. Ind. Electron.*, vol. 49, no. 4, pp. 724–738, 2002.

[9] S. Daher, J. Schmid, and F. L. M. Antunes, "Multilevel Inverter Topologies for Stand-

Alone PV Systems," *IEEE Trans. Ind. Electron.*, vol. 55, no. 7, pp. 2703–2712, 2008.

[10] K. K. Gupta, A. Ranjan, P. Bhatnagar, L. K. Sahu, and S. Jain, "Multilevel Inverter Topologies with Reduced Device Count: A Review," *IEEE Trans. Power Electron.*, vol. 31, no. 1, pp. 135–151, 2016.

[11] H. Du Toit Mouton, "A new Nonlinear PI / PID Controller for Quadrotor Posture Regulation," *IEEE Trans. Ind. Electron.*, vol. 49, no. 5, pp. 1017–1025, 2002.

[12] M. Malinowski *et al.*, "A Survey on Cascaded Multilevel Inverters," *IEEE Trans. Ind. Electron.*, vol. 57, no. 7, pp. 2197–2206, 2010.

[13] A. K. Koshti and M.N.Rao, "A Brief Review on Multilevel Inverter Topologies," *2017 Int. Conf. Data Manag. Anal. Innov.*, pp. 187–193, 2017.

[14] T. Brückner and D. G. Holmes, "Optimal Pulse-Width Modulation for Three-Level Inverters," *IEEE Trans. Power Electron.*, vol. 20, no. 1, pp. 82–89, 2005.

[15] S. K. Mondal, B. K. Bose, V. Oleschuk, and J. O. P. Pinto, "Space Vector Pulse Width Modulation of Three-Level Inverter Extending Operation Into Overmodulation Region," *IEEE Trans. Power Electron.*, vol. 18, no. 2, pp. 604–611, 2003.

[16] Venkata Yaramasu and B. Wu, *Model Predictive Control of Wind Energy Conversion Systems*. New York, NY, USA: Wiley–IEEE Press, 2017.

[17] K. K. Leung and H. S. Chung, "Dynamic Hysteresis Band Control of the Buck Converter With Fast Transient Response," *IEEE Trans. Circuits Syst.*, vol. 52, no. 7, pp. 398–402, 2005.

[18] K. Kulikowski and A. Sikorski, "New DPC Look-Up Table Methods for Three-Level AC / DC Converter," *IEEE Trans. Ind. Electron.*, vol. 63, no. 12, pp. 7930–7938, 2016.

[19] T. Orłowska-Kowalska, F. Blaabjerg, and R. Jose, "Advanced and Intelligent Control in Power Electronics and Drives.," *Stud. Comput. Intell. Springer, 2014.*, vol. 8, no. 3, pp. 72–72, 2014.

[20] P. Cortes, A. Wilson, S. Kouro, J. Rodriguez, and H. Abu-Rub, "Model Predictive Control of Multilevel Cascaded H-Bridge Inverters," *IEEE Trans. Ind. Electron.*, vol.

57, no. 8, pp. 2691–2699, 2010.

[21] P. Wipasuramonton, Z. Q. Zhu, and D. Howe, "Predictive Current Control with Current Error Correction for PM Brushless AC Drives," *IEEE Trans. Ind. Appl.*, vol. 42, no. 4, pp. 558–564, 2006.

[22] J.M. Maciejowski, "Predictive Control with Constraints," *Int. J. Adapt. Control Signal Process.*, vol. 17, no. 3, pp. 261–262, 2003.

[23] J. Rodriguez *et al.*, "State of the Art of Finite Control Set Model Predictive Control in Power Electronics," *IEEE Trans. Ind. Informatics*, vol. 9, no. 2, pp. 1003–1016, 2013.

[24] P. Cortés, M. P. Kazmierkowski, R. M. Kennel, D. E. Quevedo, and J. Rodríguez, "Predictive Control in Power Electronics and Drives," *IEEE Trans. Ind. Electron.*, vol. 55, no. 12, pp. 4312–4324, 2008.

[25] J. Rodriguez and P. Cortes, *Predictive Control of Power Converters and Electrical Drives*. New York, NY, USA: Wiley–IEEE Press, 2012.

[26] P. Cortés, M. P. Kazmierkowski, R. M. Kennel, D. E. Quevedo, and J. Rodríguez., "Predictive Control in Power Electronics and Drives," *IEEE Trans. Ind. Electron.*, vol. 55, no. 12, pp. 97–100, 2008.

[27] A. Linder, R. Kanchan, R. Kennel, and P. Stolze, "Model-Based Predictive Control of Electric Drives," *Ger. Cuvillier Verlag Göttingen*, no. November 2016, p. 256, 2010.

[28] S. Vazquez, J. Rodriguez, M. Rivera, L. G. Franquelo, and M. Norambuena, "Model Predictive Control for Power Converters and Drives : Advances and Trends," *IEEE Trans. Ind. Electron.*, vol. 64, no. 2, pp. 935–947, 2017.

[29] A. A. Ahmed, B. K. Koh, and Y. Il Lee, "A Comparison of Finite Control Set and Continuous Control Set Model Predictive Control Schemes for Speed Control of Induction Motors," *IEEE Trans. Ind. Informatics*, vol. 14, no. 4, pp. 1334–1346, 2018.

[30] J. D. Barros and J. F. Silva, "Optimal Predictive Control of Three-Phase NPC Multilevel Converter for Power Quality Applications," *IEEE Trans. Ind. Electron.*, vol. 55, no. 10, pp. 3670–3681, 2008.

[31] C. Xia, T. Liu, T. Shi, and Z. Song, "A Simplified Finite-Control-Set Model-Predictive Control for Power Converters," *IEEE Trans. Ind. Informatics*, vol. 10, no. 2, pp. 991–1002, 2014.

[32] J. D. Barros, J. F. A. Silva, and É. G. A. Jesus, "Fast-Predictive Optimal Control of NPC Multilevel Converters," *IEEE Trans. Ind. Electron.*, vol. 60, no. 2, pp. 619–627, 2013.

[33] N. Celanovic and D. Boroyevich, "A Comprehensive Study of Neutral-Point Voltage Balancing Problem in Three-Level Neutral-Point-Clamped Voltage Source PWM Inverters," *IEEE Trans. Power Electron.*, vol. 15, no. 2, pp. 242–249, 2000.

[34] J. Pou, R. Pindado, D. Boroyevich, and P. Rodríguez, "Evaluation of the Low-Frequency Neutral-Point Voltage Oscillations in the Three-Level Inverter," *IEEE Trans. Ind. Electron.*, vol. 52, no. 6, pp. 1582–1588, 2005.

[35] R. Vargas, P. Cortés, U. Ammann, J. Rodríguez, and J. Pontt, "Predictive Control of a Three-Phase Neutral-Point-Clamped Inverter," *IEEE Trans. Ind. Electron.*, vol. 54, no. 5, pp. 2697–2705, 2007.

[36] Y. Yang, H. Wen, M. Fan, M. Xie, and R. Chen, "Fast Finite-Switching-State Model Predictive Control Method Without Weighting Factors for T-Type Three-Level Three-Phase Inverters," *IEEE Trans. Ind. Informatics*, vol. 15, no. 3, pp. 1298–1310, 2019.

[37] A. K. Bonala, S. R. Sandepudi, and V. P. Muddineni, "Selective Finite-States Model Predictive Control of Grid Interfaced Three-Level Neutral Point Clamped Photovoltaic Inverter for Inherent Capacitor Voltage Balancing," *IET Power Electron.*, vol. 11, no. 13, pp. 1–9, 2018.

[38] F. Wang, Z. Li, and Z. Liu, "Model Predictive Control Methods for Three-level Sparse Neutral Point Clamped Inverter," *IEEE J. Emerg. Sel. Top. Power Electron.*, vol. 8, no. 4, pp. 4355–4366, 2019.

[39] B. Wu, *High-Power Converters and AC Drives*. Wiley–IEEE. New York, NY, USA, 2006.

[40] N. Celanovic and D. Boroyevich, "A Fast Space-Vector Modulation Algorithm for Multilevel Three-Phase Converters," *IEEE Trans. Ind. Appl.*, vol. 37, no. 2, pp. 637–

641, 2001.

[41] Y. Jiao, F. C. Lee, and S. Lu, "Space Vector Modulation for Three-Level NPC Converter With Neutral Point Voltage Balance and Switching Loss Reduction," *IEEE Trans. Power Electron.*, vol. 29, no. 10, pp. 5579–5591, 2014.

[42] L. Tarisciotti, P. Zanchetta, A. Watson, S. Bifaretti, and J. C. Clare, "Modulated Model Predictive Control for a Seven-Level Cascaded H-Bridge Back-to-Back Converter," *IEEE Trans. Ind. Electron.*, vol. 61, no. 10, pp. 5375–5383, 2014.

[43] L. Tarisciotti, P. Zanchetta, A. Watson, J. Clare, M. Degano, and S. Bifaretti, "Modulated Model Predictive Control for a Three-Phase Active Rectifier," *IEEE Trans. Ind. Appl.*, vol. 51, no. 2, pp. 1610–1620, 2015.

[44] L. Tarisciotti, P. Zanchetta, A. Watson, P. Wheeler, and S. Bifaretti, "Multiobjective Modulated Model Predictive Control for a Multilevel Solid-State Transformer," *IEEE Trans. Ind. Appl.*, vol. 51, no. 5, pp. 4051–4060, 2015.

[45] L. Tarisciotti, A. Formentini, A. Trentin, P. Zanchetta, P. Wheeler, and M. Rivera, "Modulated Predictive Control for Indirect Matrix Converter," *IEEE Trans. Ind. Appl.*, vol. 53, no. 5, pp. 4644–4654, 2017.

[46] M. Vijayagopal, P. Zanchetta, L. Empringham, L. De Lillo, L. Tarisciotti, and P. Wheeler, "Control of a Direct Matrix Converter with Modulated Model Predictive Control," *IEEE Trans. Ind. Appl.*, vol. 53, no. 3, pp. 2342–2349, 2017.

Chapter II

Deadbeat Predictive Control of Three-Level NPC Inverter

II.1 Introduction

The diode-clamped multilevel inverter employs clamping diodes and cascaded DC capacitors to produce AC voltage waveforms with multiple levels. The multilevel inverter can be generally configured as a three, four, or five-level topology [1][2], but only the three-level inverter, often known as neutral-point clamped (NPC) inverter [3], Compared with the two-level inverter, the three-level NPC inverter owns obvious advantages such as lower harmonics of the output voltages and currents, higher operation voltage and power [4][5]. In addition, they are the most suitable power converters for high-voltage high-power applications [6]–[8]. In this thesis, various aspects of the three-level NPC inverter are discussed, including the inverter topology, operating principle, device commutation, and predictive control methods. The three-level NPC inverter suffers from a basic issue that is represented in how to balance the capacitor voltages. In other words, how to keep the neutral-point (NP) potential stable and the ripple supposed [9][10]. Without NP voltage balancing techniques, due to circuit asymmetries, one of the capacitors charges while the other discharges, needing higher-rated capacitors, and leading to malfunctions such as: the deviation of the inverter output voltage from its reference, and the increase of the voltage THD due to the mismatch between the capacitor voltages, which in turn, leads to the degradation of the inverter performance [11]. Industrial applications also require long-term stability of the neutral point voltage, rather than the elimination of the low-frequency dc voltage ripple. Hence, this inverter requires a closed-loop control for currents and DC-link capacitor voltage balancing [12][13].

Due to its capability to handle multi-objective control problems. For that, Model predictive control (MPC) is considered an excellent solution that fulfills the control requirements of a three-level NPC inverter [14]–[16]. In addition, it is an attractive alternative control approach for different multilevel inverters due to its high accuracy, fast transient response, and inherent discrete nature. The basic concept of this strategy is based on the discrete-time model of the system to predict the future behavior of the control variables using the available switching states [15]. This strategy relies on the cost function, which embeds the current tracking and the DC-link capacitor voltages error. The optimal switching state that minimizes the cost function is selected and applied to the inverter in the next sampling instant [12][17].

Conventional MPC requires evaluating the cost function for all the switching states of the inverter, thus requiring a longer time for the execution process. This, in turn, imposes a high computational burden that consumes a lot of the calculations resources [18], increasing the cost of implementation. Furthermore, the selection of the weighting factor required to maintain NP voltage balancing is an intricate and time-consuming task [19][20]. Therefore, the high computational burden and multi-objective control have become a challenge for the practical implementation of MPC for multilevel inverter topologies [21][22]. For that, to reduce the computational burden the deadbeat (DB) control is used to construct the voltage vector reference [23][24]. Then, the three-level NPC inverter topology is selected and the small redundant voltage vectors are carefully tuned in order to balance the neutral-point (NP) voltage without using the weighting factor [25][26].

This chapter presents the topological structure and mathematical model of the three-level NPC inverter. An overview of conventional model predictive control for this topology is included. In addition, three improved DB predictive controllers are applied to a three-level NPC inverter and investigated their effect on the steady-state performance based on four evaluation criteria, namely: the NP voltage balancing error, the THD of the output voltage and current, the computational burden required, and the average switching frequency. The dynamic performance is evaluated and compared by studying the behavior of the competing controllers under the step-change of the reference current.

II.2 Three-level neutral point clamped (NPC) inverter

II.2.1 Inverter configuration

The simplified circuit diagram of the three-level NPC inverter is shown in Figure II.1, where V_{dc} is the input DC power supply, C is the capacitance of each capacitor, L represents the filter

inductance, R is the load resistance, i_a, i_b, and i_c are the output currents of the inverter, V_{an}, V_{bn}, and V_{cn} represent the output voltages of the inverter, V_P and V_N represent the top and the bottom capacitor voltages of the inverter, respectively. The power circuit of the NPC inverter contains three legs. Each leg consists of four switches denoted by S_{x1}, S_{x2}, S_{x3}, and S_{x4} and two diodes. The midpoint of the two clamping diodes is connected to the midpoint of the two capacitors on the DC-link.

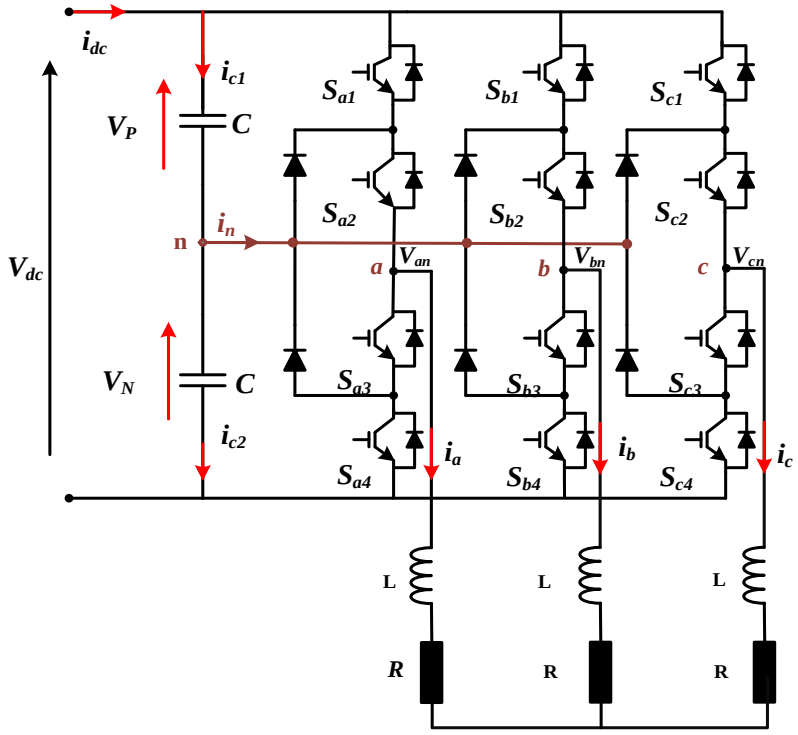

Figure II.1: The power circuit of three level NPC inverter.

II.2.2 Switching state

The switching states of each inverter phase $x \in (a,b,c)$ are summarised in Table II.1. During the switching state [P], both switches S_{a1} and S_{a2} are turned 'ON' while S_{a3} and S_{a4} are 'OFF', and the output voltage is equal to $V_{dc}/2$. As well, the switching state [O] means that the two internal switches S_{a2} and S_{a3} are 'ON' while S_{a1} and S_{a4} are 'OFF', and V_{dc} is clamped to zero. The switching state [N] signifies that the two switches S_{a3} and S_{a4} are turned 'ON' while S_{a1} and S_{a2} are 'OFF', and the output voltage is equal to $-V_{dc}/2$. These switching states generate 19 non-redundant vectors and eight redundant vectors in the $\alpha\beta$ frame. According to their length, these 27 vectors are divided into four groups as shown in Figure II.2. Finally, the 27 voltage vectors with their switching states are summarized in Table II.2.

- Zero vectors (from V_0 to V_2) are represented by three switching states: (OOO), (PPP) and (NNN). The magnitude of these vectors is equal to 0.
- Small vectors (from V_3 to V_{14}). Each small vector has two switching states, one containing P and the other containing N, and therefore can be further classified into P or N type small vector.
- Medium vectors (V_{16}, V_{18}, V_{20}, V_{22}, V_{24}, and V_{26}).
- Large vectors (V_{15}, V_{17}, V_{19}, V_{21}, V_{23}, and V_{25}).

Table II.1: Possible switching combinations of each phase $x = \{a, b, c\}$

S_x	S_{x1}	S_{x2}	S_{x3}	S_{x4}	V_{xn}
P	1	1	0	0	$V_{dc}/2$
O	0	1	1	0	*0*
N	0	0	1	1	$-V_{dc}/2$

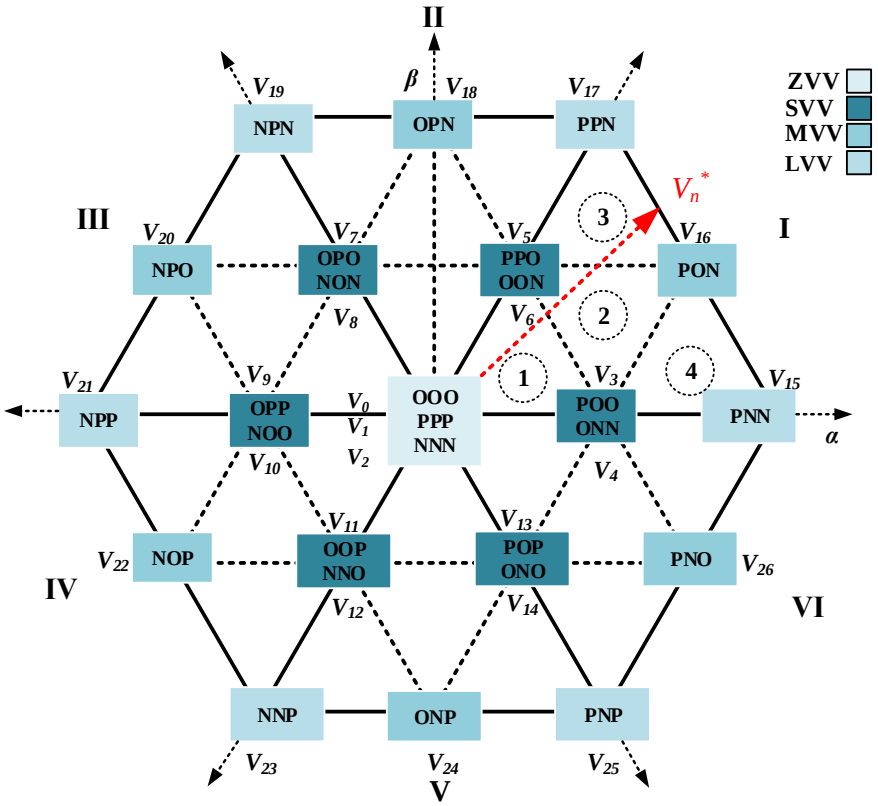

Figure II.2: Basic voltage vectors of three-level NPC inverter: zero voltage vectors (ZVV), small voltage vectors (SVV), medium voltage vectors (MVV), and large voltage vectors (LVV).

Table II.2: The switching states (S_x) and the voltage vectors (V_i) of the three-level NPC inverter

S_a	S_c	S_c	V_i
O	O	O	$V_0=0$
P	P	P	$V_1=0$
N	N	N	$V_2=0$
P	O	O	$V_3= (1/3)V_{dc}$
O	*N*	*N*	$V_4=(1/3)V_{dc}$
P	*P*	*O*	$V_5= (1/6)V_{dc} + j(\sqrt{3}/6)V_{dc}$
O	*O*	*N*	$V_6=(1/6)V_{dc} + j(\sqrt{3}/6)V_{dc}$
O	*P*	*O*	$V_7=(-1/6)V_{dc} + j(\sqrt{3}/6)V_{dc}$
N	*O*	*N*	$V_8=(-1/6)V_{dc} + j(\sqrt{3}/6)V_{dc}$
O	*P*	*P*	$V_9=(-1/3)V_{dc}$
N	*O*	*O*	$V_{10}=(-1/3)V_{dc}$
O	*O*	*P*	$V_{11}=(-1/6)V_{dc} - j(\sqrt{3}/6)V_{dc}$
N	*N*	*O*	$V_{12}=(-1/6)V_{dc} - j(\sqrt{3}/6)V_{dc}$
P	*O*	*P*	$V_{13}=(1/6)V_{dc} - j(\sqrt{3}/6)V_{dc}$
O	*N*	*O*	$V_{14}=(1/6)V_{dc} - j(\sqrt{3}/6)V_{dc}$
P	*N*	*N*	$V_{15}=(2/3)V_{dc}$
P	*O*	*N*	$V_{16}=(1/2)V_{dc} + j(\sqrt{3}/6)V_{dc}$
P	*P*	*N*	$V_{17}=(1/3)V_{dc} + j(\sqrt{3}/3)V_{dc}$
O	*P*	*N*	$V_{18}= j(\sqrt{3}/3)V_{dc}$
N	*P*	*N*	$V_{19}=(-1/3)V_{dc} + j(\sqrt{3}/3)V_{dc}$
N	*P*	*O*	$V_{20}=(-1/2)V_{dc} + j(\sqrt{3}/6)V_{dc}$
N	*P*	*P*	$V_{21}=(-2/3)V_{dc}$
N	*O*	*P*	$V_{22}=(-1/2)V_{dc} - j(\sqrt{3}/6)V_{dc}$
N	*N*	*P*	$V_{23}==(-1/3)V_{dc} -j(\sqrt{3}/3)V_{dc}$
O	*N*	*P*	$V_{24}=- j(\sqrt{3}/3)V_{dc}$
P	*N*	*P*	$V_{25}=(1/3)V_{dc} - j(\sqrt{3}/3)V_{dc}$
P	*N*	*O*	$V_{26}=(1/2)V_{dc} -j(\sqrt{3}/6)V_{dc}$

II.2.3 Discrete-time model of the system

As shown in Figure II.1, the model of the three-level NPC inverter with a three-phase resistive-inductive load is expressed as:

$$\begin{cases} L\dfrac{di_a}{dt} = V_{an} - Ri_a \\ L\dfrac{di_b}{dt} = V_{bn} - Ri_b \\ L\dfrac{di_c}{dt} = V_{cn} - Ri_c \end{cases} \tag{II.1}$$

Applying the Clarke transform, the three-level NPC inverter model in the $\alpha\beta$ stationery frame is expressed as:

$$\begin{cases} L\dfrac{di_\alpha}{dt} = V_{\alpha n} - Ri_\alpha \\ L\dfrac{di_\beta}{dt} = V_{\beta n} - Ri_\beta \end{cases} \tag{II.2}$$

According to the relationship between the DC-link bus voltage and the output switching states of the inverter, the terminal voltage of the inverter can be written as:

$$\begin{cases} V_{an} = V_{dc}(2S_a - S_b - S_c)/6 \\ V_{bn} = V_{dc}(-S_a + 2S_b - S_c)/6 \\ V_{cn} = V_{dc}(-S_a - S_b + 2S_c)/6 \end{cases} \tag{II.3}$$

The equation (II.3) can be transformed into the stationary $\alpha\beta$ reference frame as follows:

$$\begin{cases} V_{\alpha n} = V_{dc}(2S_a - S_b - S_c)/6 \\ V_{\beta n} = \sqrt{3}V_{dc}(S_b - S_c)/6 \end{cases} \tag{II.4}$$

where $V_{\alpha n}$ and $V_{\beta n}$ are the α and β components of the voltage vector, S_a, S_b, and S_c are the switching states of three inverter legs, respectively.The derivative of load current can be replaced by forward-Euler formula as follows:

$$\frac{di(t)}{dt} = \frac{i(k+1) - i(k)}{T_s} \tag{II.5}$$

By using (II.2) and (II.5), the predictive current of the inverter at the $(k + 1)^{th}$ instant can be expressed as follows:

$$\begin{cases} i_\alpha(k+1) = \dfrac{T_s}{L}\left(V_{\alpha n}(k) - Ri_\alpha(k)\right) + i_\alpha(k) \\ i_\beta(k+1) = \dfrac{T_s}{L}\left(V_{\beta n}(k) - Ri_\beta(k)\right) + i_\beta(k) \end{cases} \tag{II.6}$$

where k is the sampling period, i_α and i_β are the measured currents at k^{th} sampling instant.

From Figure II.1, the neutral point current i_n of the three-level three-phase NPC inverter can be calculated by using the combination of the output currents and switching states as follows:

$$i_n = i_{C1} - i_{C2} = -\left(S_{a1} + S_{a4}\right)i_a - \left(S_{b1} + S_{b4}\right)i_b - \left(S_{c1} + S_{c4}\right)i_c \tag{II.7}$$

The capacitor voltages dynamics are described by the capacitor differential equations [16]:

$$\begin{cases} i_{C1} = \dfrac{i_n}{2} = C\dfrac{dV_P}{dt} \\ i_{C2} = -\dfrac{i_n}{2} = C\dfrac{dV_N}{dt} = C\dfrac{d\left(V_{dc} - V_N\right)}{dt} = -C\dfrac{dV_P}{dt} \end{cases} \tag{II.8}$$

Then, the discrete-time model of the DC-link capacitor voltages are obtained by applying the forward Euler approximation as follows:

$$\begin{cases} V_P(k+1) = V_P(k) + \dfrac{1}{C}i_{C1}(k)T_s = V_P(k) + \dfrac{1}{2C}i_n(k)T_s \\ V_N(k+1) = V_N(k) + \dfrac{1}{C}i_{C2}(k)T_s = V_N(k) - \dfrac{1}{2C}i_n(k)T \end{cases} \tag{II.9}$$

II.3 Conventional model predictive control (C-MPC)

Several control strategies have been proposed for the control of power converters. The most recent method is model predictive control. This strategy is based on a prediction of the behavior of the inverter for finite number of possible voltage vector on each sampling interval. The cost function is used to evaluate the voltage vector for the next sampling interval based on the prediction model. The optimal switching state is selected and applied to the inverter during the next sampling period which minimizes the cost function. For the three-level NPC inverter, the conventional MPC scheme has two objectives, the first is to achieve a fast and accurate current

tracking, and the second is to realize the inverter NP voltage balancing by using weighting factors [14][27][28]. Thus, the cost function of the conventional MPC based on the current predictive model is expressed as:

$$g_1(k) = \left|i_\alpha^*(k+1) - i_\alpha(k+1)\right| + \left|i_\beta^*(k+1) - i_\beta(k+1)\right| + \lambda_{dc1}\left|V_P(k+1) - V_N(k+1)\right| \quad \text{(II.10)}$$

where λ_{dc1} is the weighting factor, which sets the relative importance of the phase current tracking and the NP voltage balancing. A high value of this constant implies a high priority for the balance of the capacitors [12]. The output current references in the $\alpha\beta$ reference frame $i_{\alpha\beta}^*(k+1)$ can be obtained from the second-degree Lagrange extrapolation method as follows [29]:

$$\begin{cases} i_\alpha^*(k+1) = 3i_\alpha^*(k) - 3i_\alpha^*(k-1) + i_\alpha^*(k-2) \\ i_\beta^*(k+1) = 3i_\beta^*(k) - 3i_\beta^*(k-1) + i_\beta^*(k-2) \end{cases} \quad \text{(II.11)}$$

From (II.6), (II.9), and (II.10), it can be seen that the selection of an optimal switching state for the three-level-NPC inverter by using conventional MPC requires 27 current predictions, 27 NP voltage predictions, and 27 cost function evaluations. This means that a total of 81 iterations are required in each sampling period, which increases the computational burden. Further, the heuristic selection of the weighting factor required to maintain the relative importance of these multiple control objectives between the current tracking and the NP voltage balancing is an intricate and time-consuming task.

II.4 Deadbeat predictive control

Deadbeat control is one of the most well-known predictive control methods and was proposed in last years [30][31]. A deadbeat predictive control uses a model of the system to calculate the required control variable that cancels the error between the control variable and the reference input [32]. The main advantages of this control scheme are fast dynamic response and the possibility to use any modulation method such as (PWM) or space vector modulation (SVM). This control method provides fast dynamic response than conventional MPC, with a much lower calculation burden because the optimal voltage references are directly calculated without switching state evaluation.

II.4.1 Deadbeat predictive control with weighting factor

The main idea of the voltage-based conventional MPC is to select the voltage vector that makes the predicted current close to its reference. According to (II.6), a new predictive control based on the deadbeat principle is adopted instead of the current control to reduce the computational burden [23][33]. The deadbeat (DB) control is used to construct the voltage vector reference [34]. Assuming that the controller works correctly at the $(k+1)^{th}$ instant so $i^*(k+1)=i(k+1)$, the desired reference voltages in the $\alpha\beta$ reference frame can be obtained as follows:

$$\begin{cases} V_{\alpha n}^*(k) = L\left[i_\alpha^*(k+1) - i_\alpha(k)\right]/T_S + Ri_\alpha(k) \\ V_{\beta n}^*(k) = L\left[i_\beta^*(k+1) - i_\beta(k)\right]/T_S + Ri_\beta(k) \end{cases} \tag{II.12}$$

where $V_{\alpha n}^*(k)$ and $V_{\beta n}^*(k)$ denote, respectively, the α and β components of the reference voltage at the k^{th} instant. The cost function of the MPC based on the reference voltage can be updated as:

$$g_2(k) = \left|V_{\alpha n}^*(k) - V_{\alpha n}(k)\right| + \left|V_{\beta n}^*(k) - V_{\beta n}(k)\right| + \lambda_{dc2}\left|V_P(k+1) - V_N(k+1)\right| \tag{II.13}$$

where λ_{dc2} is the weighting factor based on the DB control, which is used for the NP voltage balancing.

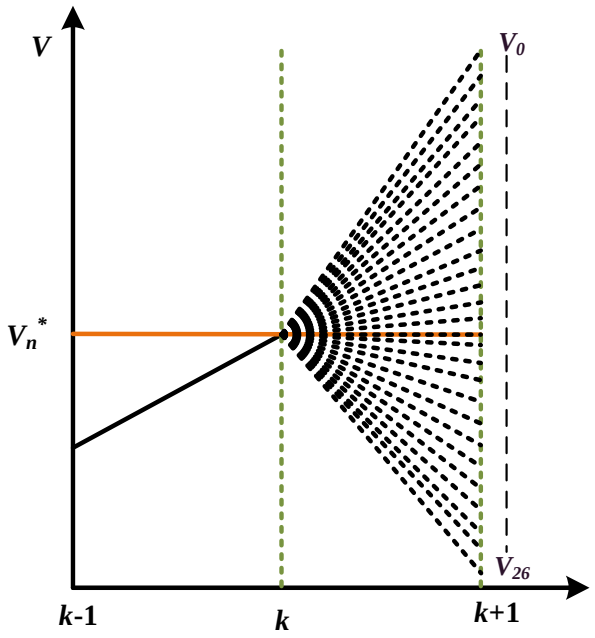

Figure II.3: The candidate voltage vectors using conventional MPC.

From (II.9), (II.12), and (II.13), as shown in Figure II.3 it can be noticed that the predictive control based on the DB control needs only one-cycle to compute the expected reference voltage, 27 NP voltage predictions, and 27 cost function evaluations; thus, a total of 55 iterations are required in each sampling period.

II.4.2 Deadbeat predictive control without weighting factor

The NP imbalance is one of the greatest challenges for the three-level NPC inverter controller design. For the conventional MPC, the weighting factor must be well-tuned to balance the NP voltage effectively. Thus, getting the proper value of the weighting factor is a tedious and time-consuming task. It can be seen in Figure II.2 that there are 12 small vectors and 6 medium vectors in the space vectors. Both medium and small voltage vectors affect the NP voltage fluctuation. The medium vectors charge and discharge the DC-link voltage depending on the polarity of three-phase currents and certainly cause an imbalance in the DC-link voltage. This imbalance can only be compensated by correctly selecting the positive/negative small vectors depending on the direction of i_n and the sign of V_P-V_N. Thus, the new cost function without weighting factors at the k^{th} instant can be expressed as:

$$g_3(k) = \left|V^*_{\alpha n}(k) - V_{\alpha n}(k)\right| + \left|V^*_{\beta n}(k) - V_{\beta n}(k)\right| \tag{II.14}$$

Taking the small vector pair V_3 (POO) and V_4 (ONN) shown in the space vector diagram in Figure II.2 as an example, the corresponding switching states are shown in Figure II.4. This pair of small vectors connect phase-a current to the neutral point *n*. According to this description, it can be concluded that the charge and discharge of the two capacitors depend on the direction of i_n as summarized in Table II.3. As the small vectors are redundant and have an opposite influence on the NP voltage, they are used for the NP voltage balancing. The voltage difference between the two capacitors of the DC-link can be defined as $\Delta V_{PN}=V_P-V_N$, where this latter should be annulled to guarantee the NP voltage balancing. As can be seen in Figure II.4 (a), $i_n=-i_a$ when V_3 (POO) is applied. So when $i_a>0$, V_P is decreased, and V_N is increased, thus making the voltage at the NP increasing. Contrarily, when V_3 (POO) is applied and $i_a<0$, the voltage at the NP decreases as V_P is increased, and V_N is decreased. On the other hand, when the redundant vector V_4 (ONN) is applied, $i_n=i_a$ as shown in Figure II.4 (b). When $i_a>0$, V_P is increased, and V_N is decreased, which makes the NP voltage decreasing. Contrarily, when $i_a<0$, V_P is decreased, and V_N is increased, which makes the NP voltage increasing. Depending on the sign of ΔV_{PN}, the appropriate redundant vector is selected to ensure $\Delta V_{PN}=0$. As an application

example, if $i_a>0$ and $\Delta V_{PN}>0$, V_3 (POO) should be selected to increase the NP voltage and annul ΔV_{PN}, if $i_a>0$ and $\Delta V_{PN}<0$, V_4 (ONN) should be selected in this case to decrease the NP voltage and annul ΔV_{PN}. Hence $\Delta V_{PN}\, i_n<0$ is the necessary condition that should be fulfilled to ensure ΔV_{PN} converges to 0.

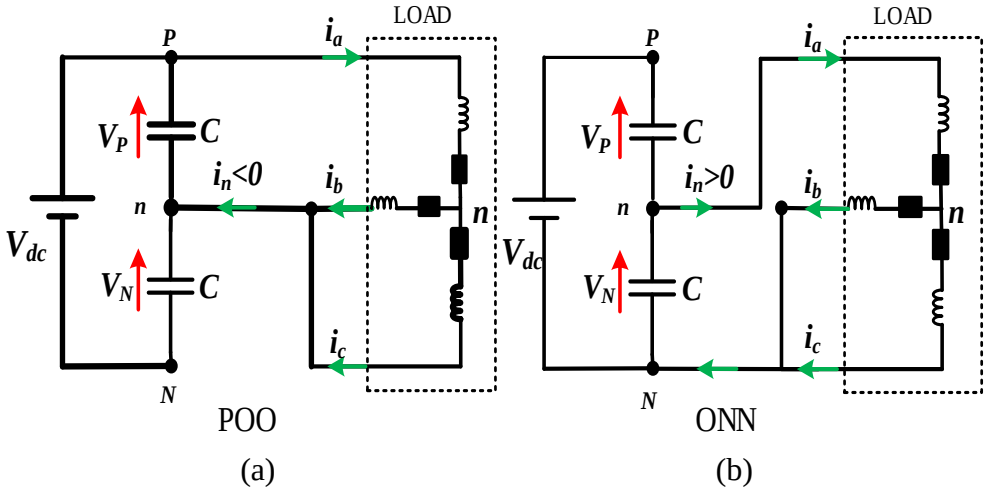

Figure II.4: Effect of different redundant small voltage vectors on the NP voltage. (a) When $i_O<0$. (b) When $i_O>0$.

Table II.3: The neutral point current generated by each vector of three-level NPC inverter

Positive small vectors	i_n	**Negative small vectors**	i_n	**Medium vectors**	I_n
V_4 **(ONN)**	$i_a(k)$	V_3 (POO)	$-i_a(k)$	V_{16} (PON)	$i_b(k)$
V_5 **(PPO)**	$i_c(k)$	V_6 (OON)	$-i_c(k)$	V_{18} (OPN)	$i_a(k)$
V_8 **(NON)**	$i_b(k)$	V_7 (OPO)	$-i_b(k)$	V_{20} (OPO)	$i_c(k)$
V_9 **(OPP)**	$i_a(k)$	V_{10} (NOO)	$-i_a(k)$	V_{22} (NOP)	$i_b(k)$
V_{12} **(NNO)**	$i_c(k)$	V_{11} (OOP)	$-i_c(k)$	V_{24} (ONP)	$i_a(k)$
V_{13} **(POP)**	$i_b(k)$	V_{14} (ONO)	$-i_b(k)$	V_{26} (PNO)	$i_c(k)$

II.4.3 19 Vectors-based DB predictive controller

The NP voltage balance became related to the redundant vectors, as explained in Section II.4.2. Each pair positive/negative small vectors (V_3 *or* V_4), (V_5 *or* V_6), (V_7 *or* V_8), (V_9 *or* V_{10}), (V_{11} *or* V_{12}), and (V_{13} *or* V_{14}) are selected for NP voltage balancing as illustrated in Figure II.5. Furthermore, the 19 vectors-based DB predictive controller requires one reference voltage prediction and 19 cost function evaluations. For that, 20 iterations are required in each sampling period.

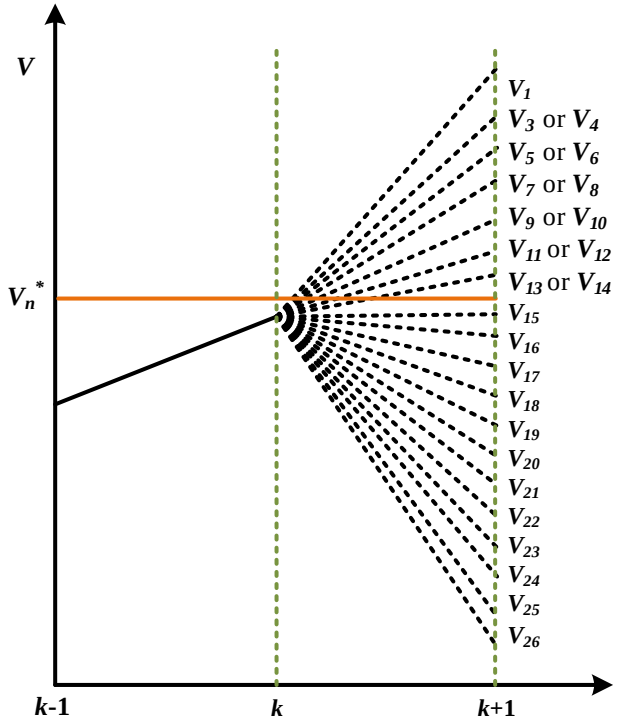

Figure II.5: The candidate voltage vectors using 19 vectors-based DB predictive controller.

II.4.4 6 Vectors-based DB predictive controller

In this method, the sector distribution method is used. 27 voltage vectors are distributed evenly over 6 sectors, where each sector has 6 vectors. Thus, the number of vectors used for the cost function evaluation is reduced to 6 vectors. Figure II.6 is inserted to illustrate the selection procedure of the optimal vector where the reference voltage vector is supposed located in the first sector, i.e., $0 \leq \theta < \pi/3$. According to the description in Section II.4.2, the positive/negative small vectors (V_3 *or* V_4) *and* (V_5 *or* V_6) are selected for the NP voltage balancing. The position of the reference voltage vector θ in the space vector diagram shown in Figure II.6 is given as:

$$\theta = \tan^{-1}\left(\frac{V_{\beta n}^{*}(k)}{V_{\alpha n}^{*}(k)}\right) \tag{II.15}$$

According to θ, the candidate voltage vectors participating in the cost function evaluation was distributed over 6 sectors, as summarized in Table II.4. It can be seen clearly that the 6 vectors-based DB predictive controller requires one reference voltage prediction and 6 cost function evaluations, which requires only 7 iterations in each sampling period.

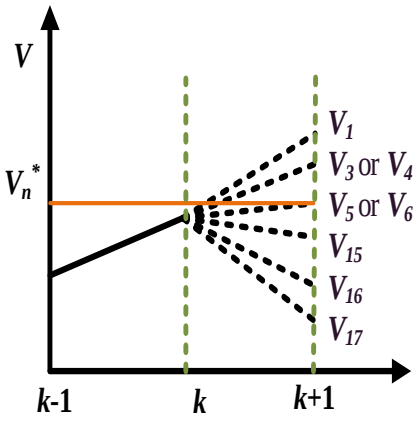

Figure II.6: The candidate voltage vectors using 6 vectors-based DB predictive controller for sector I.

Table II.4: Candidate voltage vectors of 6 vectors-based DB controller for all sectors

Sector	Candidate Voltage Vectors
I: $0 \le \theta < \pi/3$	V_1, (V_3 or V_4), (V_5 or V_6), V_{15}, V_{16}, V_{17}
II: $\pi/3 \le \theta < 2\pi/3$	V_1, (V_5 or V_6), (V_7 or V_8), V_{17}, V_{18}, V_{19}
III: $2\pi/3 \le \theta < \pi$	V_1, (V_7 or V_8), (V_9 or V_{10}), V_{19}, V_{20}, V_{21}
IV: $\pi \le \theta < 4\pi/3$	V_1, (V_9 or V_{10}), (V_{11} or V_{12}), V_{21}, V_{22}, V_{23}
V: $4\pi/3 \le \theta < 5\pi/3$	V_1,(V_{11} or V_{12}), (V_{13} or V_{14}), V_{23}, V_{24}, V_{25}
VI: $5\pi/3 \le \theta < 2\pi$	V_1, (V_{13} or V_{14}), (V_3 or V_4), V_{15}, V_{25}, V_{26}

II.4.5 3 Vectors based DB predictive controller

To further reduce the computational burden, especially the cost function calculation, while effectively maintaining the balance of the capacitor voltages, the voltage vectors were distributed over four regions for each sector. Thus, the number of voltage vectors associated with the cost function evaluation can be reduced to 3 vectors. From Figure II.7, the triangular regions for each sector can be obtained by using the position of the $\alpha\beta$ components of the reference voltage vectors $V_{\alpha n}^*$ and $V_{\beta n}^*$ in the space vector diagram as follows:

$$\begin{cases} V_{\alpha n}^* = m_n \dfrac{2}{\sqrt{3}} \sin\left(\dfrac{\pi}{3} - \left(\theta - (S_n - 1)\dfrac{\pi}{3}\right)\right) \\ V_{\beta n}^* = \dfrac{2}{\sqrt{3}} m_n \sin\left(\theta - (S_n - 1)\dfrac{\pi}{3}\right) \end{cases} \quad \text{(II.16)}$$

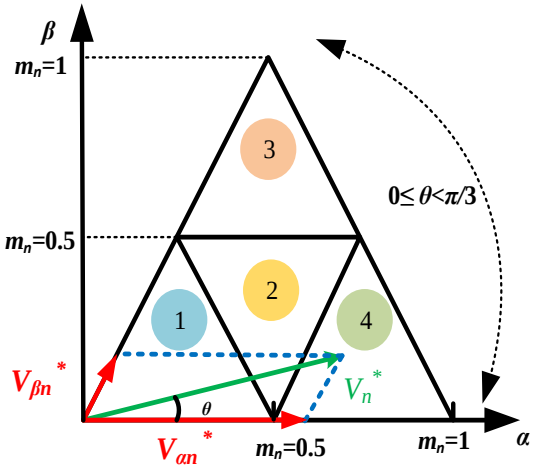

Figure II.7: Triangular regions for sector I.

The values estimated in (II.16) are used to identify the relevant triangle according to the rules given in Table II.5. Where S_n is the sector number, θ is the phase of the reference voltage vector, V_n^* *is* the complex notation of the reference voltage vector $V_n^*=V^*_{\alpha n}+jV^*_{\beta n}$, and m_n is the modulation index [3], which can be expressed as follows:

$$m_n = \sqrt{3}\frac{\left|V_n^*\right|}{V_{dc}} \tag{II.17}$$

In the case of the reference voltage vector located in the fourth region in the first sector, as illustrated in Figure II.8, the small voltage vectors (V_3 *or* V_4) are selected for NP voltage balancing using the principle explained in Section II.4.2. Furthermore, 3 vectors-based DB predictive controller involves one reference voltage prediction and three cost function evaluations. Thus, this algorithm requires only four iterations in each sampling period. Table II.6 lists the candidate voltage vectors for all sectors and regions under different conditions.

Table II.5: Region selection criteria

Regions	**Working Conditions**
1	$V_{\alpha n}^*<0.5m_n$, $V_{\beta n}^*<0.5m_n$, and $V_{\alpha n}^* + V_{\beta n}^* <0.5m_n$
2	$V_{\alpha n}^* <0.5m_n$, $V_{\beta n}^*<0.5m_n$, and $V_{\alpha n}^* + V_{\beta n}^* >0.5m_n$
3	$V_\beta >0.5m_n$
4	$V_\alpha >0.5m_n$

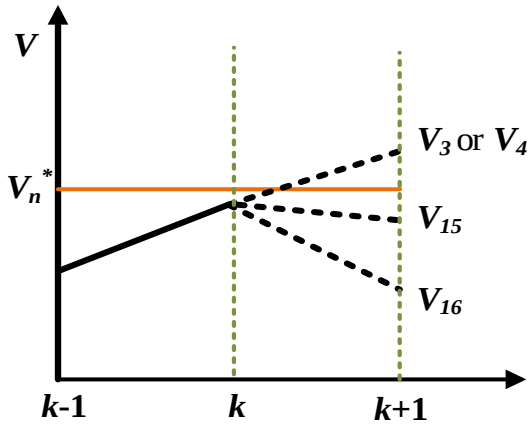

Figure II.8: The candidate voltage vectors using the 3 vectors-based DB predictive controller for sector I, region 4.

Table II.6: Candidate voltage vectors of 3 vectors-based DB predictive controller for all sectors

Sector number	Candidate Voltage Vectors	Sector number	Candidate Voltage Vectors
I-1	(V_3 or V_4), (V_5 or V_6), V_1	IV-1	(V_9 or V_{10}), (V_{11} or V_{12}), V_1
I-2	(V_3 or V_4), (V_5 or V_6), V_{16}	IV-2	(V_9 or V_{10}), (V_{11} or V_{12}), V_{22}
I-3	(V_5 or V_6), V_{16} , V_{17}	IV-3	(V_{11} or V_{12}), V_{22}, V_{23}
I-4	(V_3 or V_4), V_{15} , V_{16}	IV-4	(V_9 or V_{10}), V_{21}, V_{22}
II-1	(V_5 or V_6), (V_7 or V_8), V_1	V-1	(V_{11} or V_{12}), (V_{13} or V_{14}), V_1
II-2	(V_5 or V_6), (V_7 or V_8), V_{18}	V-2	(V_{11} or V_{12}), (V_{13} or V_{14}), V_{24}
II-3	(V_7 or V_8), V_{18}, V_{19}	V-3	(V_{13} or V_{14}), V_{24}, V_{25}
II-4	(V_5 or V_6), V_{17}, V_{18}	V-4	(V_{11} or V_{12}), V_{23}, V_{24}
III-1	(V_7 or V_8), (V_9 or V_{10}), V_1	VI-1	(V_{13} or V_{14}), (V_3 or V_4), V_1
III-2	(V_7 or V_8), (V_9 or V_{10}), V_{20}	VI-2	(V_{13} or V_{14}), (V_3 or V_4), V_{26}
III-3	(V_9 or V_{10}), V_{20}, V_{21}	VI-3	(V_3 or V_4), V_{26}, V_{15}
III-4	(V_7 or V_8), V_{19} , V_{20}	VI-4	(V_{13} or V_{14}), V_{25}, V_{26}

Finally, the voltage-based DB predictive controllers method is more attractive from the computational point of view compared with the conventional MPC method, supporting the feasibility of the real-time implementation. The overall system of the proposed control strategy is shown in Figure II.9.

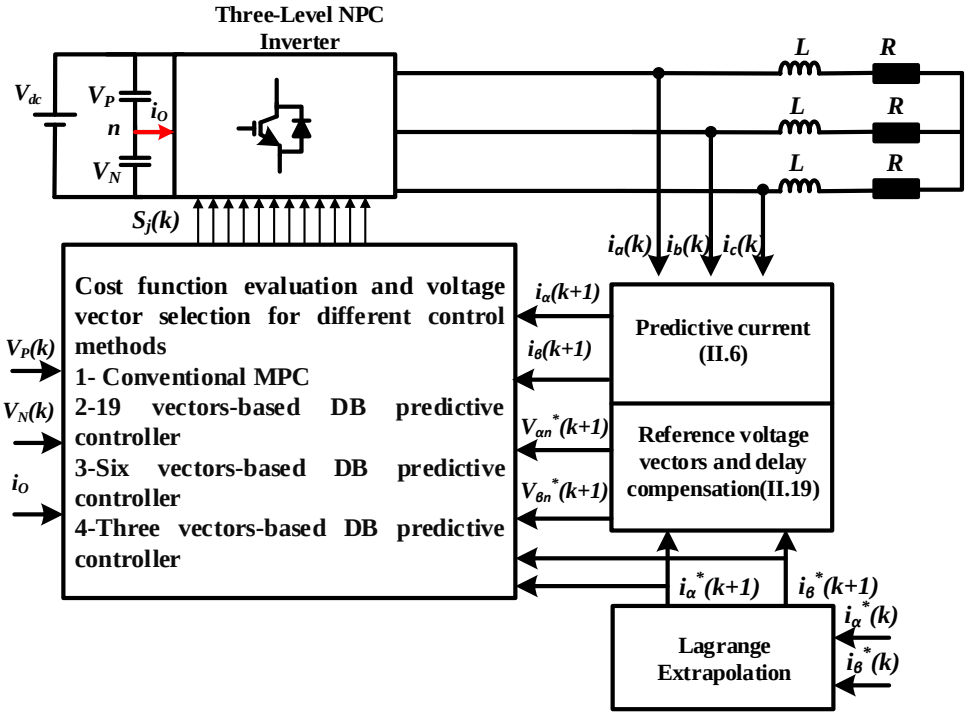

Figure II.9: Block diagram of the studied voltage-based DB predictive controllers.

II.5 Delay time compensation

When control schemes based MPC are implemented experimentally, a large number of calculations are required, introducing a considerable time delay in the actuation. The inherent calculation delay due to the utilization of processors can deteriorate the performance of the system if it is not considered in the controller design [12]. Similar compensation methods have also been proposed for other predictive control schemes such as deadbeat control. Another source of delay in these types of control schemes appears due to the need for future values of the reference variables in the cost function. Usually, the future reference is considered to be the same as the actual reference, which is a good assumption when the reference is a constant value or the sampling frequency is much higher than the frequency of the reference variable. However, during transients and with sinusoidal references, a delay between the controlled and reference variables appears. In order to eliminate this delay, the sampling time should be higher than the computational time of the MPC, so the two-step ahead prediction could be adopted for the delay compensation. This scheme is applied in the conventional MPC and the three voltage-based DB predictive controllers to compensate the calculation delay. Therefore, the discrete-time equation of the model (II.6) and (II.12) is shifted one step forward as follows [35].

$$\begin{cases} i_\alpha(k+2) = \dfrac{T_S}{L}\left(V_{\alpha n}(k+1) - Ri_\alpha(k+1)\right) + i_\alpha(k+1) \\ i_\beta(k+2) = \dfrac{T_S}{L}\left(V_{\beta n}(k+1) - Ri_\beta(k+1)\right) + i_\beta(k+1) \end{cases} \quad \text{(II.18)}$$

$$\begin{cases} V^*_{\alpha n}(k+1) = L\left[i^*_\alpha(k+2) - i_\alpha(k+1)\right]/T_s + Ri_\alpha(k+1) \\ V^*_{\beta n}(k+1) = L\left[i^*_\beta(k+2) - i_\beta(k+1)\right]/T_s + Ri_\beta(k+1) \end{cases} \quad \text{(II.19)}$$

where $i_\alpha^*(k+2)$ and $i_\beta^*(k+2)$ are α and β current references at the $(k+2)^{th}$ instant, respectively. They can be estimated using Lagrange extrapolation method as follows:

$$\begin{cases} i^*_\alpha(k+2) = 6i^*_\alpha(k) - 8i^*_\alpha(k-1) + 3i^*_\alpha(k-2) \\ i^*_\beta(k+2) = 6i^*_\beta(k) - 8i^*_\beta(k-1) + 3i^*_\beta(k-2) \end{cases} \quad \text{(II.20)}$$

The cost functions of the conventional MPC and the three voltage-based DB predictive controllers given in (II.10), (II.13), and (II.14) are updated by (II.21), (II.22), and (II.23), respectively, as follows:

$$g_{N1}(k+1) = \left|i^*_\alpha(k+2) - i_\alpha(k+2)\right| + \left|i^*_\beta(k+2) - i_\beta(k+2)\right| + \lambda_{dc2}\left|V_P(k+1) - V_N(k+1)\right| \quad \text{(II.21)}$$

$$g_{N2}(k+1) = \left|V^*_{\alpha n}(k+1) - V_{\alpha n}(k+1)\right| + \left|V^*_{\beta n}(k+1) - V_{\beta n}(k+1)\right| + \lambda_{dc2}\left|V_P(k+1) - V_N(k+1)\right| \quad \text{(II.22)}$$

$$g_{N3}(k+1) = \left|V^*_{\alpha n}(k+1) - V_{\alpha n}(k+1)\right| + \left|V^*_{\beta n}(k+1) - V_{\beta n}(k+1)\right| \quad \text{(II.23)}$$

II.6 Simulation results

In order to validate the effectiveness of deadbeat predictive control for three-level NPC inverter, the control scheme has been simulated using MATLAB software with the parameters shown in Table A.1. Moreover, to verify the steady-state and the dynamic performance, we perform a comparison between the conventional and the three voltage-based DB predictive controllers with the same parameters. From the results presented in Figure II.10 and Figure II.11, it can be seen clearly that the 3 vectors-based DB controller obtains an accurate current tracking ability with a low THD 1.27 % and low current ripple. Moreover, this simulation clearly demonstrated the ability of the proposed DB controllers algorithms to track reference currents with a fast dynamic response compared to the conventional MPC method.

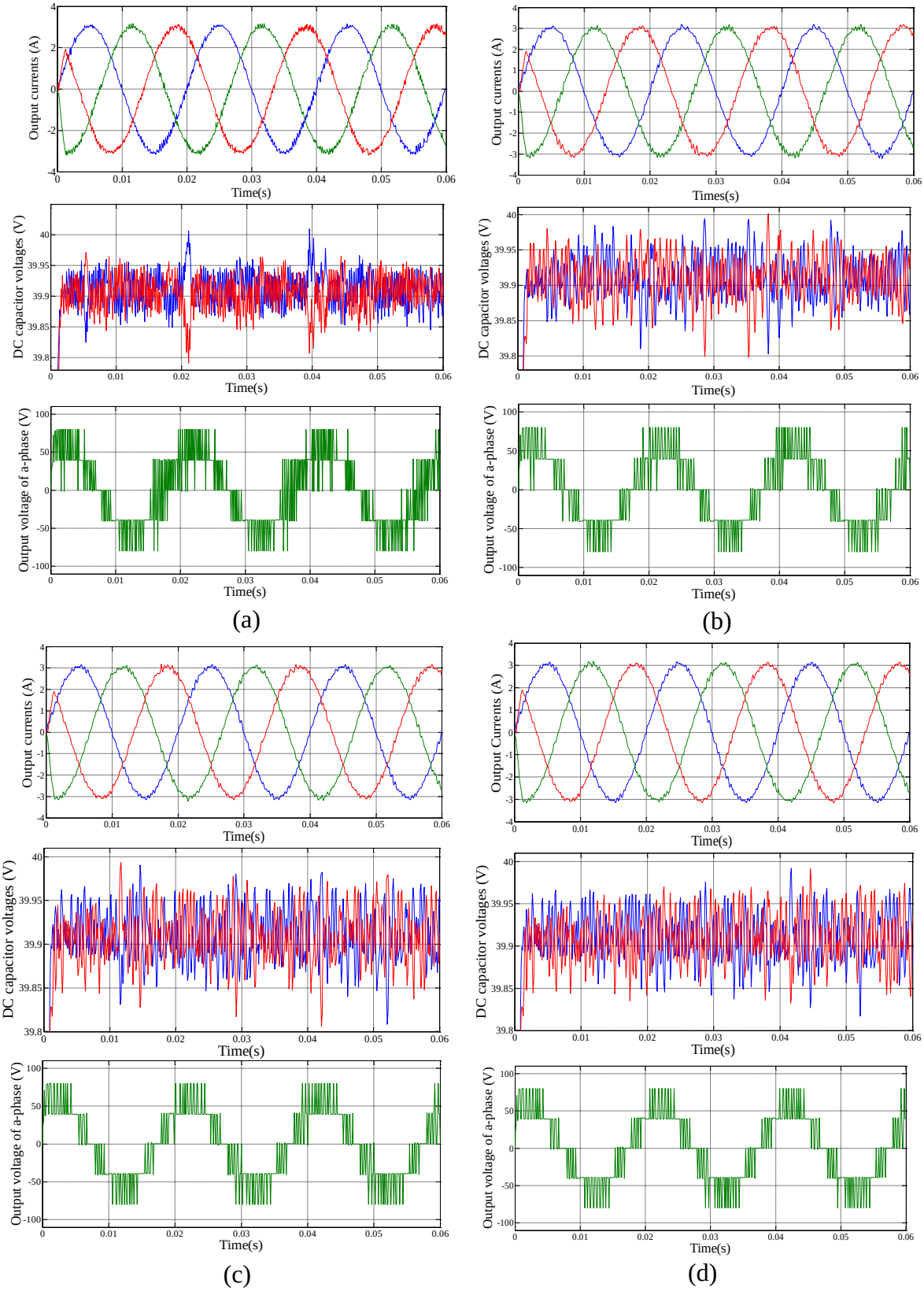

Figure II.10: Simulation results of (a) Conventional MPC. (b) 19 vectors-based DB predictive controller. (c) 6 vectors-based DB predictive controller. (d) 3 vectors-based DB predictive controller.

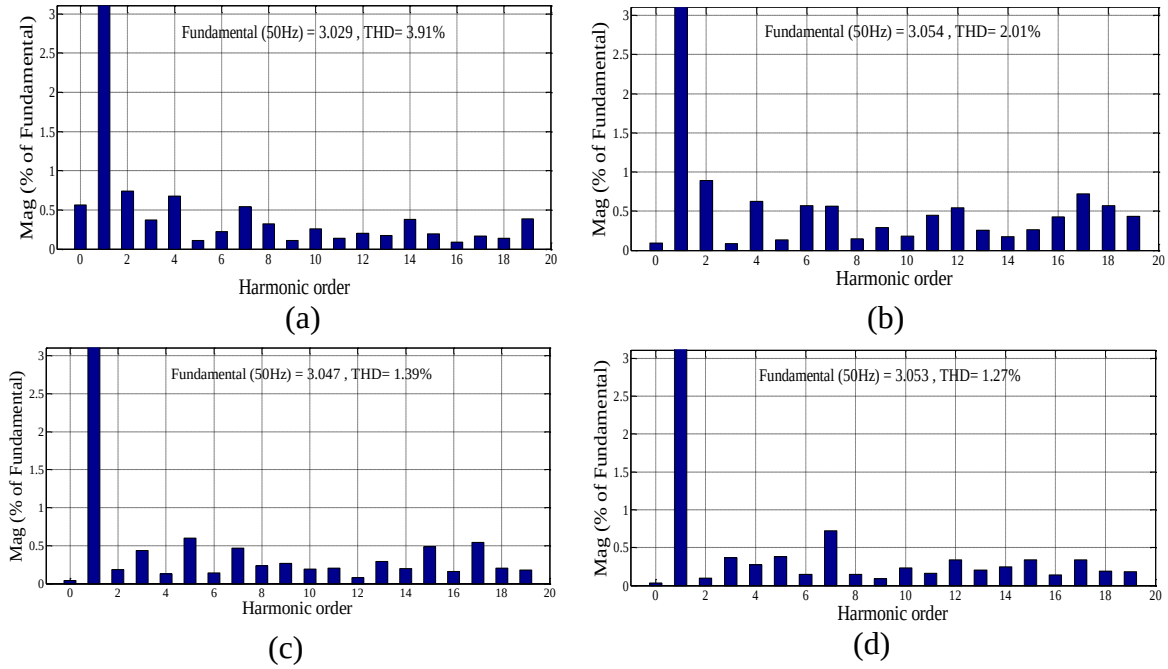

Figure II.11: Harmonics spectrum of phase-a current. (a) Conventional MPC. (b) 19 vectors-based DB predictive controller. (c) 6 vectors-based DB predictive controller. (d) 3 vectors-based DB predictive controller.

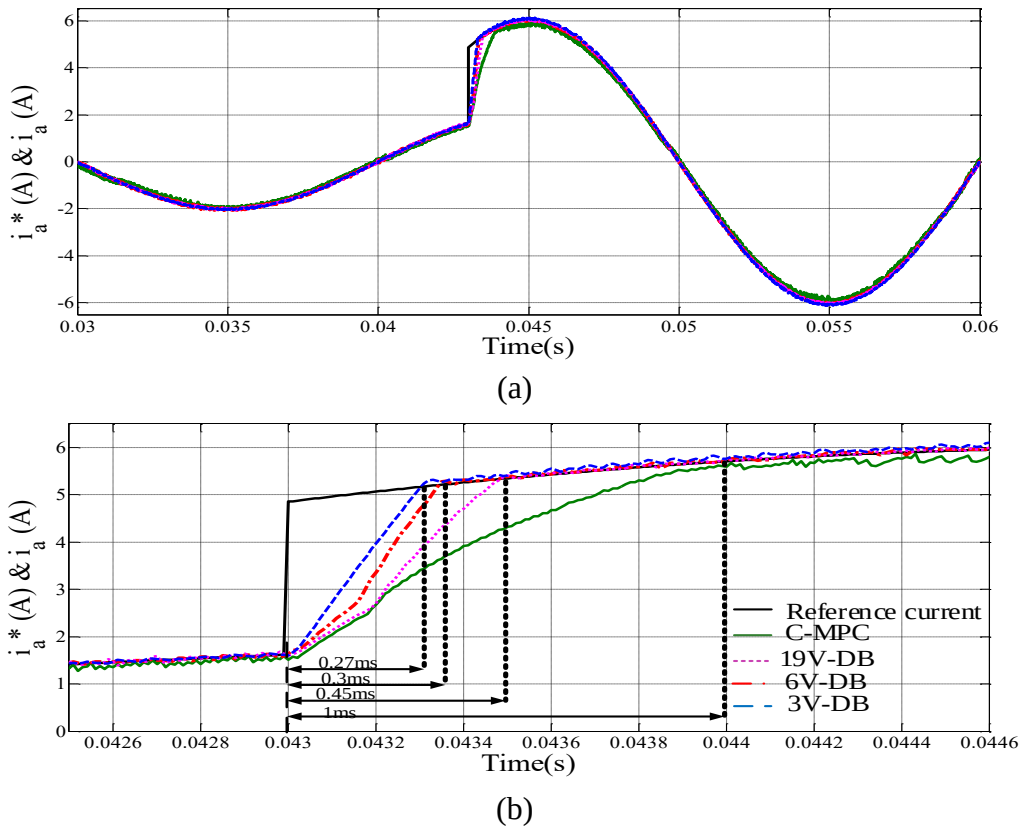

Figure II.12: (a) Simulation dynamic-state performance of competing predictive algorithms. (b) Zoom part of step-change.

For more clarification, simulation tests have been carried to evaluate the dynamic performance of different conventional and improved DB predictive controllers during step change of the reference current from 2A to 6A as shown in Figure II.12. Table II.7 shows the settling time of all computing MPC algorithms. It shows that the 3 vectors-based DB predictive controller has the fastest dynamic response with the lowest settling time (0.27ms) compared to the other algorithms.

From the simulation results presented, it is clear that the 3 vectors-based DB predictive controller method obtains an accurate current tracking ability with a low THD and low current ripple. Moreover, this simulation clearly demonstrated the ability of the proposed 3 vectors-based DB predictive control algorithm to track reference currents with a fast dynamic response.

II.7 Experimental results

The performance of the conventional and the three voltage-based DB predictive controllers applied for the three-level NPC inverter is illustrated also through experimental results. The experimental test bench used includes a three-level NPC inverter powered by a DC power supply feeding an *R-L* load, the parameters of this experiment tests are shown in Table A.1. To validate the performance of the three voltage-based DB predictive controllers, three tests are carried out to evaluate both steady state and dynamic performance of all competing MPC algorithms: Test 1: The amplitude and the frequency of the output reference currents are set as 3 A and *f*=50 Hz, respectively. Test 2: the amplitude of the output reference current is stepped from 1A to 3A, and the reference frequency is kept constant at *f*=50 Hz. Test 3: the amplitude of the reference current is suddenly changed from 3A to 1A, and the frequency is the same as Case 3.

II.7.1 Neutral-point voltage balancing error

In order to investigate the performance of the weighting factor for balancing NP voltage, the conventional MPC method is tested under different weighting factor values to obtain the optimal value of λ_{dc1} for lower NP voltage error ΔV_{PN} and lower THD, the weighting factor is changed from 0.01 to 100 as shown in Figure II.13. From this experimental test, it can be seen that when λ_{dc1} is increasing the conventional MPC method succeeded in maintaining the NP voltage balance, on other hand the THD increased. Notice that the best weighting factor value is 1 for NP voltage balancing and lower THD value. Through this test, the weighting factor for NP voltage balancing is finally set as λ_{dc1}=1 for the conventional MPC.

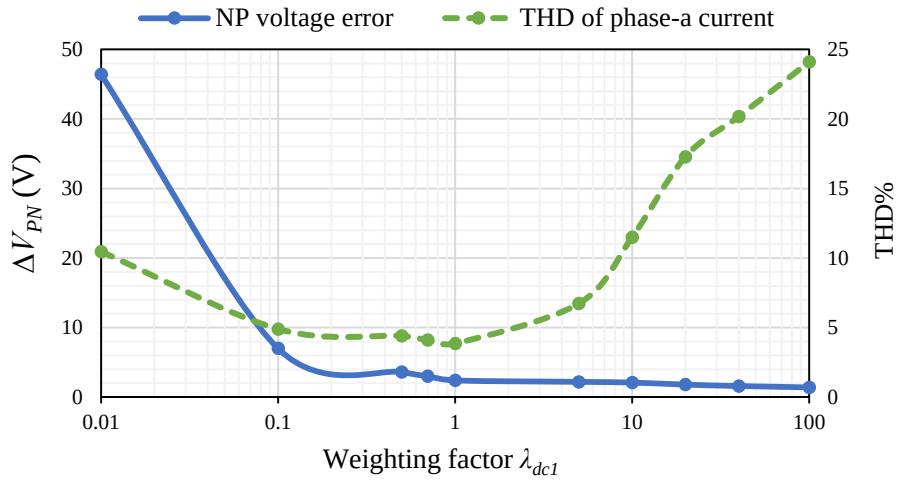

Figure II.13: Experimental results of the THD of phase-a current and the NP voltage error with different weighting factor values.

II.7.2 Steady-state performance

The performance of the conventional MPC and the improved DB predictive controllers are compared for steady-state operation of the three-level NPC inverter. In this test, the weighting factor for NP voltage balancing is fixed as λ_{dc1}=1 for the conventional MPC. Figure II.14 shows the experimental waveforms of the inverter output currents i_a, i_b, and i_c, the line-to-line voltage V_{ab}, the capacitor voltages V_P and V_N, and the harmonic spectrum of phase-a current for conventional and the three voltage-based DB predictive controllers under Test 1. From the experimental results, notice that the conventional MPC and the three voltage-based DB predictive controllers can effectively regulate the NP voltage and the fluctuation is lower than 1V.

Figure II.14 (a) illustrates the experimental waveforms of the conventional MPC method. Notice that the output currents keep tracking the sinusoidal form with high ripples. On the other hand, as depicted in Figure II.14 (b)–(d), it can be seen that the three improved DB predictive controllers have achieved accurate tracking of the given currents with better quality and lower ripples without using the weighting factor. Furthermore, according to the measured THDs of output currents shown in Table II.7, it can be seen that the conventional MPC has a high distortion of THD=3.886%. In contrast, the 3 vectors-based DB predictive controller owns the best output current quality with a low distortion of THD=1.081% compared to the other improved DB predictive controllers. The current THD in the three vectors-based DB predictive controller is reduced by nearly 72% compared with conventional MPC.

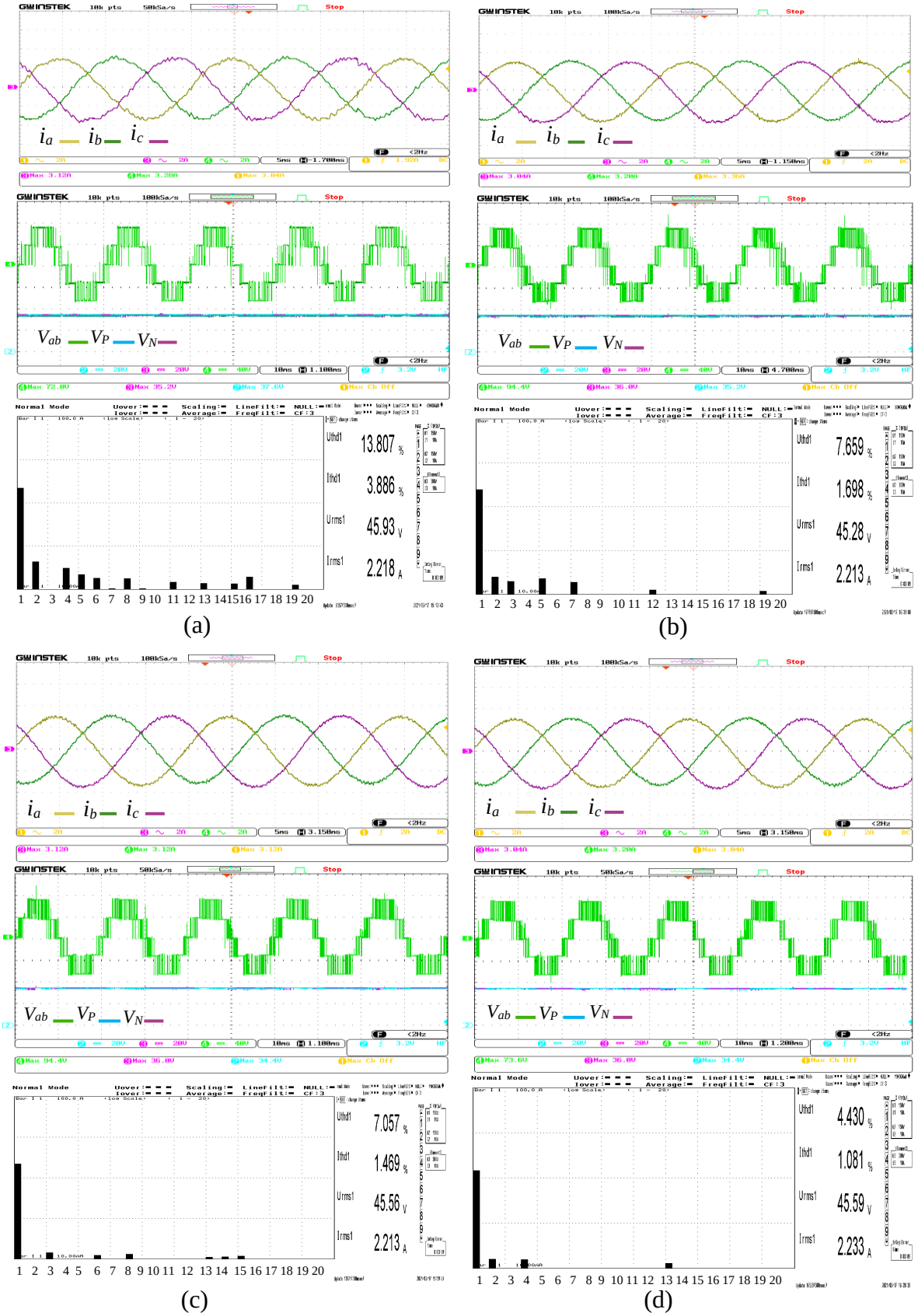

Figure II.14: Steady-state experimental waveforms with harmonics spectrum of phase a current for Test 1. (a) Conventional MPC. (b) 19 vectors-based DB predictive controller. (c) 6 vectors-based DB predictive controller. (d) 3 vectors-based DB predictive controller.

II.7.3 Computational burden required

For all predictive algorithms, the interruption time is set to be the same, i.e., all algorithms are executed with a sampling time of 100μs. The computational burden required by the competing MPC algorithms are given as 92μs for the conventional MPC, 56μs for 19 vectors-based DB predictive controller, 41μs for 6 vectors-based DB predictive controller, and only 36μs for 3 vectors-based DB predictive controller. As shown in Table II.7, it can be observed that the execution time of the 3 vectors-based DB predictive controller is reduced by nearly 60%, which greatly reduces the computational burden compared with conventional MPC.

II.7.4 Average switching frequency

The average switching frequency is adopted for a fair comparison of the competing MPC algorithms. The average switching frequency is the number of switching cycles per unit of time [36]. It can be expressed as:

$$f_{sw} = \frac{n_{sw}}{12T_s} \tag{II.24}$$

where n_{sw} is the total number of switching cycles over the duration T_s and 12 is the total number of switches in the inverter. As can be observed in Table II.7, the average switching frequency of the 3 vectors-based DB predictive controller is the lowest (f=1.8 kHz) compared to the other MPC algorithms.

II.7.5 Dynamic performance

To investigate the transient behavior of the competing MPC algorithms, the conventional and the improved DB predictive controllers are analyzed under different test conditions (Test 2 and Test 3). Figure II.15 displays the experimental waveforms of the phase-a current i_a, line-to-line voltage V_{ab}, and the capacitor voltages (V_P and V_N).

In this experiment, it can be seen that the deadbeat predictive controllers own good dynamic performance for different dynamic conditions with the current reference suddenly increased or decreased. Furthermore, the deadbeat predictive controllers own very similar dynamic performance with a quick response without affecting the normal operation of the system. A synchronized output current is always well obtained.

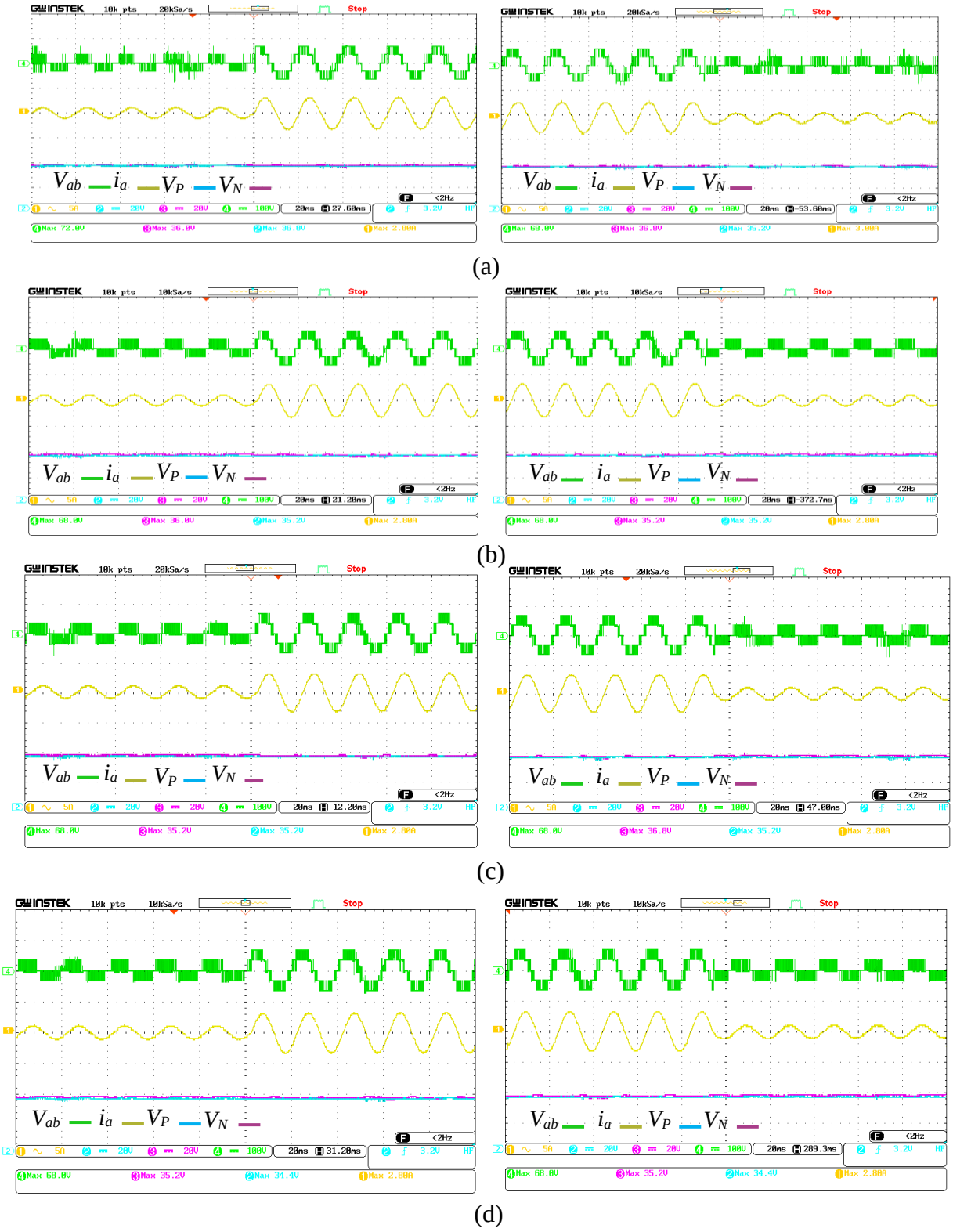

Figure II.15: Dynamic experimental waveforms for Test 2 and Test 3. (a) Conventional MPC. (b) 19 vectors-based DB predictive controller. (c) 6 vectors-based DB predictive controller. (d) 3 vectors-based DB predictive controller.

Table II.7: Comparative study between the competing predictive algorithms

Controller	Average switching frequency	Computational burden	THD	Dynamic response
Conventional MPC	2.4kHz	92µs	3.886%	1ms
19V-DB	2kHz	56µs	1.698%	0.45ms
6V-DB	1.9kHz	41µs	1.469%	0.3ms
3V-DB	1.8kHz	36µs	1.081%	0.27ms

II.8 Parameter sensitivity test

The conventional MPC and the DB predictive controller are dependent on the exact parameters of the *R-L* filter model. Any parameter mismatch in the model would make the calculated of voltage reference deviate from its optimal value. This means that both methods in their basic implementation are sensitive to variations in the load parameters. In this test, the parameter sensitivity of the improved DB predictive controllers is analyzed and compared to the parameter sensitivity of the conventional MPC for a three-level NPC inverter. The effects of variations in the controller parameters R and L were analyzed using simulation studies, which are investigated by changing the electric-circuit parameters in the algorithms within the range from−50% to +50% of their nominal values. It was concluded that the most significant effect in the control performance is produced when the inductance L is misidentified by the control system. For more clarification, seven points are taken into account within the established range. For simplicity purposes, only one parameter is varied at a time. The root mean square (RMS) value and THD of the output current are selected as the performance indicator.

The RMS current error is chosen because it is suitable for evaluating how exactly the real current follows the reference current instantaneously. It can be calculated as follow:

$$RMS_i = \sqrt{\frac{\int_{T_i}^{T_f} \left(i^*(t) - i(t)\right)^2 dt}{T_f - T_i}} \tag{II.25}$$

where $i^*(t)$ is the reference current and $i(t)$ is the measured current. T_f and T_i are the higher and lower boundaries for the time interval chosen, respectively.

The variations in the RMS current error of phase-a and the THD of the output current phase-a for *L* variation are shown in Figure II.16 (a) and (b). Notice that, the three voltage-based DB predictive controllers outperform the conventional MPC. As expected, the worst performance THD and RMS error of output current were obtained with the conventional MPC. Otherwise, it can be clearly seen that the 6 and 3 vectors-based DB predictive controllers almost identical THD and RMS error, thus means the conventional MPC has the highest parameter sensitivity compared to the improved DB predictive controllers.

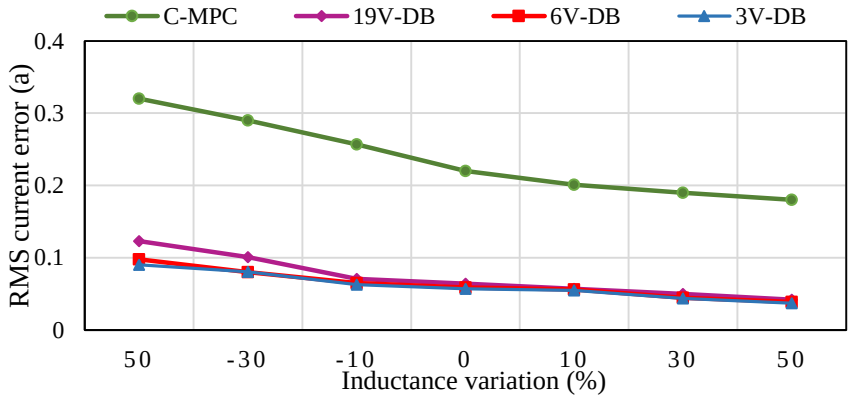

(a)

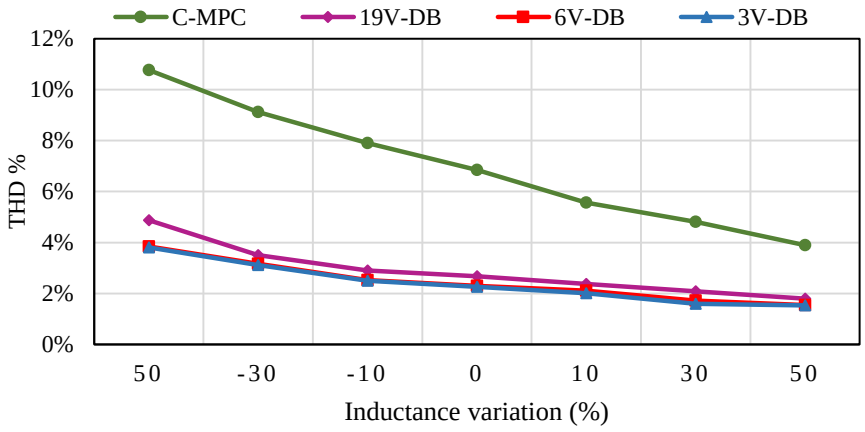

(b)

Figure II.16: Sensitivity of the conventional MPC and three voltage-based DB predictive controllers with different inductor arm variations. (a) RMS current error. (b) THD %.

II.9 Power loss analysis

Figure II.17 shows power losses analysis as a function of different load types (R_1=10Ω, R_2=100Ω, L_1=10mH, L_2=100mH). It can be seen during the parameter mismatch that the 6 and 3 vectors-based DB predictive controllers show the lowest power losses, while the 19 vectors-

based DB predictive controllers and the conventional MPC show the most considerable power losses. Moreover, from the power losses analysis results, it can be observed that the switching losses have small values in MOSFETs and zero in diodes (P_{d_sw}=0) for the conventional MPC and the three voltage-based DB predictive controllers because of the use of SiC MOSFETs and DIODEs high-performance characteristics.

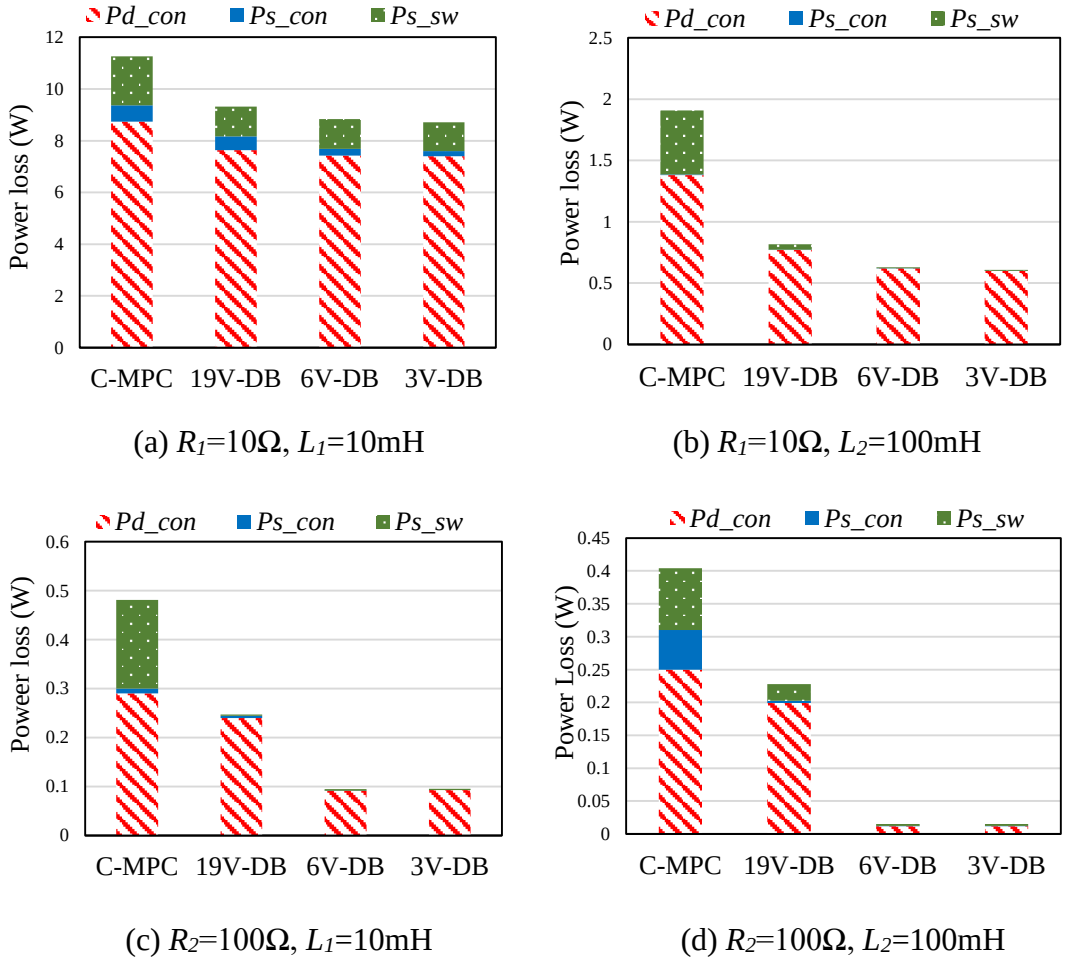

Figure II.17: Power losses distribution of semiconductor devices versus various load types (*R-L*) for conventional MPC and three voltage-based DB predictive controllers.

II.10 Conclusion

In this Chapter, three improved DB predictive controllers applied to a three-level NPC inverter are investigated. A comprehensive comparison study of the improved DB predictive controllers with the conventional MPC has been conducted in terms of computational burden, current THD, NP voltage balancing, average switching frequency, and dynamic response. Some conclusions can be summarized as follows: 1) The conventional MPC method suffers from a long computation burden and tedious tuning of weighting factors. It also can be observed that

the THD of the injecting currents is 3.886%. 2) The improved DB predictive controllers eliminate the weighting factors for balancing the NP voltage and takes full play of utilizing the negative and positive small voltage vectors to balance the NP voltage, which simplifies the control implementation. 3) Compared with the three improved DB algorithms, the number of voltage vectors involved in the predictive model and cost function evaluation is reduced to three, which simplifying the control implementation. By using the 3 vectors-based DB predictive controller, it can be seen that the execution time is reduced by nearly 60% compared with the other two algorithms, which significantly reduces the computational resources for implementation. 4) The improved DB predictive controllers show less sensitivity concerning the mismatch in the filter inductance and have the lowest power losses than conventional MPC methods.

The evaluation results show that all three enhanced DB predictive controllers have a fast dynamic response and good balancing of the NP voltage without using the weighting factor. The 3 vectors-based DB predictive controller is the best in the output current quality of the inverter, low computational burden, less average switching frequency, and has the lowest THD value (1.081%). Both 6 and 3 vector-based DB predictive controllers show the lowest power losses.

II.11 Chapter references

[1] N. S. Choi, J. G. Cho, and G. H. Cho, "A General Circuit Topology of Multilevel Inverter," *PESC '91 Rec. 22nd Annu. IEEE Power Electron. Spec. Conf.*

[2] F. Z. Peng, "A Generalized Multilevel Inverter Topology with Self Voltage Balancing," *IEEE Trans. Ind. Appl.*, vol. 37, no. 2, pp. 611–618, 2001.

[3] B. Wu, *High-Power Converters and AC Drives*. Wiley–IEEE. New York, NY, USA, 2006.

[4] N. Yousefpoor, S. H. Fathi, N. Farokhnia, S. Member, and H. A. Abyaneh, "THD Minimization Applied Directly on the Line-to-Line Voltage of Multilevel Inverters," *IEEE Trans. Ind. Electron.*, vol. 59, no. 1, pp. 373–380, 2012.

[5] D. Floricau, E. Floricau, and G. Gateau, "New Multilevel Converters With Coupled Inductors : Properties and Control," *IEEE Trans. Ind. Electron.*, vol. 58, no. 12, pp. 5344–5351, 2011.

[6] Z. Du, L. M. Tolbert, and J. N. Chiasson, "Reduced Switching Frequency Computed PWM Method for Multilevel Converter Control," *Proc. IEEE 36th Annu. PESC, Recife, Brazil, Jun. 2005, pp. 2560–2564.*, no. July, 2005.

[7] Y. Xiong, D. Chen, X. Yang, C. Hu, and Z. Zhang, "Analysis and Experimentation of A New Three-phase Multilevel Current-Source Inverter Yu," *Proc. IEEE 35th Annu. PESC, Aachen, Ger. Jun. 2004, pp. 548–551.*, pp. 4–7, 2004.

[8] P. Correa, M. Pacas, and J. Rodríguez, "Predictive Torque Control for Inverter-Fed Induction Machines," *IEEE Trans. Ind. Electron.*, vol. 54, no. 2, pp. 1073–1079, 2007.

[9] N. Celanovic and D. Boroyevich, "A Comprehensive Study of Neutral-Point Voltage Balancing Problem in Three-Level Neutral-Point-Clamped Voltage Source PWM Inverters," *IEEE Trans. Power Electron.*, vol. 15, no. 2, pp. 242–249, 2000.

[10] J. Pou, R. Pindado, D. Boroyevich, and P. Rodríguez, "Evaluation of the Low-Frequency Neutral-Point Voltage Oscillations in the Three-Level Inverter," *IEEE Trans. Ind. Electron.*, vol. 52, no. 6, pp. 1582–1588, 2005.

[11] L. Lin, Y. Zou, Z. Wang, and H. Jin, "Modeling and Control of Neutral-Point Voltage Balancing Problem in Three-Level NPC PWM Inverters," *2005 IEEE 36th Power Electron. Spec. Conf.*, pp. 861–866, 2005.

[12] J. Rodriguez and P. Cortes, *Predictive Control of Power Converters and Electrical Drives*. New York, NY, USA: Wiley–IEEE Press, 2012.

[13] V. Yaramasu and B. Wu, *Model Predictive Control of Wind Energy Conversion Systems*. New York, NY, USA: Wiley–IEEE Press, 2017.

[14] R. Vargas, P. Cortés, U. Ammann, J. Rodríguez, and J. Pontt, "Predictive Control of a Three-Phase Neutral-point-clamped Inverter," *IEEE Trans. Ind. Electron.*, vol. 54, no. 5, pp. 2697–2705, 2007.

[15] J. D. Barros and J. F. Silva, "Optimal Predictive Control of Three-Phase NPC Multilevel Converter for Power Quality Applications," *IEEE Trans. Ind. Electron.*, vol. 55, no. 10, pp. 3670–3681, 2008.

[16] A. Calle-Prado, S. Alepuz, J. Bordonau, J. Nicolas-Apruzzese, P. Cortés, and J.

Rodriguez, "Model Predictive Current Control of Grid- Connected Neutral-Point Clamped Converters to Meet Low Voltage Ride-Through Requirements," *IEEE Trans. Ind. Electron.*, vol. 62, no. 3, pp. 1503–1514, 2015.

[17] Soumya Ranjan Mohapatra and V. Agarwal, "Model Predictive Controller with Reduced Complexity for Grid Tied Multilevel Inverters," *IEEE Trans. Ind. Electron.*, vol. 66, no. 11, pp. 8851–8855, 2019.

[18] R. Vargas, P. Cortés, U. Ammann, J. Rodríguez, and J. Pontt, "Predictive Control of a Three-Phase Neutral-Point-Clamped Inverter," *IEEE Trans. Ind. Electron.*, vol. 54, no. 5, pp. 2697–2705, 2007.

[19] C. A. Rojas, J. Rodríguez, F. Villarroel, J. R. Espinoza, C. A. Silva, and M. Trincado, "Weighting Factors," *IEEE Trans. Ind. Electron.*, vol. 60, no. 2, pp. 681–690, 2013.

[20] Y. Xu, Y. He, and S. Li, "Logical Operation-Based Model Predictive Control for Quasi-Z-Source Inverter," *IEEE J. Emerg. Sel. Top. Power Electron.*, vol. 9, no. 1, pp. 1039–1051, 2021.

[21] X. Xing and H. Chen, "A Fast-Processing Predictive Control Strategy for Common Mode Voltage Reduction in Parallel," *IEEE J. Emerg. Sel. Top. Power Electron.*, vol. 9, no. 1, pp. 316–326, 2019.

[22] J. Rodriguez *et al.*, "State of the Art of Finite Control Set Model Predictive Control in Power Electronics," *IEEE Trans. Ind. Informatics*, vol. 9, no. 2, pp. 1003–1016, 2013.

[23] J. D. Barros, J. F. A. Silva, and É. G. A. Jesus, "Fast-Predictive Optimal Control of NPC Multilevel Converters," *IEEE Trans. Ind. Electron.*, vol. 60, no. 2, pp. 619–627, 2013.

[24] C. Xia, T. Liu, T. Shi, and Z. Song, "A Simplified Finite-Control-Set Model-Predictive Control for Power Converters," *IEEE Trans. Ind. Informatics*, vol. 10, no. 2, pp. 991–1002, 2014.

[25] X. Xing, X. Li, F. Gao, C. Qin, and C. Zhang, "Improved Space Vector Modulation Technique for Neutral-Point Voltage Oscillation and Common-Mode Voltage Reduction in Three-Level Inverter," *IEEE Trans. Power Electron.*, vol. 34, no. 9, pp. 8697–8714, 2019.

[26] F. Wang, Z. Li, and Z. Liu, "Model Predictive Control Methods for Three-level Sparse Neutral Point Clamped Inverter," *IEEE J. Emerg. Sel. Top. Power Electron.*, vol. 8, no. 4, pp. 4355–4366, 2020.

[27] R. Vargas, P. Cortés, U. Ammann, J. Rodríguez, and J. Pontt, "Predictive Control of a Three-Phase Neutral-Point-Clamped Inverter," *IEEE Trans. Ind. Electron.*, vol. 54, no. 5, pp. 2697–2705, 2007.

[28] N. Bekhoucha, N. Mesbahi, and S. Ouchen, "Predictive Current Control of Three Level Neutral Point Clamped Grid Connected Inverter in Photovoltaic Generation Systems," *Int. Conf. Electr. Sci. Technol. Maghreb, Cist. 2018*, pp. 1–6, 2019.

[29] M. Odavic, V. Biagini, P. Zanchetta, M. Sumner, and M. Degano, "One-Sample-Period-Ahead Predictive Current Control for High-Performance Active Funt Power Filters," *IET Power Electron.*, vol. 4, no. 4, pp. 414–423, 2011.

[30] S. Park, F. Kang, M. H. Lee, and C. Kim, "A New Single-Phase Five-Level PWM Inverter Employing a Deadbeat Control Scheme," *IEEE Trans. POWER Electron.*, vol. 18, no. 3, pp. 831–843, 2003.

[31] O. Kukrer, "Deadbeat Control of a Three-Phase Verter with an Output LC Filter," *IEEE Trans. Power Electron.*, vol. 11, no. 1, pp. 16–23, 1996.

[32] X. Zhang, B. Hou, and Y. Mei, "Deadbeat Predictive Current Control of Permanent-Magnet Synchronous Motors with Stator Current and Disturbance Observer," *IEEE Trans. Power Electron.*, vol. 32, no. 5, pp. 3818–3834, 2017.

[33] X. Wang, W. Xu, Y. Zhao, and X. Li, "Modified MPC Algorithm for NPC Inverter Fed Disc Coreless Permanent Magnet Synchronous Motor," *IEEE Trans. Appl. Supercond.*, vol. 26, no. 7, 2016.

[34] N. Bekhoucha, M. Kermadi, N. Mesbahi, and S. Mekhilef, "Performance Investigation of Deadbeat Predictive Controllers for Three-Level Neutral Point Clamped Inverter," *IEEE J. Emerg. Sel. Top. Power Electron.*, vol. 10, no. 1, pp. 1165–1177, 2022.

[35] P. Cortes, J. Rodriguez, C. Silva, and A. Flores, "Delay Compensation in Model Predictive Current Control of a Three-Phase Inverter," *IEEE Trans. Ind. Electron.*, vol.

59, no. 2, pp. 2011–2013, 2012.

[36] Y. Yang, H. Wen, M. Fan, M. Xie, R. Chen, and Y. Wang, "A Constant Switching Frequency Model Predictive Control Without Weighting Factors for T-Type Single-Phase Three-Level Inverters," *IEEE Trans. Ind. Electron.*, vol. 66, no. 7, pp. 5153–5164, 2019.

Chapter III

Modulated Model Predictive Control of Three-Level NPC Inverter

III.1 Introduction

The MPC was considered as an alternative control scheme due to its fast dynamic response, simple inclusion of nonlinearities and constraints, multivariable control using a single control loop, etc. However, the inherent variable switching frequency is another issue that needs careful consideration, for the conventional model predictive control (C-MPC); only one voltage vector is utilized in each control cycle, which leads to the variable switching frequency for the inverter output. Furthermore, it suffers from heavy computational burden and cumbersome weighting factors tuning, which hinders the control performance improvement [1][2]. In order to solve the issue of variable switching frequency for the conventional MPCs, several strategies have been proposed in the literature to maintain the switching frequency fixed or inside a narrow range [3]–[6]. A variant of the MPC method was introduced with an intrinsic modulation scheme named modulated model Predictive Control (M^2PC) with the aim of improving the performance of conventional MPC [7]–[11]. This control method intends to improve the output electrical power quality of the system with an intrinsic modulator while preserving the advantages of MPC [12]–[14]. The use of a modulator allows better output of the switching state that resembles the input reference. With relation to PI controllers with modulator, much faster control response and possibly reduced current ripples are expected from M^2PC. Space vector modulation (SVM) was selected as the intrinsic modulator due to is efficient use of selected voltage vectors for finite switching power systems. Moreover, in these M^2PC methods, the redundant positive and negative small voltage vectors are employed in each control cycle with

adjusted dwell time calculation to eliminate the imbalance of the neutral-point (NP) voltage [13][14].

This chapter presented modulated predictive control M²PC for three-level NPC inverter, the proposed M²PC methods with the five-segments and nine-segments are compared in terms of the steady-state, dynamic performances, and parameter sensitivity. Furthermore, an extensive power losses analysis of the inverter's switching devices is carried out using PLECS software, where conduction losses, switching losses, and efficiency under different filter parameters and switching frequencies.

III.2 Principle of modulated model predictive control

The M^2PC algorithm is an appropriate intrinsic modulation scheme for the MPC algorithm combining both MPC [17] and SVM [5] algorithms are introduced. A symmetric SVM pattern with adjacent states has been preferred for reducing the output current harmonics and NP voltage ripple. The majority of the NP voltage balancing schemes used in SVM rely on some form of manipulation of redundant small vectors, where the relative duration of positive and negative small vectors is usually adjusted in order to compensate the NP voltage error [18][19]. To facilitate the dwell time calculation, three voltage vectors are selected in each region, then the reference voltage V_n^* is calculated according to the 'volt-second balancing' [20]. When V_n^* falls into region 3 of sector I as shown in Figure III.1, the three nearest vectors are V_{17}, V_{16}, and V_5, that is, the product of the reference voltage V_n^* and sampling period T_s equals the sum of the voltage multiplied by the time interval of chosen space vectors as follows:

$$\begin{cases} V_{17}d_a + V_{16}d_b + V_5 d_c = V_n^* T_s \\ d_a + d_b + d_c = T_s \end{cases} \tag{III.1}$$

where d_a, d_b, and d_c are the dwell times for V_{17}, V_{16}, and (V_5 or V_6), respectively. The vector's duty cycles have investigated in [15] as:

$$\begin{cases} d_a = T_s \dfrac{g_{16}g_5}{g_5g_{17} + g_5g_{16} + g_{17}g_{16}} \\ d_b = T_s \dfrac{g_{17}g_5}{g_5g_{17} + g_5g_{16} + g_{17}g_{16}} \\ d_c = T_s \dfrac{g_{16}g_{17}}{g_5g_{17} + g_5g_{16} + g_{17}g_{16}} \end{cases} \tag{III.2}$$

where the cost function values g_j (j=0…26) for each voltage vector are calculated by using (II.13), taking into account that the zero vectors and every two pairs of redundant small-voltage vectors have the same output voltage. Thus, it has the same dwell times.

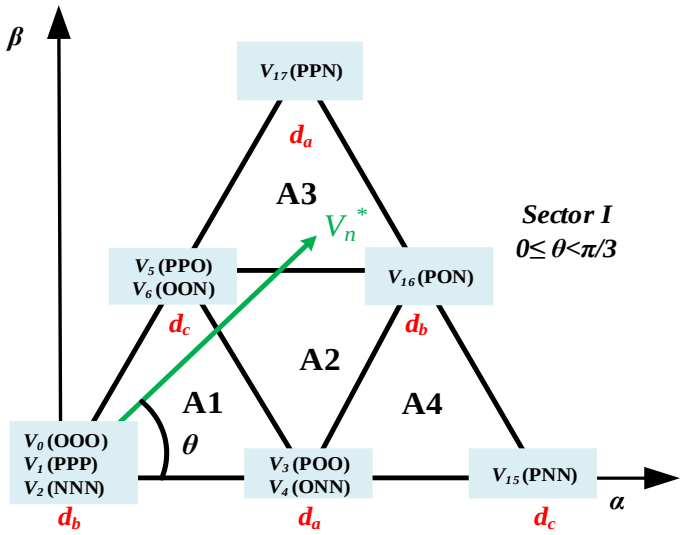

Figure III.1: Voltage vectors and their application time in sector I.

III.2.1 Effect of switching states on neutral-point voltage

As shown in Figure III.2, the voltage vectors except for large- and zero-voltage vectors affect the neutral point voltage balancing. As shown in Figure III.2 (a), although the zero vector (OOO) is connected to the neutral point O, the total sum of the currents is zero. Thus, it does not affect the neutral-point voltage balancing. As shown in Figure III.2 (b), large vector (PNN) does not affect the neutral-point voltage balancing because the neutral-point O is disconnected. Figure III.2 (c) shows the inverter operation with the P-type small voltage vector (POO). Because the P-type switching states are connected between the positive DC-link and neutral point O, the neutral-point current flows into the neutral-point point O, and the neutral-point voltage is increased. On the other hand, the N-type small vector (OON) decreases the neutral-point voltage since the three phases are connected between the neutral-point point and the negative DC-link, as shown in Figure III.2 (d). As shown in Figure III.2 (e), medium vector (PON) also affects the neutral-point voltage. Depending on the current direction of the phase connected to the neutral point, the neutral-point voltage increases or decreases with the medium vector. Among the four types of vectors for three-level inverter, only the medium and small vectors influence the neutral-point voltage balance. The medium vector charges or discharges

the two DC-link capacitors with different current direction and causes the neutral-point voltage oscillation. This oscillation can be eliminated by adjusting the dwell time of the small vector.

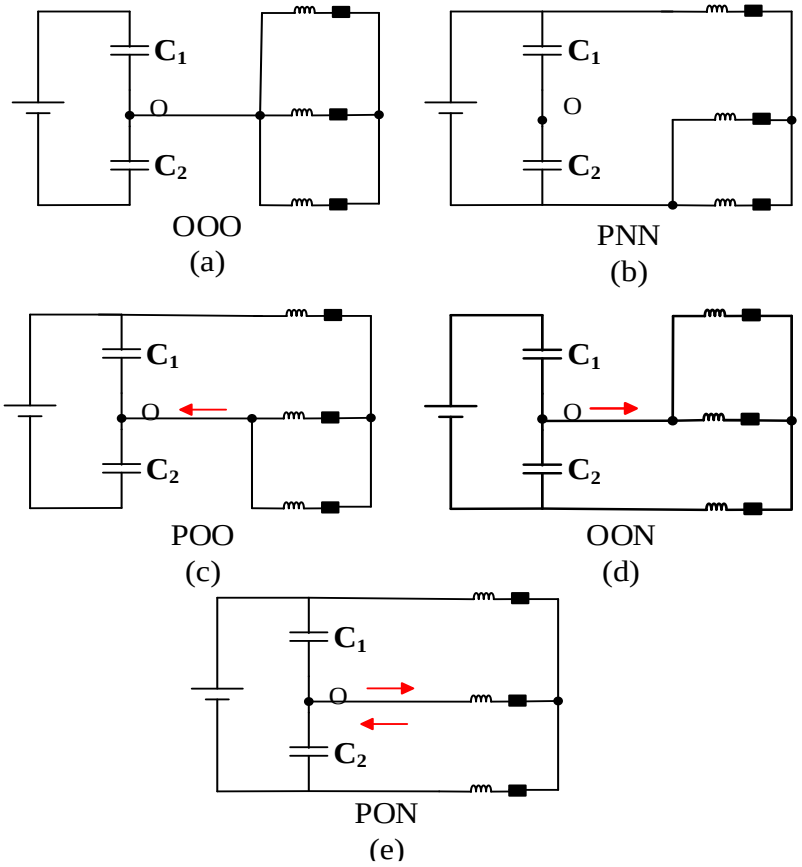

Figure III.2: Effects of voltage vectors on the neutral-point voltage balancing.

III.2.2 Five-segments based M²PC method

According to the description above, with the space voltage vectors selected and their dwell times calculated, the next step is to arrange the switching pattern. Figure III.3 shows a typical five-segments switching sequence for sector I, the sampling period T_s is divided into five segments sequence for the three selected vectors V_0, (V_3 or V_4), and (V_5 or V_6). The NP voltage imbalance is regulated using the duty cycle ratio of positive and negative small vectors.

According to this description, two conditions can be obtained for NP voltage balancing as follows, when $V_P > V_N$, the voltage vector V_3 (POO) is selected to reduces V_P and increases V_N. When $V_P < V_N$, the voltage vector V_4 (ONN) is selected to reduces V_N and increases V_P. Table III.1 lists the candidate voltage vectors for four regions of sector I. The application times and switching patterns for other large sectors can be obtained in the same way.

Table III.1: Five-segments switching sequence for sector I

	A1		A2		A3		A4	
Segments	$V_P>V_N$	$V_P<V_N$	$V_P>V_N$	$V_P<V_N$	$V_P>V_N$	$V_P<V_N$	$V_P>V_N$	$V_P<V_N$
1st	V_0 OOO	V_4 ONN	V_{16} PON	V_4 ONN	V_{16} PON	V_6 OON	V_{15} PNN	V_4 ONN
2nd	V_3 POO	V_6 OON	V_3 POO	V_6 OON	V_{17} PPN	V_{16} PON	V_{16} POO	V_{15} PNN
3rd	V_5 PPO	V_0 OOO	V_5 PPO	V_{16} PON	V_5 PPO	V_{17} PPN	V_3 POO	V_{16} PON
4th	V_3 POO	V_6 OON	V_3 POO	V_6 OON	V_{17} PPN	V_{16} PON	V_{16} PON	V_{15} PNN
5th	V_0 OOO	V_4 ONN	V_{16} PON	V_4 ONN	V_{16} PON	V_6 OON	V_{15} PNN	V_4 ONN

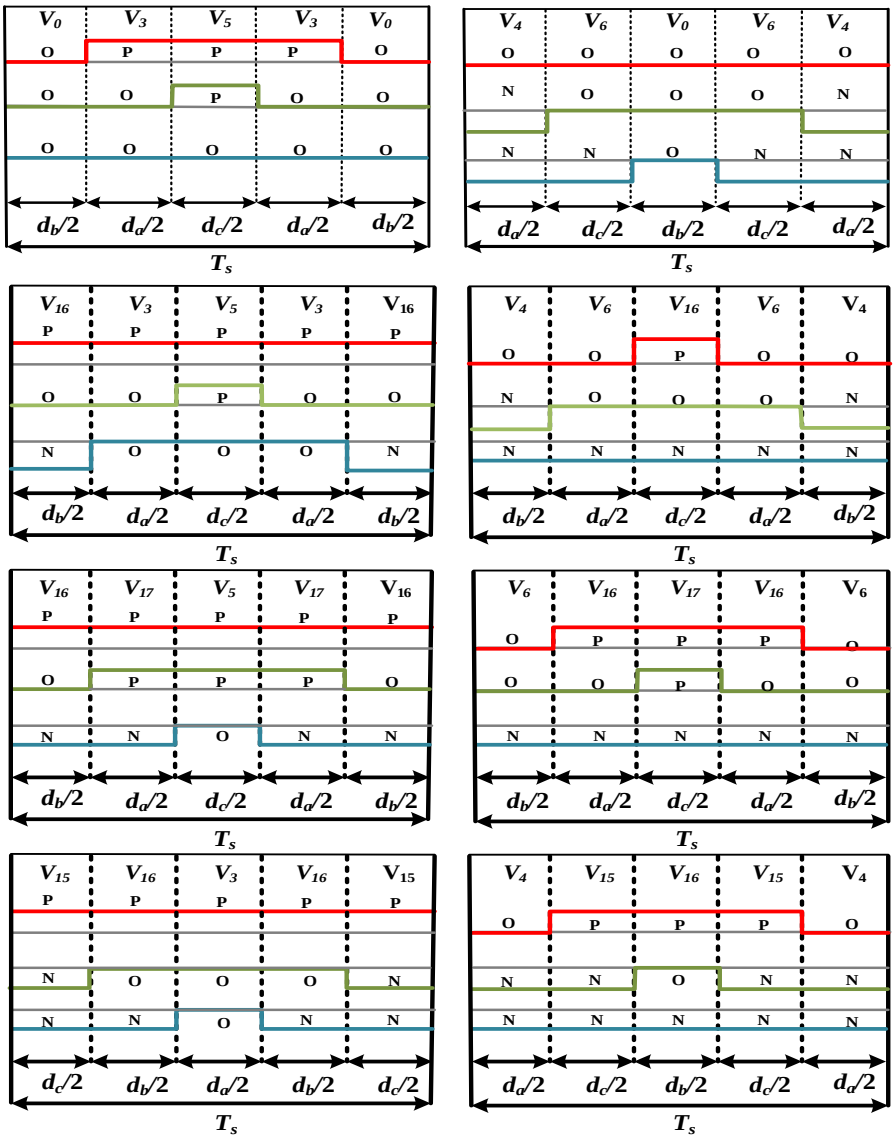

(a) (b)

Figure III.3: Switching patterns of five-segments based M²PC method in sector I. (a) $V_P>V_N$. (b) $V_P<V_N$.

III.2.3 Nine-segments based M^{2}PC method

The previous algorithm suffers from the redundancy of switching patterns to maintain NP voltage balancing in each simpling period T_s, which leads to increase the switching loss and the computational burden. To eliminate this issue, nine-segments based M^{2}PC Method is investigated in [21], which is based on NP voltage balancing factor ΔV as:

$$\Delta V = \left(V_p - V_N\right) / V_{dc} \tag{III.3}$$

The NP voltage balancing of the three-level NPC inverter is realized by adjusting the execution durations of the redundant positive and negative small voltage vectors by using (III.4), considering the opposite effect of both on the NP voltage. Assume that $\boldsymbol{V_n^*(k)}$ falls in the sector I region A1, the application times of redundant positive and negative small voltage vectors V_3 (POO), V_4 (ONN), V_5 (PPO), and V_6 (OON) can be expressed by:

$$\begin{cases} d_{POO} = \left(1+\Delta V\right) d_a / 2 \\ d_{ONN} = \left(1-\Delta V\right) d_a / 2 \\ d_{PPO} = \left(1+\Delta V\right) d_c / 2 \\ d_{OON} = \left(1-\Delta V\right) d_c / 2 \end{cases} \tag{III.4}$$

From Figure III.2, it can be seen that d_a is the dwell time of V_3 and V_4, and d_c is the dwell time *of* V_5 and V_6, can be expressed as follows:

$$\begin{cases} d_a = d_{POO} + d_{ONN} \\ d_c = d_{PPO} + d_{OON} \end{cases} \tag{III.5}$$

Table III.2: Nine-segments switching sequence for sector I

	Switching Segments								
A1	V_4	V_6	V_0	V_3	V_5	V_3	V_0	V_6	V_4
	ONN	OON	OOO	POO	PPO	POO	OOO	OON	ONN
A2	V_4	V_6	V_{16}	V_3	V_5	V_3	V_{16}	V_6	V_4
	ONN	OON	PON	POO	PPO	POO	PON	OON	ONN
A3		V_6	V_{16}	V_{17}	V_5	V_{17}	V_{16}	V_6	
		OON	PON	PPN	PPO	PPN	PON	OON	
A4		V_4	V_{15}	V_{16}	V_3	V_{16}	V_{15}	V_4	
		ONN	PON	PON	POO	PON	PNN	ONN	

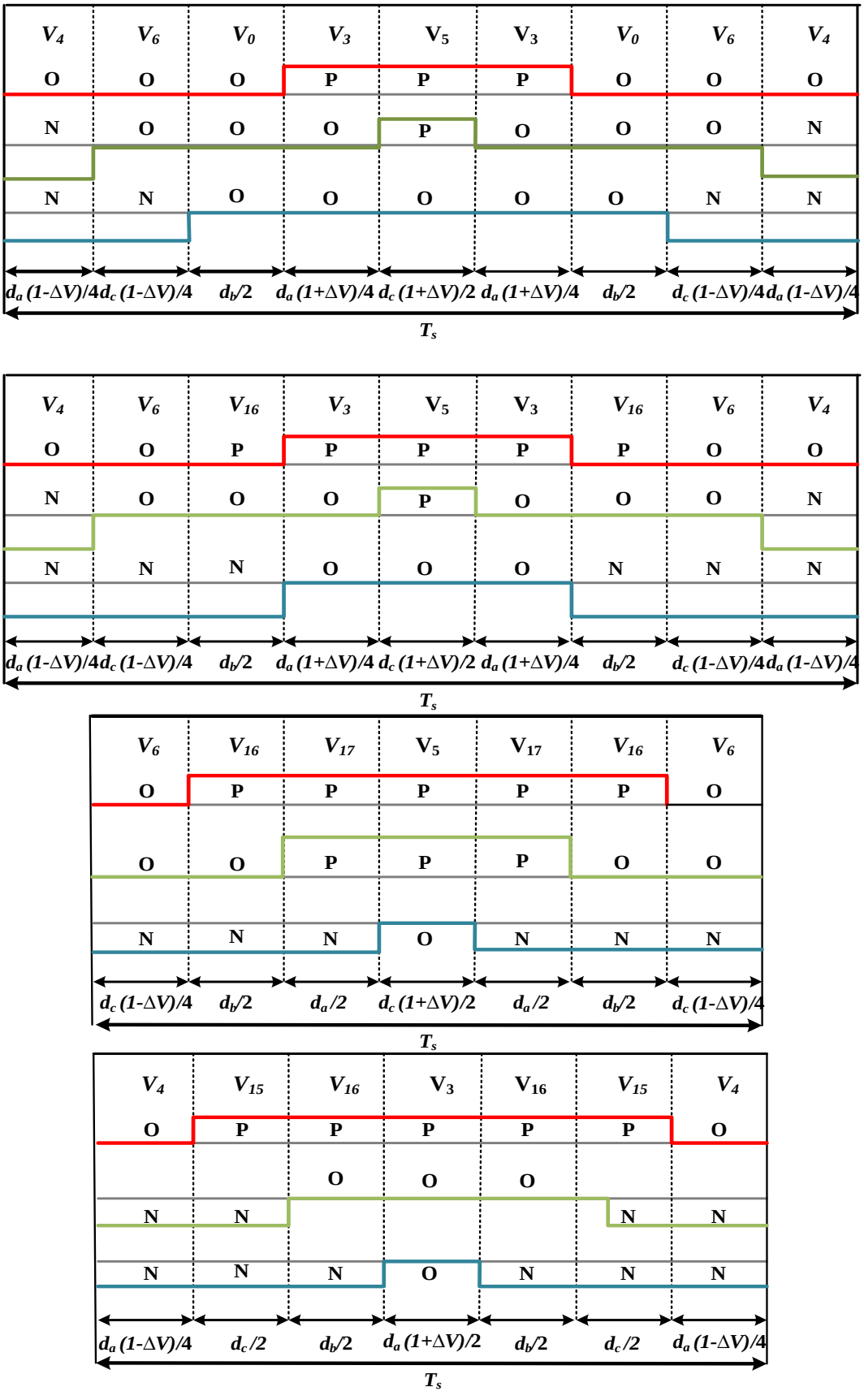

Figure III.4: Switching pattern for nine-segments based M^{2}PC method in sector I.

Based on the above analysis, the application times and switching pattern for nine-segments based M²PC method in sector I are illustrated in Figure III.4. Table III.2 summarizes all the switching sequences of different voltage vectors in the first sector. The main structure of the competing M²PC methods is shown in Figure III.5. The main difference between the three algorithms appears in the number of segments switching patterns used in each sampling period T_s, The delay compensation describes in chapter (II) has been implemented for the competing M²PC methods to avoid delays caused by digital implementation.

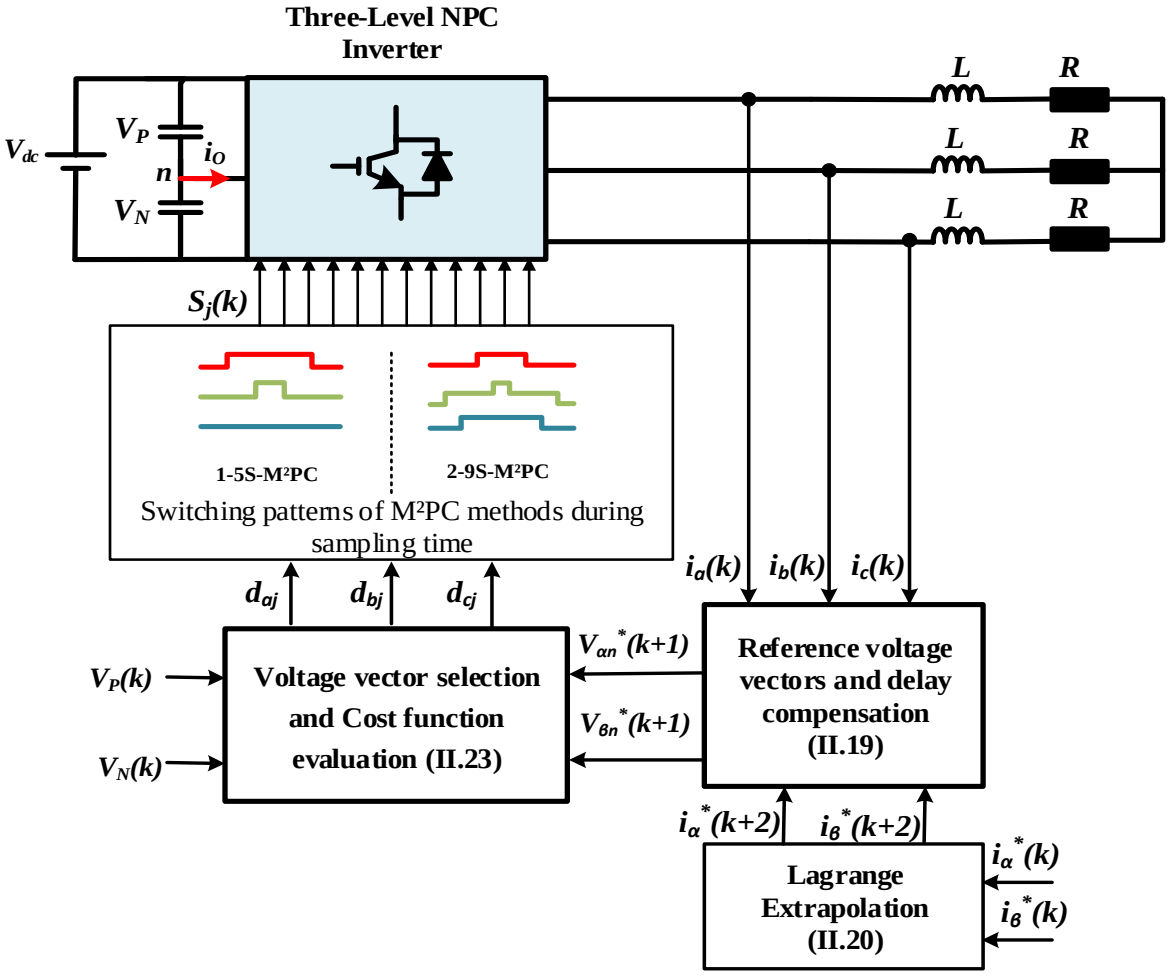

Figure III.5: Block diagram of the studied M²PC methods.

III.3 Simulation results

In order to validate the effectiveness of the proposed M²PC methods for three-level NPC inverter, the control scheme has been simulated using MATLAB software. The simulation parameters used in this chapter are the same ones used in the previous chapter. To prove the effect of NP voltage balance, current tracking, and THD, the proposed M²PC methods are compared in Figure III.6 and Figure III.7.

Figure III.6 present the simulation waveforms of the inverter output currents i_a, i_b, and i_c, line-to-line inverter voltage V_{ab}, and the capacitor voltages V_P and V_N respectively, for competing M²PC methods. It can be seen clearly that both M²PC methods has best current tracking, and can effectively regulate the NP voltage error.

From Figure III.7, it can be obtained that the total harmonic distortion (THD) of current is 1.62% for proposed. On the other hand, from Figure III.7 (a) the five-segments based M²PC has the highest THD value 2.95% of the phase-a output current, and the nine-segment based M²PC has the lowest THD value 1.62%. It can be concluded that the increase of segments number inside the switching pattern makes the output currents get more accurate tracking with low distortion.

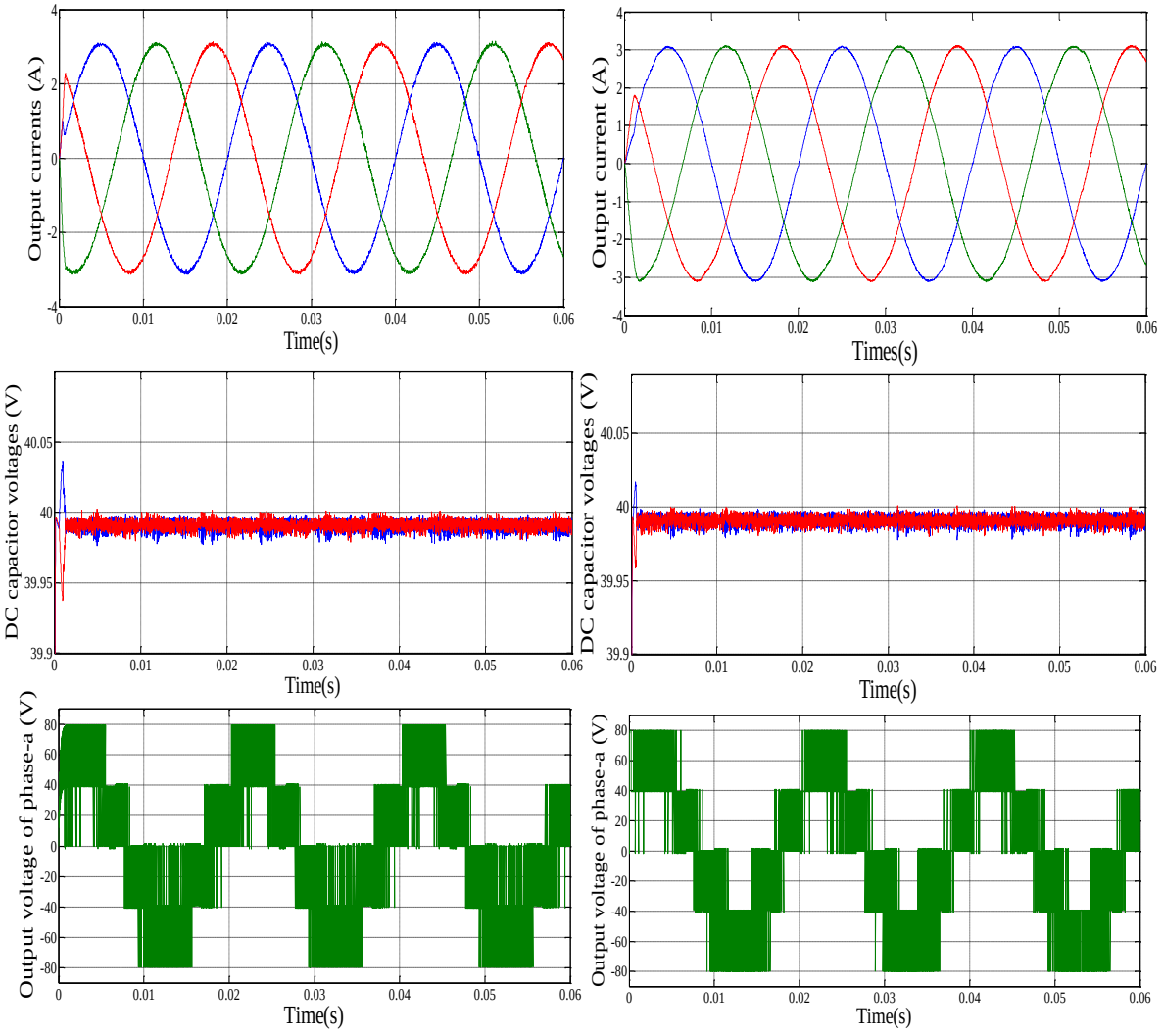

(a) (b)

Figure III.6: Steady-state simulation results of: (a) Five-segments based M²PC method. (b) Nine-segments based M²PC method.

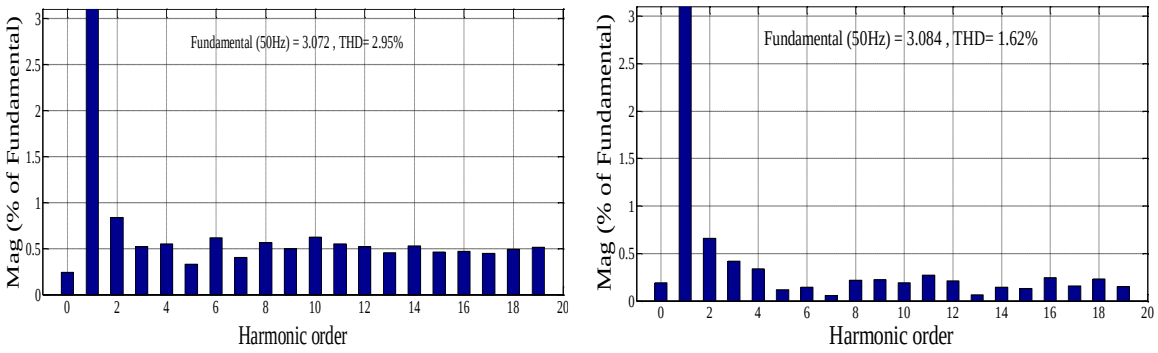

(a) (b)

Figure III.7: Harmonics spectrum of phase-a current. (a) Five-segments based M^{2}PC method. (b) Nine-segments based M^{2}PC method.

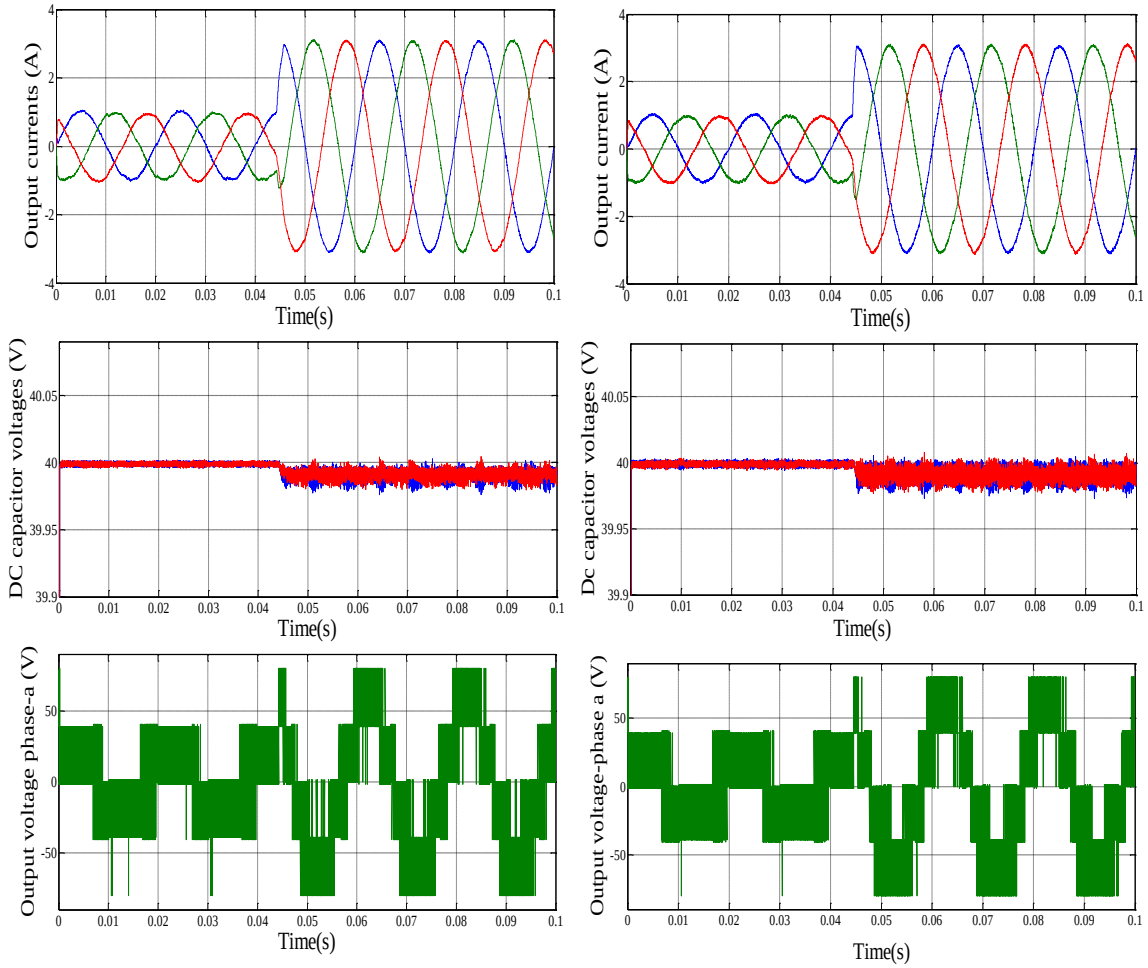

(a) (b)

Figure III.8: Dynamic simulation waveforms of modulated MPC methods: (a) Five-segments based M²PC method. (b) Nine-segments based M²PC method.

Figure III.8 show the dynamic simulation waveforms of three-phase output currents i_b, i_b, and i_c, line-to-line voltage V_{ab}, and and the capacitor voltages V_P and V_N for the proposed M²PC methods. In this test, the reference current of the inverter changes from 1A to 3A. Both M²PC methods respond quickly to this change without affecting the balance of the NP voltage, also the output current is always well obtained.

Furthermore, it can be seen clearly from Figure III.9 that the nine-segments based M²PC method has the fastest dynamic response with the lowest settling time (0.12ms) compared to the other five-segments based M²PC method .

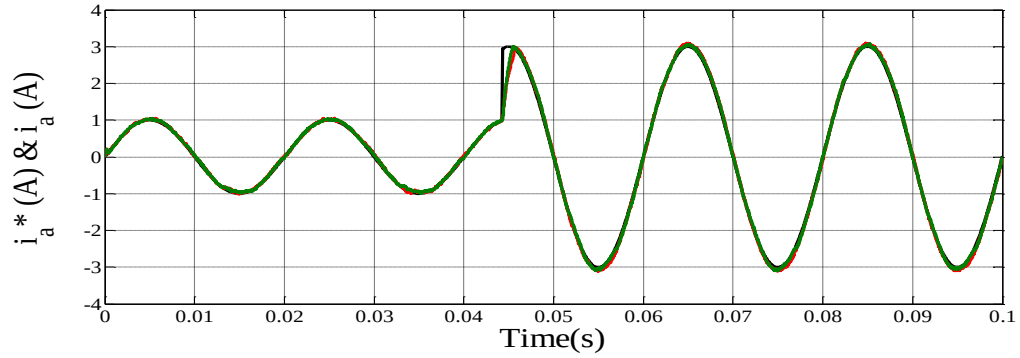

(a)

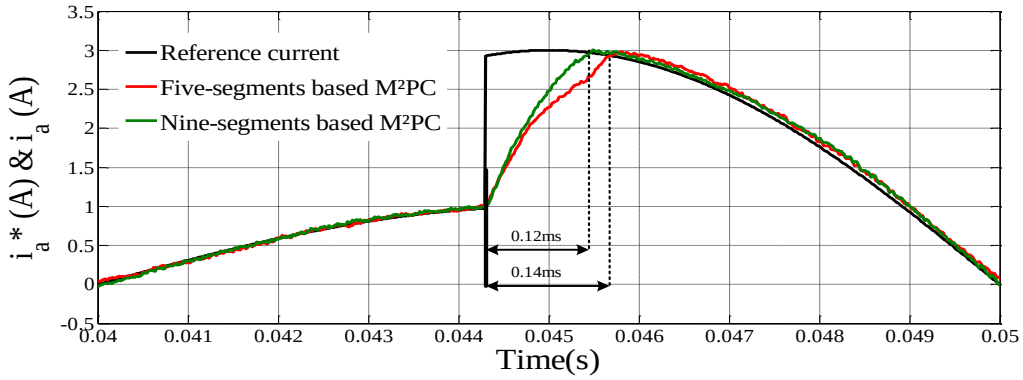

(b)

Figure III.9: (a) Simulation dynamic-state performance of both M²PC methods. (b) Zoom part of step-change.

III.4 Experimental results

The controllers are implemented using DS1104 real-time controller board with associated I/Os. The controller parameters are given in Table A.1. The experimental setup is shown in Appendix B. The sampling period of the controller is set to 80 µs. To validate the performance of the proposed M²PC methods, four tests are carried out to evaluate both steady-state and dynamic performance of different modulated MPC algorithms at a fixed operating frequency

(f=50Hz). Test 1: the amplitude and the frequency of the output reference currents are set as 2A and f=50 Hz. Test 2: the amplitude and the frequency of the output reference currents are set as 3A. Test 3: the amplitude of the output reference current is stepped from 3A to 1A. Test 4: the amplitude of the reference current is suddenly changed from 1A to 3A.

III.4.1 Steady-state response

The performance of competing M^{2}PC methods is compared for the steady-state operation. In this section, two test conditions are defined when the reference current i^*=2A, and then for i^*=3A. Figures III.10 and III.11 show the experimental results of Test 1 and 2, respectively, of i_a, i_b, and i_c current waveforms, line-to-line inverter voltage V_{ab}, the capacitor voltages V_P and V_N, and harmonic spectrum of phase-a current for different M^{2}PC methods.

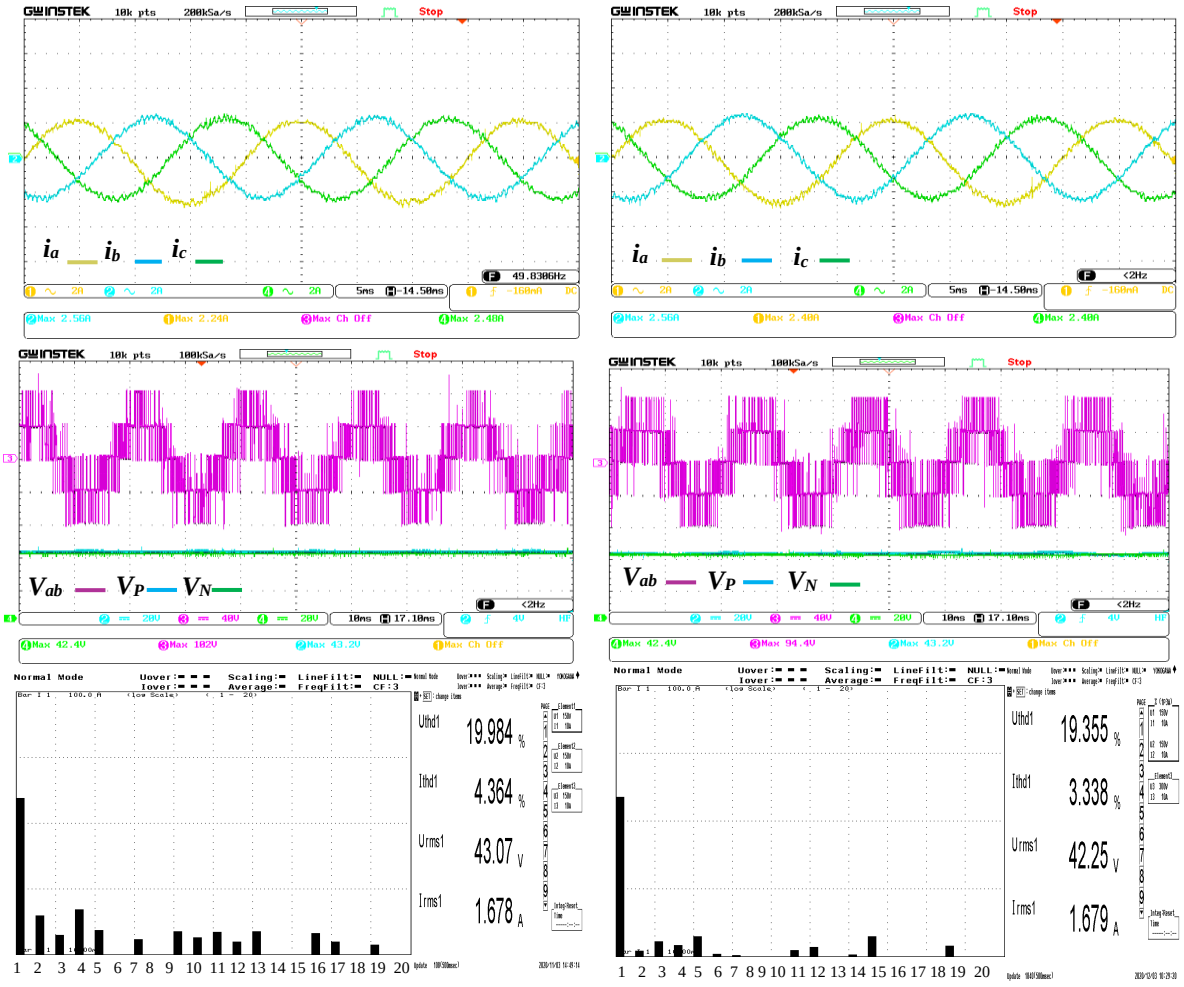

(a) (b)

Figure (III.10): Steady-state experimental waveforms with harmonics spectrum of phase-a current for Test 1: (a) Five-segments based M^{2}PC method. (b) Nine-segments based M^{2}PC method.

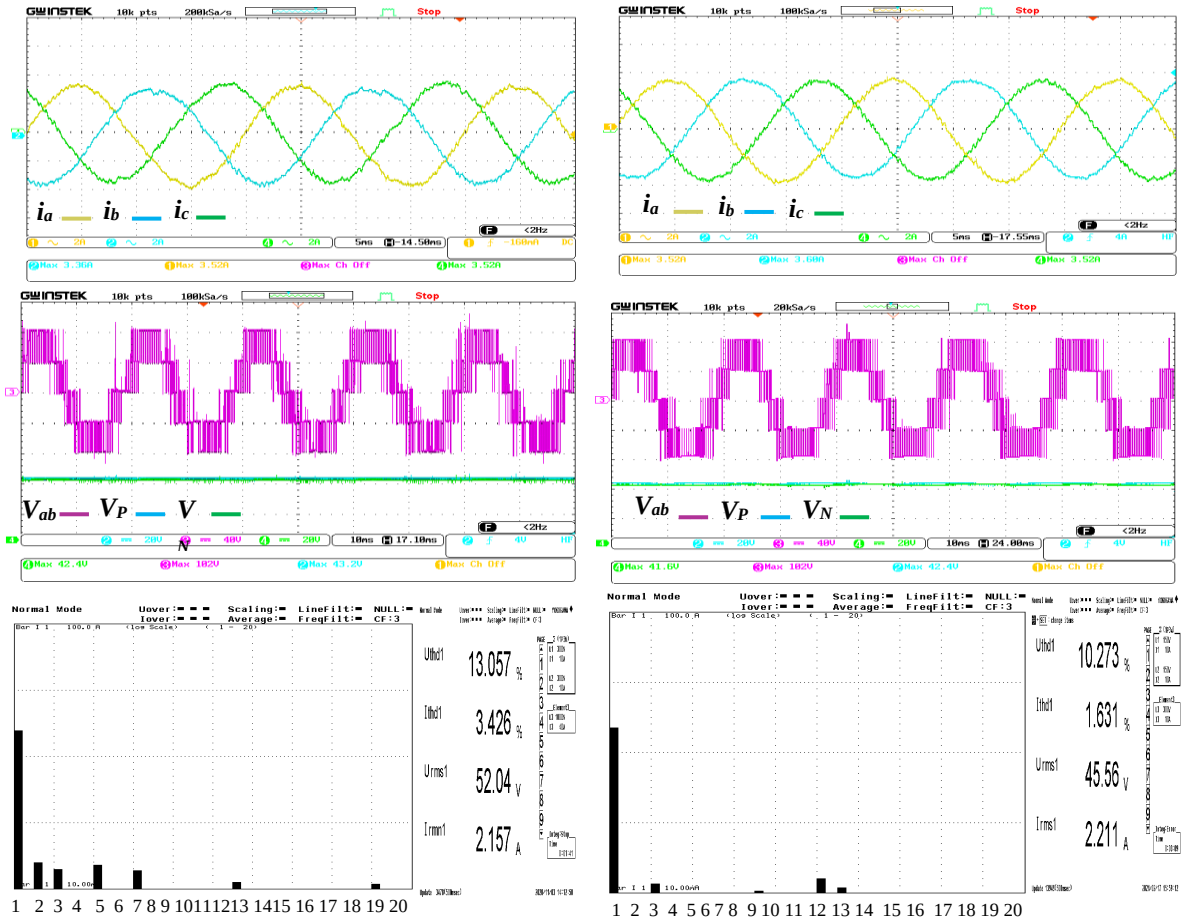

(a) (b)

Figure III.11: Steady-state experimental waveforms with harmonics spectrum of phase-a current for Test 2: (a) Five-segments based M^{2}PC method. (b) Nine-segments based M^{2}PC method.

From these experimental waveforms, the main conclusions can be drawn as: 1) It can be clearly seen that all three M^{2}PC algorithms are producing good sinusoidal output current and accurate tracking of the reference current. 2) From the steady-state experimental waveforms, it can be seen that five-segments and nine-segments M^{2}PC methods can effectively regulate the NP voltage, where the maximum ripple of the three M^{2}PC methods is less than 1V. Therefore, it can be concluded that the positive and negative small voltage vectors controlled effectively the NP voltage. 3) Form Figure III.10 (b) and Figure III.11 (b), it can be noticed that the THD of the output phase-a current of the nine-segments based M^{2}PC method is the lowest. On the other hand, from Figure III.10 (a) and Figure III.11 (a) the five-segments based M^{2}PC has the highest THD value of the phase-a output current. Therefore, according to the measured THDs of output currents shown in Table III.3, it can be concluded that the increase of segments number inside the switching pattern makes the output currents get more accurate tracking with

low distortion. As expected, the proposed nine-segments based M²PC has the lowest THD 1.631%.

III.4.2 Dynamic response

The dynamic response of the competing M²PC methods is evaluated under step change of the reference current. Figure III.12 (a) and (b) show respectively the experimental waveforms of phase-a current, line-to-line voltage V_{ab}, and the capacitor voltages (V_P, V_N). In this test, the reference current of the inverter changes from 3A to 1A, and then form 1A to 3A. As it can be seen in Figure III.12 (a) and (b), the three M²PC methods respond quickly to this change without affecting the normal operation of the system. A synchronized output current is always well obtained. In addition, it can be seen that both M²PC methods have a good NP voltage balancing capability during transient waveforms.

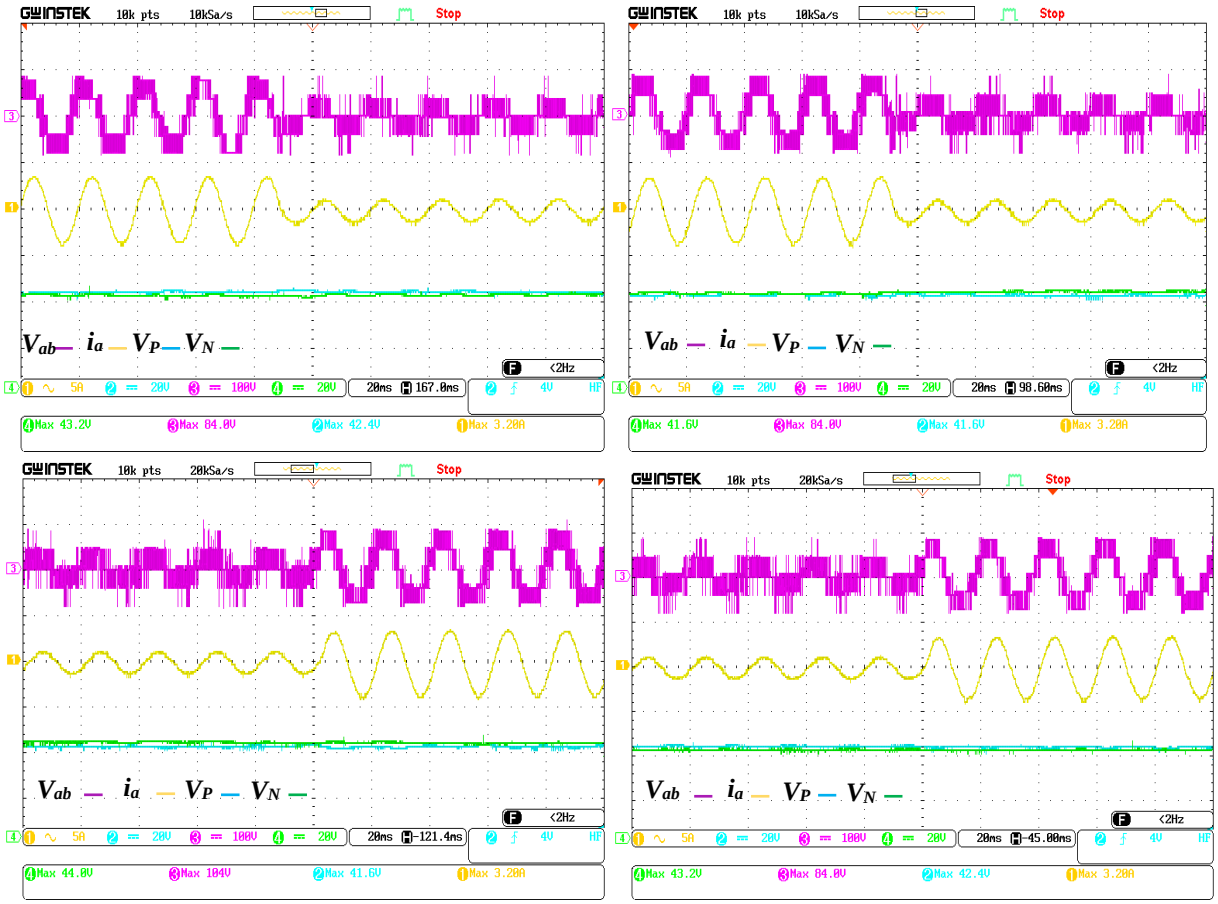

(a) (b)

Figure III.12: Dynamic experimental waveforms for Test 3 and Test 4: (a) Five-segments based M²PC method. (b) Nine-segments based M²PC method.

Table III.3: THD comparison for the proposed M²PC methods

M^2PC Methods	THD% Test(1)	THD% Test (2)
Five-segments based M^2PC	4.364%	3.338%
Nine-segments based M^2PC	3.338%	1.631%

III.4.3 Computational burden

The execution time for the proposed M²PC methods is compared with the conventional MPC method, the interruption time is set to be the same, i.e., all algorithms are executed with a sampling time of 80µs. The computational burden required by the competing algorithms are given as 76µs for the conventional MPC, 23µs for five-segments M²PC methods, and 15µs for the nine-segments based M²PC method. As shown in Figure III.13, it can be observed that the computational burden of the proposed deadbeat control is reduced by nearly 80% compared with conventional MPC method.

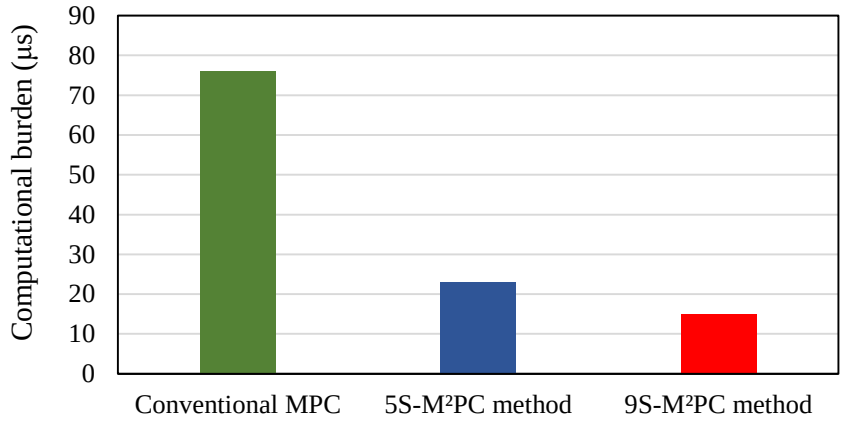

Figure III.13: Computational burden comparison.

III.5 Parameter sensitivity

In this section, the parameter sensitivity of the proposed nine-segments based M^2PC method discussed in this work is analyzed and compared to the parameter sensitivity of the five-segments based M^2PC method for the three-level NPC inverter. The effects of variations in the load parameters *R*, *L* (in ±50% and in ±10%) were analyzed using simulation studies for the

M^{2}PC methods. It was concluded that the most significant effect in the control performance is produced when the inductance *L* is misidentified by the control system,

The measured THD values of the inverter output current for the MP^{2}C methods under Test 2 are shown in Table III.4. Notice that, the THD of the output current is decreased with the increased of the inductance. Otherwise, these results show that the proposed nine-segments based M^{2}PC method is very less sensitive to parameter mismatch compared to the five-segment method. Also, it can be seen when *L* is changed from ±10%, THD variation is less sensitive to the change for the both M^{2}PC methods.

Table III.4: THD comparison with different *L* values

Methods	Base case	+50%	+10%	-10%	-50%
Five-segments based M^{2}PC	3.426%	3.221%	3.362%	3.574%	5.213%
Nine-segments based M^{2}PC	1.631%	2.193%	2.331%	2.524%	3.87%

III.6 Power losses analysis

Figure III.14 shows power losses analysis as a function of different load types (R_1=10Ω, R_2=100Ω, L_1=10mH, L_2=100mH). It can be seen during the parameter mismatch that the nine-segments based M²PC method show the lowest power losses, while the five-segment based M²PC show the most considerable power losses. From Table III.5, it can be seen that, the proposed nine-segments has the lowest total power losses for *R*=10Ω and *L*=10mH compared by five-segments based M^{2}PC method. Furthermore, from the power losses analysis results, notice that the conduction losses are very approximate for diodes and switches in the M^{2}PC methods regardless of the change in the inductance and resistor values .Also, it can be observed that the switching losses have small values in MOSFETs and zero in diodes (P_{d_sw}=0) for the M²PC methods because of the use of SiC MOSFETs and DIODEs high-performance characteristics.

Figure III.15 shows the efficiency versus switching frequency curve. The maximum efficiency achieved using the three M^{2}PC methods is around 98% in different frequency values with a slight drop when the frequency increases. At any frequency, the highest efficiency is always recorded by the proposed nine-segments based M^{2}PC. Table III.4 compares the efficiency and the total power losses of the three competing M^{2}PC methods. Clearly, the

proposed nine-segments based M²PC owns the highest efficiency and the lowest total power losses compared five-segment method.

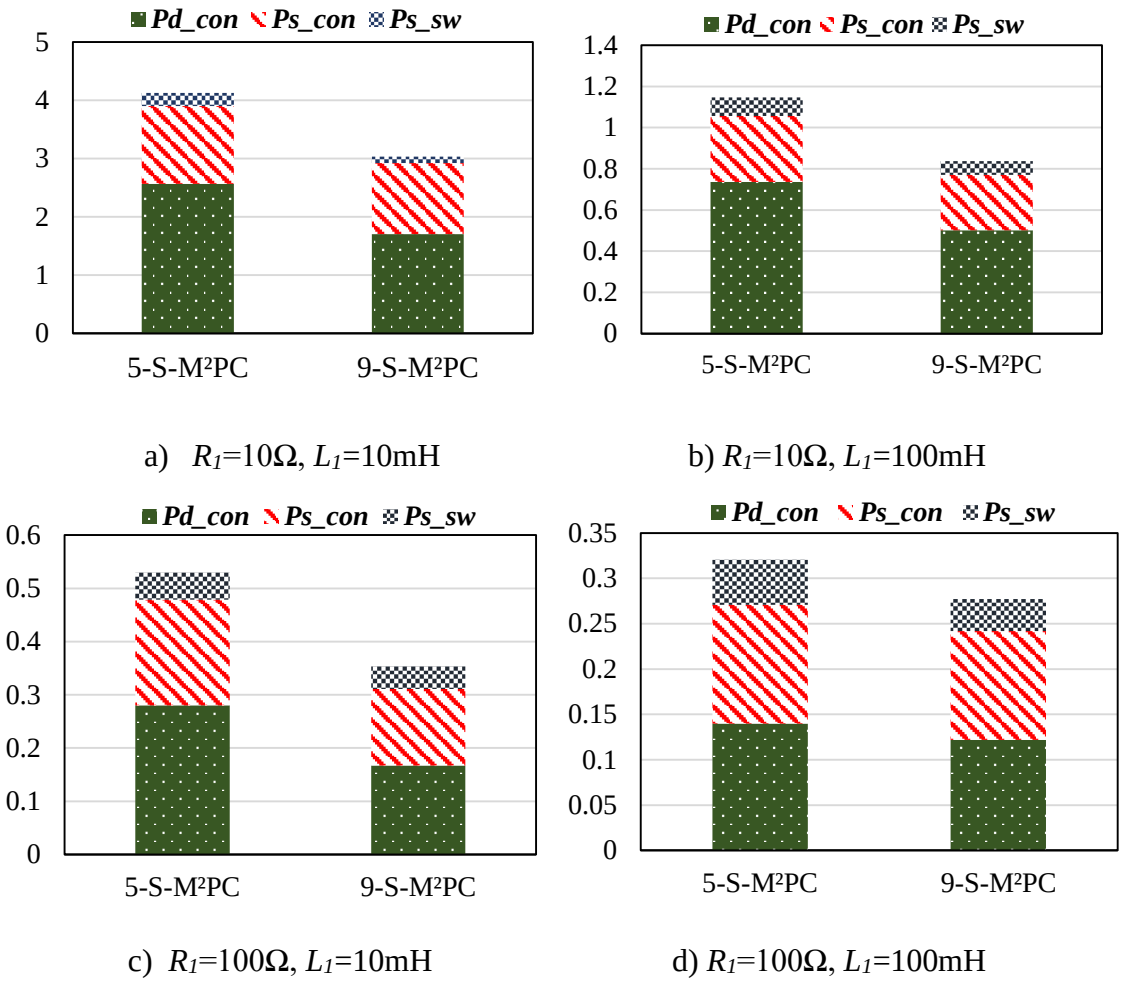

Figure III.14: Power loss distribution of semiconductors devices [*Pd_con, Ps_con, and Ps_sw* represents conduction losses of diode, conduction losses of switch, switching losses of switch respectively].

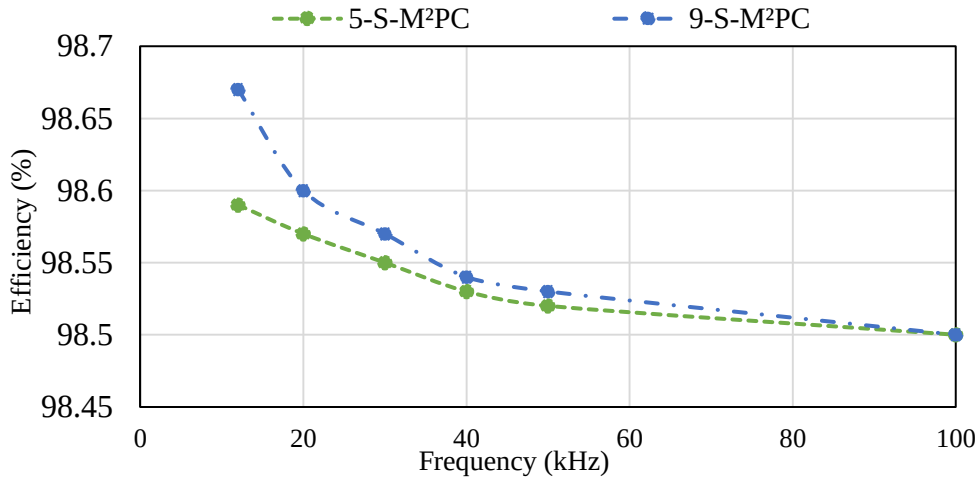

Figure III.15: Efficiency curve versus the switching frequency for *L*=10mH, and *R*=10 Ω.

Table III.5: Power losses and efficiency comparison for three MP²C methods

M²PC Methods	Efficiency (12kHz)	Total power losses (R=10Ω, L=10mH)
Five-segments based M²PC	98.59%	4.126W
Nine-segments based M²PC	98.67%	3.022W

III.7 Conclusion

In this chapter, two models modulated model predictive control M²PC with constant switching frequency and low complexity for three-level NPC inverter has been proposed. From experimental and simulation results and PLECS losses analysis, several key findings can be inferred as: 1) The proposed M²PC methods have good output current quality, while the proposed nine-segments based M²PC method owns the best value of the output current THD which equals to 1.741%. 2) The both M²PC methods have perfect capability in the NP voltage balancing in the steady-state performance and dynamic response. 3) The proposed nine-segments based M²PC method shows less sensitivity regarding the mismatch in the filter inductance than the other M²PC methods. 4) From the power losses analysis results, it can be seen that, the nine-segments based M²PC have shown the lowest power losses and the best efficiency.

III.8 Chapter references

[1] V. Yaramasu, M. Rivera, M. Narimani, B. Wu, and J. Rodriguez, "Model Predictive Approach for a Simple and Effective Load Voltage Control of Four-Leg Inverter with an Output LC Filter," *IEEE Trans. Ind. Electron.*, vol. 61, no. 10, pp. 5259–5270, 2014.

[2] S. Vazquez *et al.*, "Model Predictive Control: A Review of its Applications in Power Electronics," *IEEE Ind. Electron. Mag.*, vol. 8, no. 1, pp. 16–31, 2014.

[3] L. Tarisciotti *et al.*, "Model Predictive Control for Shunt Active Filters With Fixed Switching Frequency," *IEEE Trans. Ind. Appl.*, vol. 53, no. 1, pp. 296–304, 2017.

[4] F. Herrera, R. Cardenas, M. Rivera, J. A. Riveros, and P. Wheeler, "Predictive Voltage Control Operating at Fixed Switching Frequency of a Neutral-Point Clamped Converter," *2019 IEEE 15th Brazilian Power Electron. Conf. 5th IEEE South. Power Electron. Conf.*, 2019.

[5] D. Zhou, Z. Quan, Y. Li, and J. Zou, "A General Constant-Switching-Frequency Model-Predictive Control of Multilevel Converters with Quasi-PS-PWM/LS-PWM Output," *IEEE Trans. Power Electron.*, vol. 35, no. 11, pp. 12429–12441, 2020.

[6] M. Rivera, "Predictive Current Control for a VSI with Reduced Common Mode Voltage Operating at Fixed Switching Frequency," *IEEE Int. Symp. Ind. Electron.*, vol. 2015–Septe, pp. 980–985, 2015.

[7] D. Xiao, K. S. Alam, M. P. Akter, S. M. S. I. Shakib, D. Zhang, and M. Rahman, "Modulated Model Predictive Control for Four-Leg Inverters with Online Duty Ratio Optimization," *IEEE Trans. Ind. Appl.*, vol. 56, no. 3, pp. 3114–3124, 2020.

[8] L. Tarisciotti, P. Zanchetta, A. Watson, S. Bifaretti, and J. C. Clare, "Modulated Model Predictive Control for a Seven-Level Cascaded H-Bridge Back-to-Back Converter," *IEEE Trans. Ind. Electron.*, vol. 61, no. 10, pp. 5375–5383, 2014.

[9] L. Tarisciotti, P. Zanchetta, A. Watson, J. Clare, M. Degano, and S. Bifaretti, "Modulated Model Predictive Control for a Three-Phase Active Rectifier," *IEEE Trans. Ind. Appl.*, vol. 51, no. 2, pp. 1610–1620, 2015.

[10] L. Tarisciotti, P. Zanchetta, A. Watson, P. Wheeler, and S. Bifaretti, "Multiobjective Modulated Model Predictive Control for a Multilevel Solid-State Transformer," *IEEE Trans. Ind. Appl.*, vol. 51, no. 5, pp. 4051–4060, 2015.

[11] M. Vijayagopal, P. Zanchetta, L. Empringham, L. De Lillo, L. Tarisciotti, and P. Wheeler, "Control of a Direct Matrix Converter With Modulated Model-Predictive Control," *IEEE Trans. Ind. Appl.*, vol. 53, no. 3, pp. 2342–2349, 2017.

[12] Q. Wang *et al.*, "A Low-Complexity Optimal Switching Time Modulated Model Predictive Control for PMSM with Three-Level NPC Converter," *IEEE Trans. Transp. Electrif.*, vol. 6, no. 3, pp. 1188–1198, 2020.

[13] M. Rivera *et al.*, "Modulated Model Predictive Control (M2PC) with Fixed Switching Frequency for an NPC Converter," *Int. Conf. Power Eng. Energy Electr. Drives*, pp. 623–628, 2015.

[14] H. Mahmoudi, M. Aleenejad, and R. Ahmadi, "Modulated Model Predictive Control of

Modular Multilevel Converters in VSC-HVDC Systems," *IEEE Trans. Power Deliv.*, vol. 33, no. 5, pp. 2115–2124, 2018.

[15] F. Donoso, A. Mora, R. Cardenas, A. Angulo, D. Saez, and M. Rivera, "Finite-Set Model-Predictive Control Strategies for a 3L-NPC Inverter Operating with Fixed Switching Frequency," *IEEE Trans. Ind. Electron.*, vol. 65, no. 5, pp. 3954–3965, 2018.

[16] Y. Yang, H. Wen, M. Fan, M. Xie, R. Chen, and Y. Wang, "A Constant Switching Frequency Model Predictive Control Without Weighting Factors for T-Type Single-Phase Three-Level Inverters," *IEEE Trans. Ind. Electron.*, vol. 66, no. 7, pp. 5153–5164, 2019.

[17] J. Rodriguez and P. Cortes, *Predictive Control of Power Converters and Electrical Drives*. New York, NY, USA: Wiley–IEEE Press, 2012.

[18] X. Xing, X. Li, F. Gao, C. Qin, and C. Zhang, "Improved Space Vector Modulation Technique for Neutral-Point Voltage Oscillation and Common-Mode Voltage Reduction in Three-Level Inverter," *IEEE Trans. Power Electron.*, vol. 34, no. 9, pp. 8697–8714, 2019.

[19] C. Q. Xiang, C. Shu, D. Han, B. K. Mao, X. Wu, and T. J. Yu, "Improved Virtual Space Vector Modulation for Three-Level Neutral-Point-Clamped Converter with Feedback of Neutral-Point Voltage," *IEEE Trans. Power Electron.*, vol. 33, no. 6, pp. 5452–5464, 2018.

[20] B. Wu, *High-Power Converters and AC Drives*. Wiley–IEEE. New York, NY, USA, 2006.

[21] Y. Yang *et al.*, "Multiple-Voltage-Vector Model Predictive Control with Reduced Complexity for Multilevel Inverters," *IEEE Trans. Transp. Electrif.*, vol. 6, no. 1, pp. 105–117, 2020.

Chapter IV

Comparative Study of Proposed MPC Strategies for Three-Level NPC Grid-Connected Photovoltaic System

IV.1 Introduction

In the last years, due to its high accuracy, fast transient response, model predictive control (MPC) has been applied to various power electronic applications, including motor drives, grid-connected inverters, active power filters, renewable energy systems, etc.[1]–[3]. Unlike the classic linear control methods, applying MPC can decouple the interdependent control loops and eventually enhance the dynamic response, which have been proven to be suitable serve as the interface between distributed energy resources ref, micro-grid [4], and renewable energy system such as solar energy [5] and wind energy [4].

Renewable energy-based distributed energy sources are becoming more attractive, on both economic and technological scales [6][7]. Photovoltaic (PV) arrays are among the most used renewable energy sources, due to their advantages, it consists of no moving parts. Do not produce any noise and maintenance costs are minimal. It is also a clean source of energy. Amount of energy produced by the sun is so large, that in one hour it can provide more than enough energy for human population in one year. However, due to the low efficiency of current solar panels, conversion of sunlight into electrical power is very poor. This efficiency further decreases if there is no load matching between the input side (PV array output) and the output side (load). To maximize the power derived from the solar panel it is important to operate the panel at its maximum power point, hence an increase in output efficiency {Merging Citations}. Electrical energy can be produced through photovoltaic arrays and make it available to the public utilization through grid-connected PV systems. In the last years, these systems have been

widely investigated in numerous research works in order to enhance the energy harvesting from the PV arrays and to inject the produced PV power into the grid with high grid current quality. Furthermore, it is gaining today the most interest over traditional stand-alone PV systems, which suffer from several drawbacks, such as unavoidable costly and bulky batteries and their regular maintenance [11][12].

This chapter presents the control of a three-level NPC inverter grid-connected photovoltaic (PV) generation system. Firstly, the mathematical models of the PV array and the boost converter are introduced. In addition, the maximum power point tracking (MPPT) algorithm, which allows maximal power conversion into the grid, has been included. This method is capable of extracting maximum power from each of the independent PV arrays connected to each DC link voltage level. Then, the predictive controllers are used to regulate the current supplied to the grid and to perform the balancing of the DC-link capacitor voltages. Finally, in order to validate the effectiveness of the proposed control strategies, simulation tests are carried out using MATLAB and Simulink with different irradiations modes.

IV.2 Configurations of grid-connected PV system

The energy of PV system usually has different output characteristics, and for this reason, a power-conditioning interface between the PV system and the grid is required to match the characteristics of the PV system and the requirements of the grid connections such as voltage, frequency, active and reactive power control, harmonic minimization [13][14]. The three-level inverters are attractive topologies for both high-power and low-power PV systems due to the outstanding efficiency and lower THD compared with the conventional two level inverter [15]. The configurations of PV systems can be divided into an AC module, string, multi-string, and central configurations depending on the rated power of the PV system. Typically, neutral point clamped (NPC) inverter topology is widely used for from a string inverter configuration of small power to a central inverter configuration of high power. A typical grid-connected PV system has more than one power-processing stage as shown in Figure IV.1. The first stage is usually a DC–DC boost converter, which draws the maximum available power from the PV system by incorporating MPPT, and it boosts in the DC-link-voltage level. The output of this stage is inverted using a three-level NPC inverter before feeding to the grid.

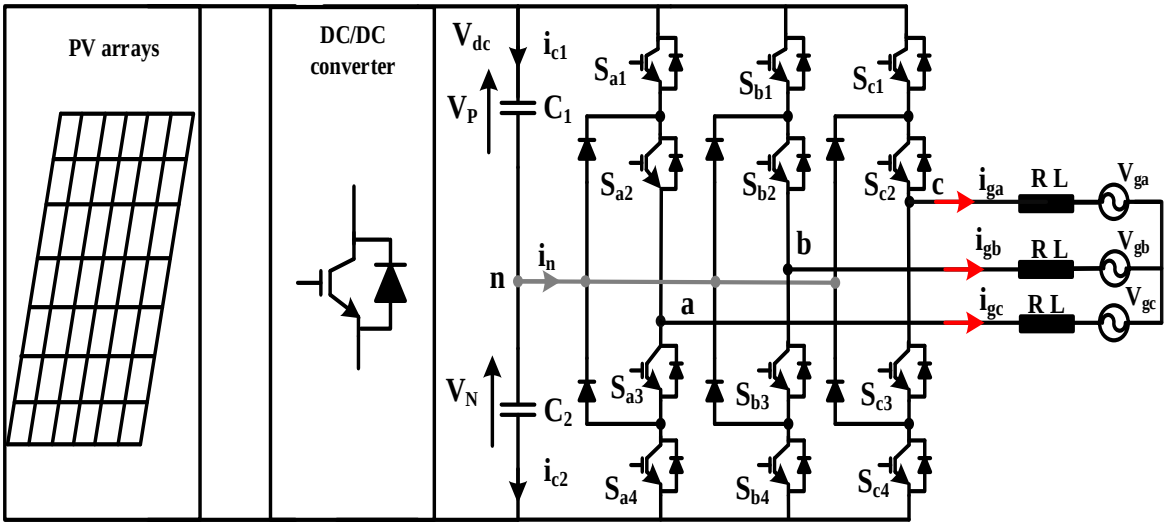

Figure IV.1: Three-phase three-level NPC grid-connected PV system.

IV.3 Modeling the PV power conversion chain

IV.3.1 Photovoltaic array model

A photovoltaic cell is basically a p-n semiconductor junction diode which converts solar irradiation into electricity. It is constituted of a light generated current source, a parallel diode, a parallel resistance, and a series resistance. Photovoltaic cells are grouped together in order to form photovoltaic modules [16][17], which are combined in series and parallel to provide the desired output power as shown in Figure IV.2.

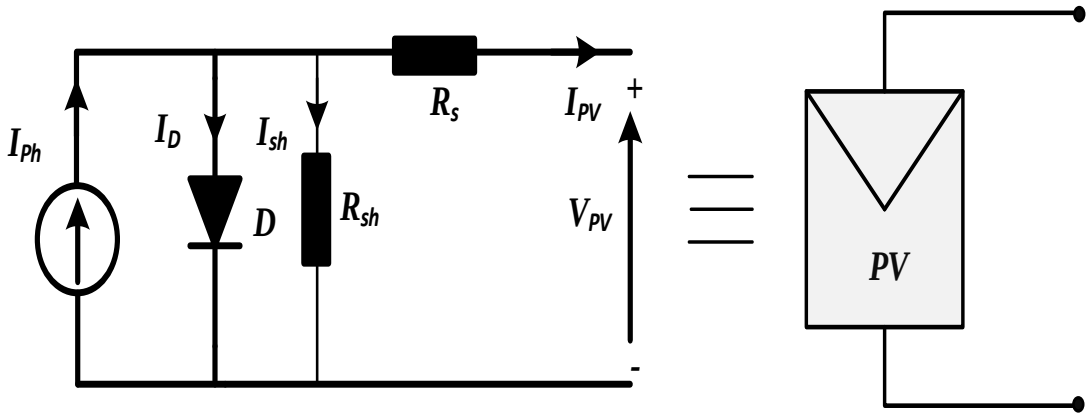

Figure IV.2: Simplified equivalent circuit of solar cell

From the equivalent circuit it is evident that the current produced by the solar cell is equal to that produced by the current source, minus that which flows through the diode, minus that which flows through the shunt resistor:

$$I_{PV} = I_{ph} - I_D - I_{sh} \tag{IV.1}$$

The current through these elements is governed by the voltage across them:

$$V_j = V + R_s I \tag{IV.2}$$

By the Shockley diode equation, the current diverted through the diode is:

$$I_D = I_0 \left\{ \exp\left[\frac{qV_j}{nkT} \right] - 1 \right\} \tag{IV.3}$$

By Ohm's law, the current diverted through the shunt resistor is:

$$I_{sh} = \frac{V_j}{R_{sh}} \tag{IV.4}$$

Substituting these into the first equation produces the characteristic equation of a solar cell, which relates solar cell parameters to the output current and voltage:

$$I_{PV} = I_{ph} - I_0 \left[\left(\exp\left(q \frac{V + R_s I}{nkT} \right) \right) - 1 \right] - \frac{V + R_s I}{R_{sh}} \tag{IV.5}$$

where I is the solar-cell output current(A), V is the solar cell output voltage (V), I_{PV} is the light generated current(A), I_0 is the cell reverse saturation current(A), q is the electronic charge q=1.6×10^{-19}C, n the dimensionless factor, k is Boltzmann's constant k=1.3807×10^{-23}JK^{-1}, T is the cell temperature (K), R_s is the series resistance (Ω), and R_{sh} is the parallel resistance (Ω).

As the solar irradiance varies over time and depending on the climatic conditions, the power output also varies. The performance of a photovoltaic cell is presented by its I-V and P-V curves which are produced for several irradiance levels and several cell temperature levels. The variation of current and power versus voltage curve under various irradiation levels and temperatures are shown in Figure IV.3. The power conversion capacity is reduced in only two cases: raising the cell temperature and low sunlight. MPPT technique based on P&O method

has been used interestingly in PV systems is developed to identify the MPP; the electrical specification is shown in Table A.2.

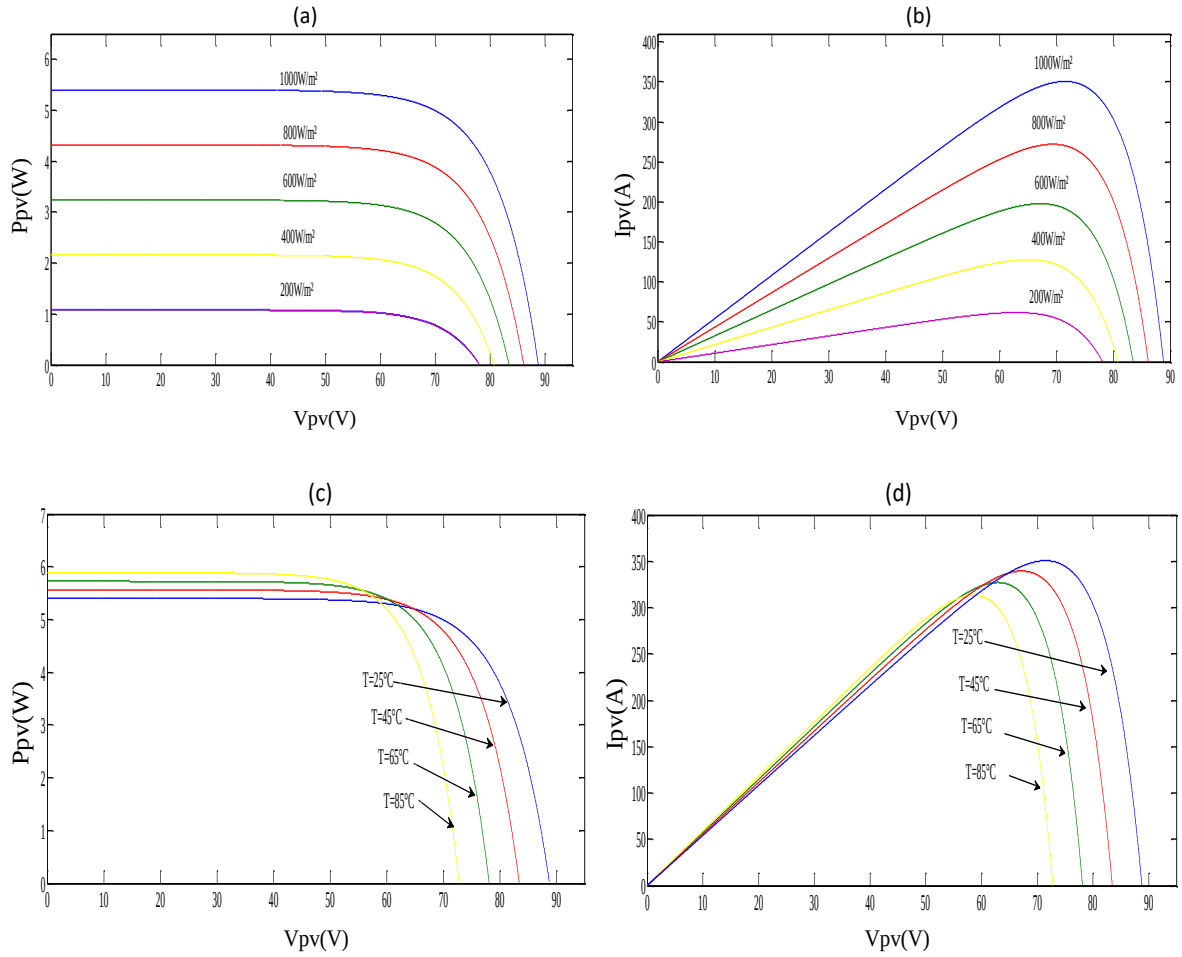

Figure IV.3: (a) P-V characteristic variable irradiance, (b) I-V characteristic variable irradiance, (c) P-V characteristic variable temperature, (d) I-V characteristic variable temperature.

IV.3.2 DC-DC boost converter model

The DC-DC power converter is necessary to the photovoltaic generating process as though it insure the adaptation of a photovoltaic array panel and the load. In this field, various DC-DC converters are realized like the Buck converter, the Boost converter and the Buck-Boost converter. The use and the choice of the required one depend on desired performance criteria. In this framework, the DC-DC converter is connected to the PV array panel, in order to track the maximum power generation. In this instance, we adopt a boost converter as the required DC-DC power one as shown in Figure IV.4.

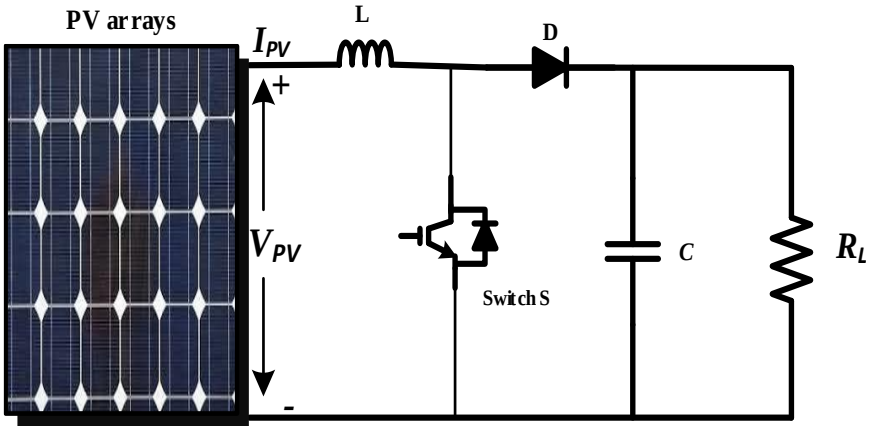

Figure IV.4: DC-DC boost converter.

The equivalent circuit of the boost converter during two switching cases is shown in Figure IV.5, where the operating principle is divided into two different parts depending on the state of the switch.

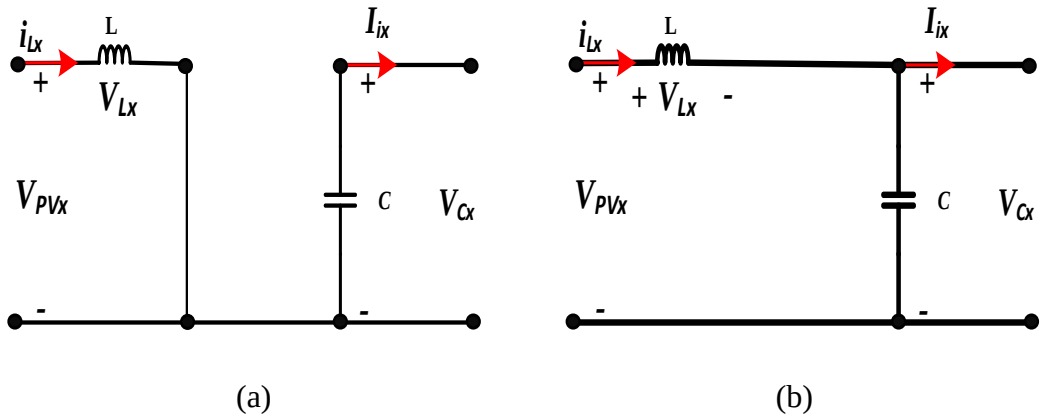

Figure IV.5: Equivalent DC-DC boost converter circuits. (a**)** switch ON. (b**)** switch OFF.

When the switch *S* is ON (*S* = 1), the boost converter can described as follows:

$$\begin{cases} L\dfrac{di_{Lx}(t)}{dt} = V_{PVx}(t) \\ C\dfrac{dV_{cx}(t)}{dt} = -i_{ix}(t) \end{cases} \quad x = 1,2,3,4 \tag{IV.6}$$

where i_{Lx} , V_{PVx} and V_{cx} are the inductor current, the PV voltage and DC-link capacitor voltage, respectively. When the switch S is Off (S=0), the boost converter equations is expressed as:

$$\begin{cases} L\dfrac{di_{Lx}(t)}{dt} = V_{PVx}(t) - V_{cx}(t) \\ C\dfrac{dV_{cx}(t)}{dt} = i_{Lx}(t) - i_{ix}(t) \end{cases} \quad \text{(IV.7)}$$

Equations (IV.6) and (IV.7) can be rewritten in term of boost switch control S as:

$$\begin{cases} L\dfrac{di_{Lx}(t)}{dt} = -(1-S)V_{PVx}(t) - V_{cx}(t) \\ C\dfrac{dV_{cx}(t)}{dt} = (1-S)i_{Lx}(t) - i_{ix}(t) \end{cases} \quad \text{(IV.8)}$$

By approximating the derivatives in (IV.8) using Euler forward method, the discrete time model of the DC-DC boost converter considering the sampling time T_{sc} is given as follows:

$$\begin{cases} i_{Lx}(k+1) = \dfrac{T_{sc}}{L}((S-1)V_{PVx}(k) - V_{cx}(k)) + i_{Lx}(k) \\ V_{cx}(k+1) = \dfrac{T_{sc}}{C}((1-S)i_{Lx}(k) - i_{ix}(k)) + V_{cx}(k) \end{cases} \quad \text{(IV.9)}$$

IV.4 Proposed system controllers

The block diagram of different control strategies applied for a three-level NPC inverter grid connected PV system is shown in Figure IV.6. To increase efficiency and decrease the cost of PV system, it is needed to operate PV panels at MPP (Maximum Power Point). Numerous MPPT algorithms developed in literature for example Perturb & Observe (P&O) [18][19]. A perturb and observe MPPT algorithm is used to obtain the reference DC-link voltage as shown in Figure IV.6 (a). Due to the intermittent nature of PV system, the generated power has a variable nature. The DC-link plays an important role in transferring this variable power from PV system to the grid. The error between the measured DC-link voltage V_{dc} and the reference V^*_{dc} is used to control the output active current of the inverter, at the same time, the unbalanced reactive power can be compensated, also is used to maintain the DC-link voltage at a specified value, the control of this inverter requires the estimation of reference active and reactive power components injecting currents as shown in Figure IV.6 (b). Furthermore, the DC to AC

conversion requires that the current injected to the grid presents low harmonic distortion, with the ability to achieve a unity power factor, and to exhibit robustness properties in front of system's perturbations such as radiance changes or load variations. As a consequence, the design of a control technique becomes of high interest for interconnection of PV units to the power grid as shown in Figure IV.6 (c). The performance of the proposed predictive algorithms approach is compared in detail with the classical MPC to emphasise the merits.

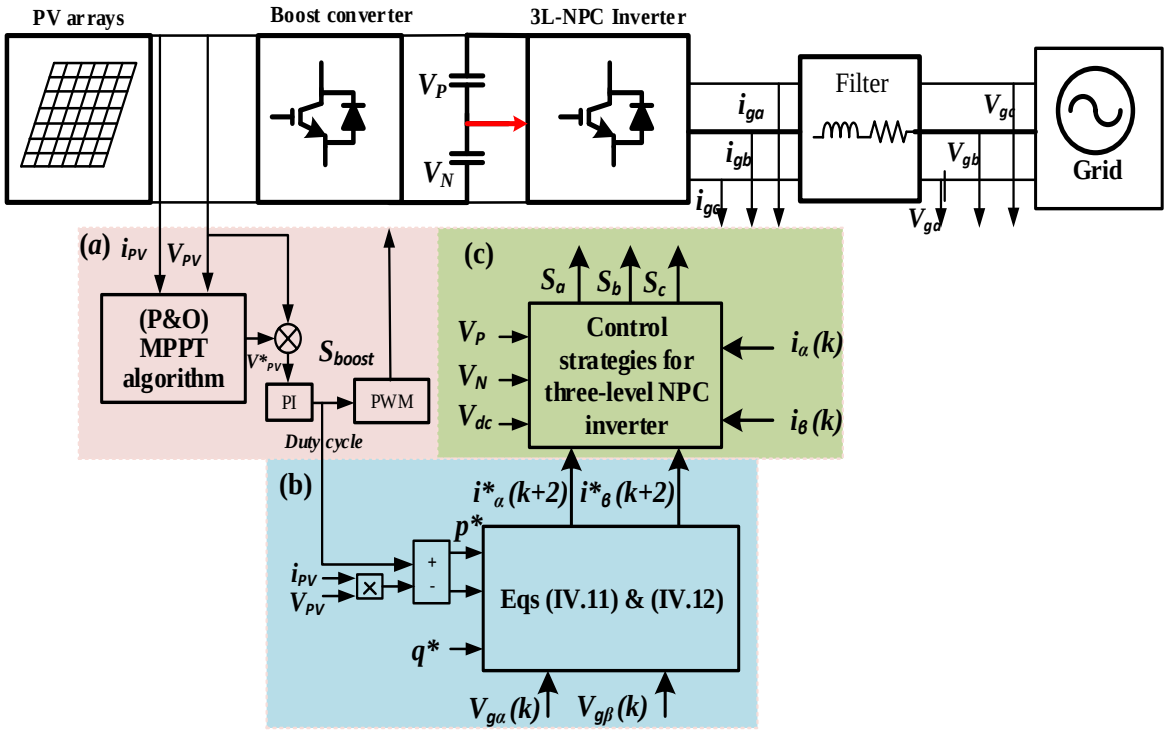

Figure IV.6: Block diagram of grid connected PV system three-level NPC inverter with reference current generation.

IV.4.1 Maximum power point tracker control

Maximum power utilization of photovoltaic (PV) power sources at any given time, to extract the maximum power generated by a solar cell, the solar system has to be equipped with a maximum power point tracker. It helps to operate the PV system at the maximum output power point for a given set of conditions, thereby maximizing the array efficiency [20]. The MPPT does this by constantly controlling the PV voltage or current independently regardless of the load connected [21]. The MPPT technology is commonly implemented in the DC-DC converters, but due to technological advancements in recent times, now it can also be

implemented in the DC-AC inverters. Although, several MPPT methods are available, the most commonly practiced is perturb and observe so it will be used in our present study.

The problem considered by MPPT methods is to automatically find the voltage V_{MPP} or current I_{MPP} at which a PV array delivers maximum power under a given temperature and irradiance. In P&O method, the MPPT algorithm is based on the calculation of the PV output power and the power change by sampling both the PV Array current and voltage. The tracker operates by periodically incrementing or decrementing the solar array voltage [22]–[24]. If a given perturbation leads to an increase (decrease) in the output power of the PV, then the subsequent perturbation is generated in the same (opposite) direction. The duty cycle of the DC chopper is varied and the process is repeated until the maximum power point has been reached. Actually, the system oscillates about the MPP. Reducing the perturbation step size can minimize the oscillation. However, small step size slows down the MPPT. For different values of irradiance and cell temperatures, the PV array would exhibit different characteristic curves. Each curve has its maximum power point. It is at this point, where the corresponding maximum voltage is supplied to the converter. Figure IV.7 shows the flowchart of P&O MPPT technique.

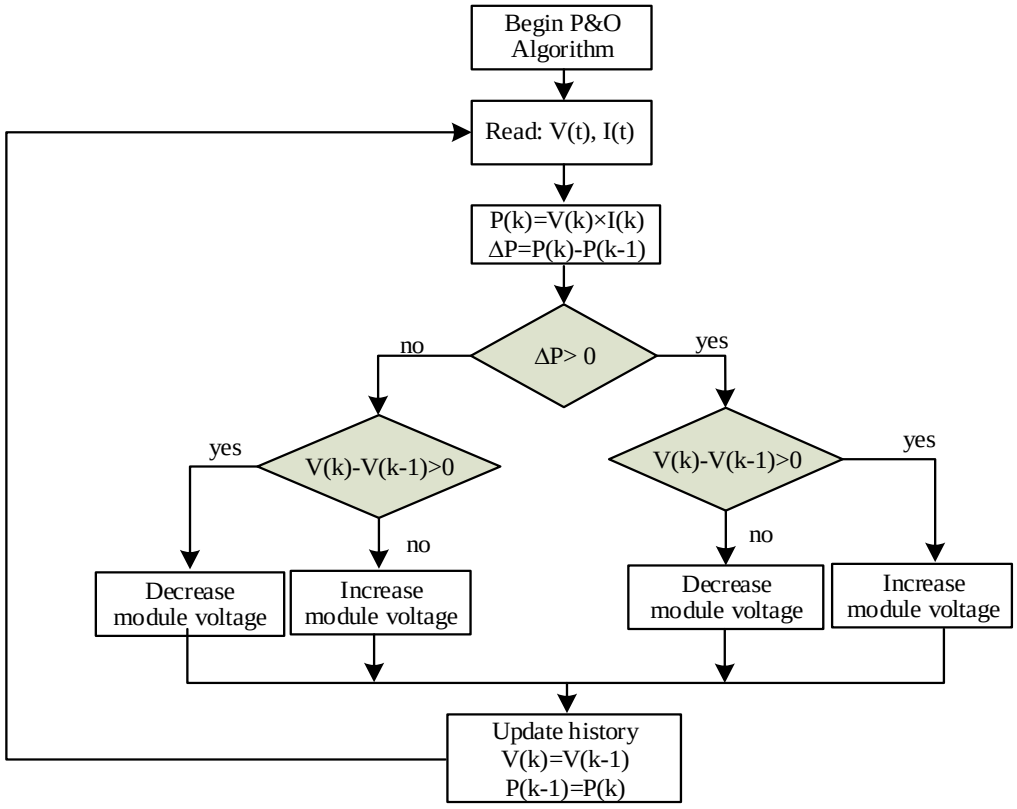

Figure IV.7: Flowchart of P&O MPPT technique.

IV.4.2 Boost control

The double loop control method of voltage and current is achieved for the boost converter by controlling the voltage of the PV to its reference V^*_{PV} provided by perturbed and observed MPPT algorithm [25]. The output of the voltage loop controller and the PV current compensation deliver the current reference i^*_{PV} of the inner loop current controller. Whereas the current control loop and the PV voltage compensation give the duty cycle of the converter as indicated by:

$$\begin{cases} i^*_{PV} = i_{PV} - PI\left(V^*_{PV} - V_{PV}\right) \\ D^* = 1 - \left(V_{PV} - PI\left(i^*_{PV} - i_{PV}\right)\right)/V_{dc} \end{cases} \quad \text{(IV.10)}$$

IV.4.3 The reference active and reactive components of injecting currents

In this section, the control of the three-level NPC inverter is realized by adjusting the reference of the power $S^* = P^* + j\,Q^*$ supplied to the grid. Notice that the current reference of the inner control loop can be obtained through the active power and reactive power references (i.e., P^* and Q^*) [26], as shown in Figure IV.6, The reference currents $i^*_{g\alpha}$ and $i^*_{g\beta}$ are calculated as:

$$\begin{cases} i^*_{g\alpha}(k) = \dfrac{2}{3}\left(\dfrac{V_{g\alpha}(k)P^*(k) + V_{g\beta}(k)Q^*(k)}{V^2_{g\alpha}(k) + V^2_{g\beta}(k)}\right) \\ i^*_{g\beta}(k) = \dfrac{2}{3}\left(\dfrac{V_{g\beta}(k)P^*(k) - V_{g\alpha}(k)Q^*(k)}{V^2_{g\alpha}(k) + V^2_{g\beta}(k)}\right) \end{cases} \quad \text{(IV.11)}$$

The reference currents obtained are extrapolated to estimate the currents in $(k+2)^{th}$ sample by using Lagrange extrapolation [27] approach as given below:

$$i^*_{g\alpha\beta}(k+2) = 6i^*_{g\alpha\beta}(k) - 8i^*_{g\alpha\beta}(k-1) + 3i^*_{g\alpha\beta}(k-2) \quad \text{(IV.12)}$$

These reference currents are traced by applying an appropriate switching state to the inverter. However, from the perspective of three-level NPC inverter, the DC-link capacitor voltage balancing is also an equally important objective.

IV.4.4 Modeling and control DC-AC inverter

Inverter technology is the key technology to have reliable and safe grid interconnection operation of the PV system. It is also required to generate high-quality power to actuality system with reasonable cost. To meet these requirements, updated technologies of power electronics are applied for PV inverters such as three-level NPC inverter. The schematic diagram of control strategies of three-level NPC inverter is shown in Figure IV.2 (c), where V_{gabc} and i_{gabc} are the grid voltages and currents of each phase, while L_f and R_f are the parameters of the output filter, V_n is the inverter voltage vectors, and V_P and V_N are the DC-link voltages of capacitors C_1 and C_2, respectively. Therefore, under steady state operation, the dynamic of the grid currents can be modeled by the following equation:

$$\frac{di_g}{dt} = -\frac{R}{L} i_g + \frac{1}{L}\left(V_n - V_g\right) \tag{IV.13}$$

Equation (IV.13) is discretized using the zero-order hold method, considering a sampling period T_s:

$$i_{g\alpha\beta}(k+1) = a_d i_{g\alpha\beta}(k) + b_d\left(V_{n\alpha\beta}(k) - V_{g\alpha\beta}(k)\right) \tag{IV.14}$$

Being $a_d = e^{-\frac{R}{L}T_s}$, and $b_d = \frac{1}{R}(1 - e^{-\frac{R}{L}T_s})$.

In addition, the discrete-time model of the DC-link capacitor voltages is discussed in chapter II in (II.9) as:

$$\begin{cases} V_P(k+1) = V_P(k) + \dfrac{1}{C} i_{C1}(k) T_s = V_P(k) + \dfrac{1}{2C} i_O(k) T_s \\ V_N(k+1) = V_N(k) + \dfrac{1}{C} i_{C2}(k) T_s = V_N(k) - \dfrac{1}{2C} i_O(k) T \end{cases} \tag{IV.15}$$

According to the description in chapter II. The new reference voltage vector $V_\alpha^*(k+2)$ and $V_\beta^*(k+2)$ can be obtained as:

$$\begin{cases} V_{\alpha n}^*\left(k+1\right) = L\left[i_\alpha^*\left(k+2\right) - i_\alpha\left(k+1\right)\right]/T_s + R i_\alpha\left(k+1\right) + V_{g\alpha}(k) \\ V_{\beta n}^*\left(k+1\right) = L\left[i_\beta^*\left(k+2\right) - i_\beta\left(k+1\right)\right]/T_s + R i_\beta\left(k+1\right) + V_{g\beta}(k) \end{cases} \tag{IV.16}$$

The inherent variable switching frequency computational burden are other issues that need careful consideration. These issues resulted a wide harmonic spectrum that extends from the fundamental frequency to half of the sampling frequency, as discussed in chapter (III) the modulated model predictive control M²PC it was a good solution for this issues. Hence, the main control objectives of the proposed control methods for three-level NPC grid-connected PV system are the reference current tracking and DC-link capacitor voltage balancing. The control block diagram of the proposed predictive techniques, which has been implemented on the three-level NPC grid-connected PV system, is shown in Figure IV.8.

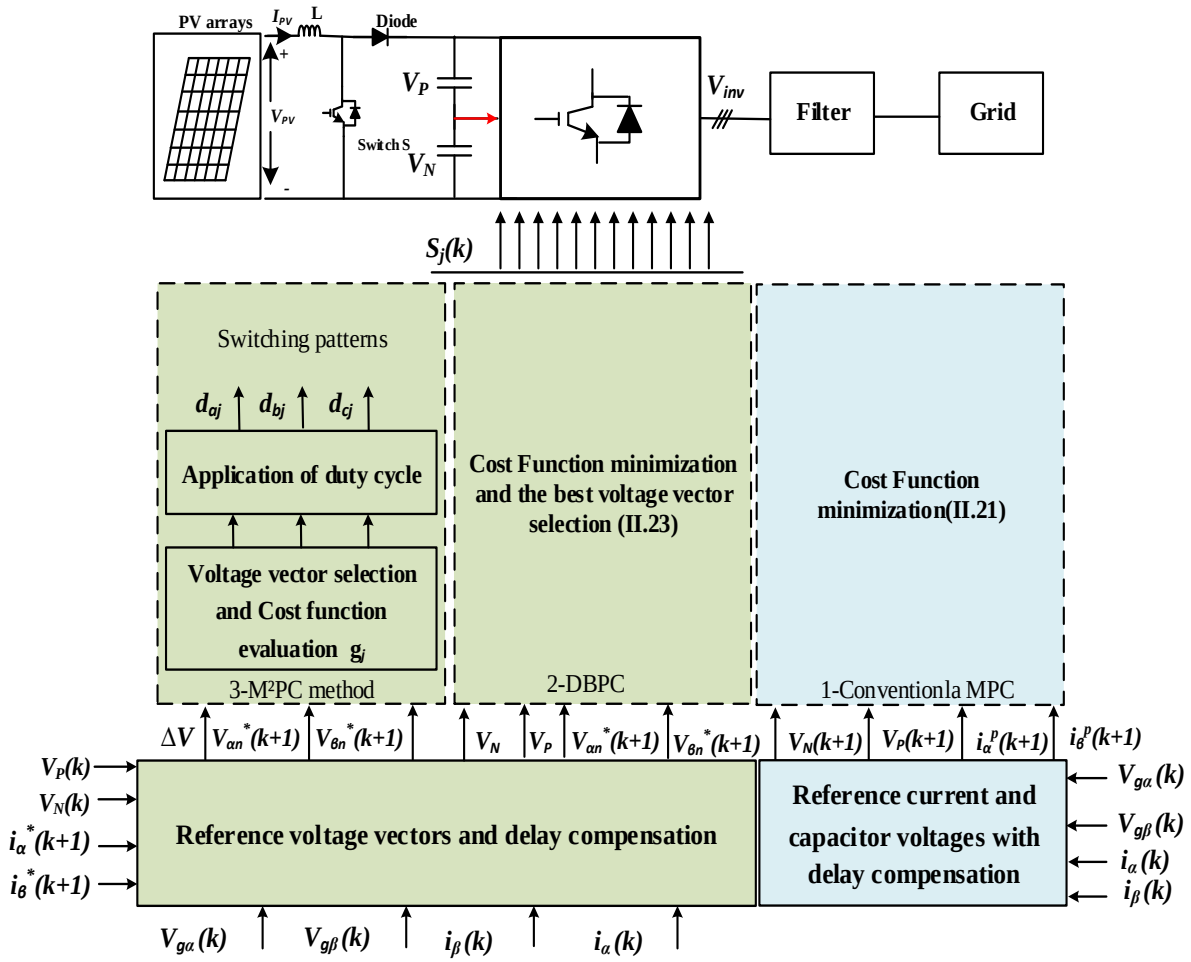

Figure IV.8: The control block diagram of grid connected three-level NPC inverter.

IV.5 Simulation results

In order to validate the effectiveness of the proposed control strategies for three-level NPC inverter grid-connected PV system, the whole control scheme were carried out using MATLAB/Simulink where the parameters for PV system, boost converter and the R_g, L_g filter are illustrated in Table A.2. Where the MPPT algorithm by P&O is used to control the DC / DC converter, while the competing MPC algorithms technique is used for the control the three-level NPC inverter (see Figure IV.8). To illustrate this performance, a stepped solar irradiance profile, as shown in Figure IV.9. The performance of the proposed system is tested under static and dynamic operating regimes.

The performance of proposed control strategies applied of the three-level NPC grid-connected PV system is compared in the steady-state operation. The simulation results corresponding to the steady-state operation of the conventional MPC, 3 vectors-based DB control, and M²PC control are shown in Figure IV.10.

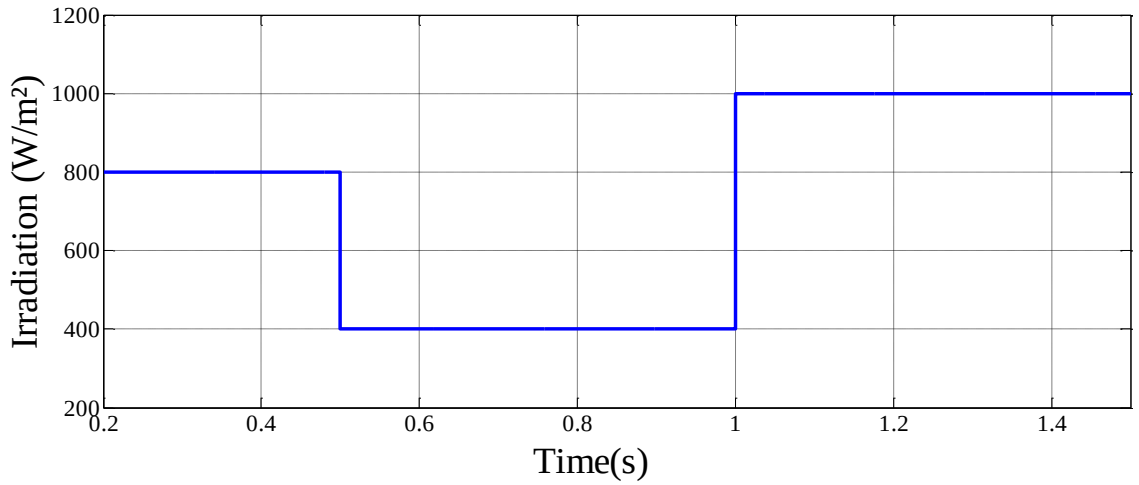

Figure IV.9: Evaluation of irradiations.

Figure IV.10 (a), (b), and (c) shows the simulation waveforms of the inverter output currents i_{ga} , i_{gb}, and i_{gc}, the capacitor voltages V_P and V_N, and the harmonic spectrum of phase-a current for conventional and the three voltage-based DB predictive controller and nine-segments based M²PC method. From the simulation results, it can be seen that the M²PC method get more accurate current with THD=2.23% compared by the 3 vectors-based DB predictive and conventional MPC, also it can effectively regulate the NP voltage without using the weighting factor.

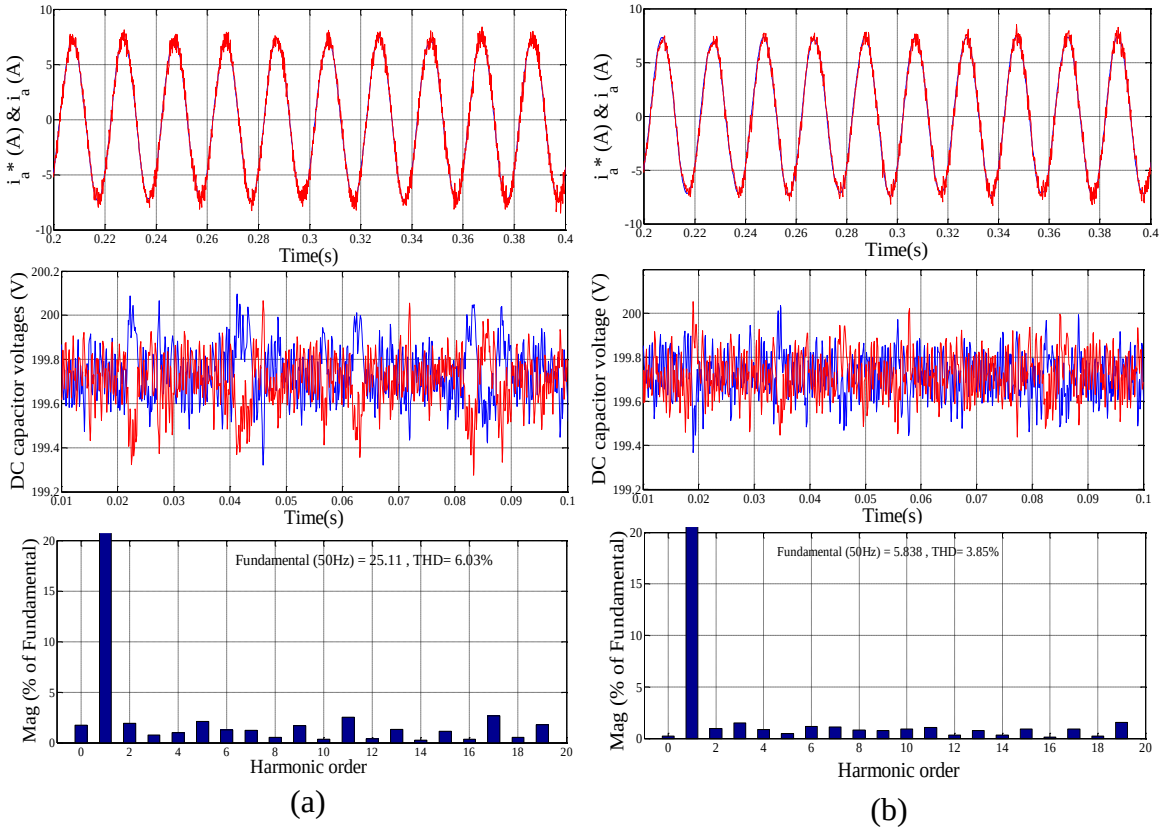

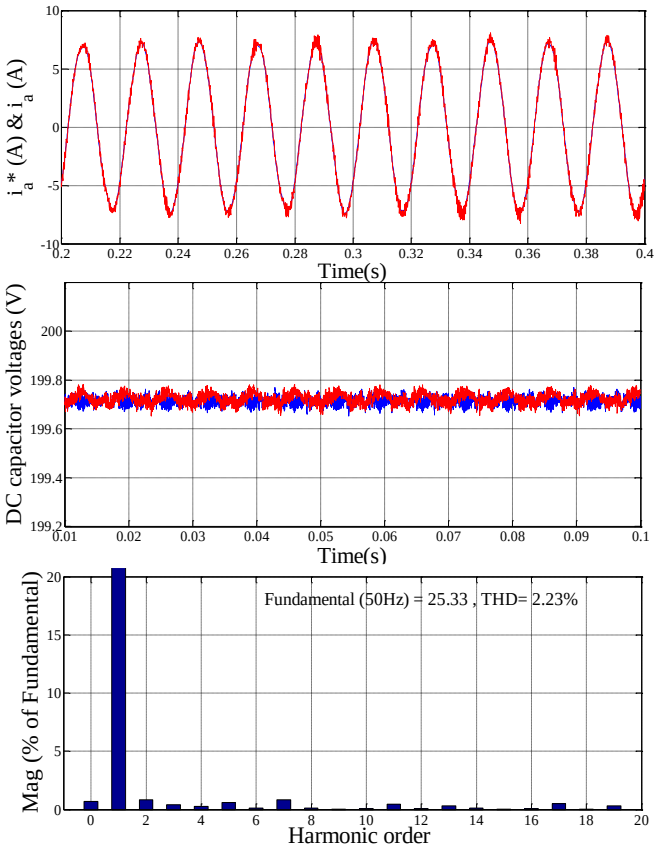

Figure IV.10: Steady-state simulation results for three-level NPC grid connected PV system after inserting the PV generator at E =1000W / m². (a) Conventional MPC. (b) 3 vectors-based DB control. (c) Nine-segments based M²PC method.

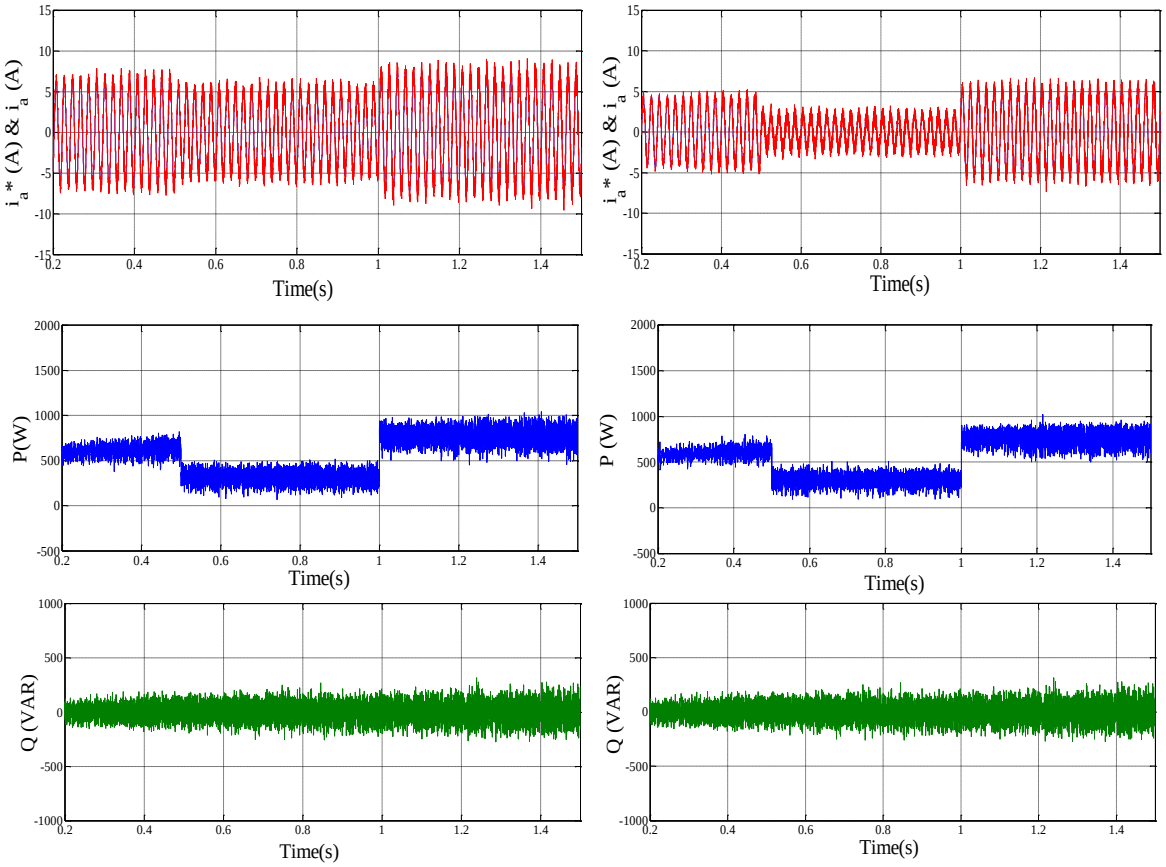

(a) (b)

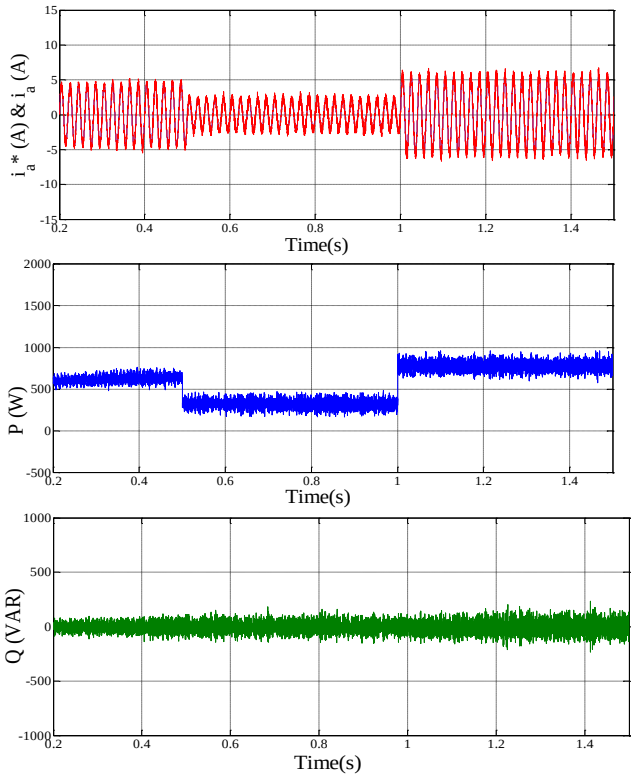

(c)

Figure IV.11: Simulation results of proposed control methods with different irradiation values. (a) Conventional MPC, (b) 3V-based DB predictive control, (c) Nine-segments based M²PC method.

As shown in Figure IV.11, a sudden decrease in solar irradiation from 800 to 400 W/m² at instant 0.5 s is applied. The grid currents track their references in both three-vectors based DB predictive control and M²PC methods accurately (Figure IV.11 (a) and (b)), and the M²PC method has the lowest THD compared by the other method, on the other hand, it can be seen clearly that active and reactive power follow their references perfectly with less oscillation for M²PC method. Then, a large sudden increase in the solar irradiation from 400 to 1000 W/m² at instant 1 s is performed, it can be seen clearly that the M²PC method has the best accuracy tracking compared to the other methods.

The computational burden required by the proposed algorithms are given as 97μs for the conventional MPC, 40μs for 3 vectors-based DB predictive controller, 20μs of nine-segment based M²PC method. As shown in Table IV.1, it can be observed that the execution time of the nine-segments is reduced by nearly 80%, which greatly reduces the computational burden compared with conventional MPC.

Table IV.1: Computational burden comparison of the proposed system

Methods	**Computational burden**
Conventional MPC	97μs
3-V DB predictive control	40μs
Nine-segments based M²PC	20μs

IV.6 Conclusion

This chapter presents the performance for three control strategies applied for three-level NPC grid-connected PV system. The MPPT control based on P&O method, have been investigated. The theoretical background is described, and the advantages and disadvantages of each application are studied through analyses and a series of simulations. A comprehensive comparison and evaluation are implemented for the four methods from several aspects such as algorithm complexity, steady state performance, current THD, computational burden, and NP voltage balance. The results show that the M²PC method can provides best steady state and dynamic performance compared to the conventional MPC methods.

IV.7 Chapter references

[1] A. Mora, R. Cárdenas-Dobson, R. P. Aguilera, A. Angulo, F. Donoso, and J. Rodriguez, "Computationally Efficient Cascaded Optimal Switching Sequence MPC for Grid-Connected Three-Level NPC Converters," *IEEE Trans. Power Electron.*, vol. 34, no. 12, pp. 12464–12475, 2019.

[2] P. Santis, D. Sáez, R. Cárdenas, and A. Núñez, "Pareto-Based Modulated Model Predictive Control Strategy for Power Converter Applications," *Electr. Power Syst. Res.*, vol. 171, no. September 2017, pp. 158–174, 2019.

[3] J. Rodriguez, S. Bernet, P. K. Steimer, and I. E. Lizama, "A Survey on Neutral-Point-Clamped Inverters," *IEEE Trans. Ind. Electron.*, vol. 57, no. 7, pp. 2219–2230, 2010.

[4] F. Katiraei and M. R. Iravani, "Transients of a Micro-Grid System with Multiple Distributed Energy Resources," *Proc. Int. Conf. Power Syst. Transients 2005 (IPST 2005)*, pp. 1–6, 2005.

[5] J. Selvaraj and N. A. Rahim, "Multilevel Inverter For Grid-Connected PV System Employing Digital PI Controller," *IEEE Trans. Ind. Electron.*, vol. 56, no. 1, pp. 149–158, 2009.

[6] M. Pickl and S. Aramco, "The Future of Offshore Oil Drilling-An Evaluation of the Economic, Environmental and Political Consequences of the Deepwater Horizon Incident," *Energy Environ.*, vol. 23, no. May, 2016.

[7] S. R. Bull, "Renewable Energy Today and Tomorrow," *Proc. IEEE*, vol. 89, no. 8, 2001.

[8] D. La Manna, V. Li Vigni, E. Riva Sanseverino, V. Di Dio, and P. Romano, "Reconfigurable Electrical Interconnection Strategies for Photovoltaic Arrays: A Review," *Renew. Sustain. Energy Rev.*, vol. 33, pp. 412–426, 2014.

[9] C. E. Chamberlin, P. Lehman, J. Zoellick, and G. Pauletto, "Effects of Mismatch Losses in Photovoltaic Arrays," *Sol. Energy*, vol. 54, no. 3, pp. 165–171, 1995.

[10] M. C. Alonso-García, J. M. Ruiz, and W. Herrmann, "Computer Simulation of Shading Effects in Photovoltaic Arrays," *Renew. Energy*, vol. 31, no. 12, pp. 1986–1993, 2006.

[11] D. H. W. Li, K. L. Cheung, T. N. T. Lam, and W. W. H. Chan, "A Study of Grid-

Connected Photovoltaic (PV) System in Hong Kong," *Appl. Energy*, vol. 90, no. 1, pp. 122–127, 2012.

[12] R. Wai and W. Wang, "Grid-Connected Photovoltaic Generation System," *IEEE Trans. Circuits Syst.*, vol. 55, no. 3, pp. 953–964, 2008.

[13] E. Romero-cadaval, G. Spagnuolo, and L. G. Franquelo, "Grid-Connected Photovoltaic Generation Plants," *Ieee Ind. Electron. Mag.*, no. September, pp. 6–20, 2013.

[14] S. Kouro, L. I. Jose, V. Dimitri, and L. G. Franquelo, "Grid-Connected Photovoltaic Systems: An Overview of Recent Research and Emerging PV Converter Technology," *Ieee Ind. Electron. Mag.*, no. March, pp. 47–61, 2015.

[15] H. Boumaaraf, A. Talha, and O. Bouhali, "A Three-Phase NPC Grid-Connected Inverter for Photovoltaic Applications Using Neural Network MPPT," *Renew. Sustain. Energy Rev.*, vol. 49, pp. 1171–1179, 2015.

[16] A. Massoud, "A Matlab / Simulink-Based Photovoltaic Array Model Employing SimPowerSystems Toolbox," *J. Energy Power Eng.*, pp. 1965–1975, 2012.

[17] A. Islam, N. Mohammad, and P. K. S. Khan, "Modeling and Performance Analysis of a Generalized Photovoltaic Array in Matlab," *2010 Jt. Int. Conf. Power Electron. Drives Energy Syst. 2010 Power India*, no. December 2017, 2010.

[18] J.M.Enrique, J.M.Andújar, and M.A.Bohórquez, "A Reliable , Fast and Low Cost Maximum Power Point Tracker for Photovoltaic Applications," *Sol. Energy*, vol. 84, pp. 79–89, 2010.

[19] M. G. Villalva, J. R. Gazoli, and E. R. Filho, "Comprehensive Approach to Modeling and Simulation of Photovoltaic Arrays," vol. 24, no. 5, pp. 1198–1208, 2009.

[20] D. P. Hohm, "Comparative Study of Maximum Power Point Tracking Algorithms Using an Experimental, Programmable, Maximum Power Point Tracking Test Bed," *Conf. Rec. Twenty-Eighth IEEE Photovolt. Spec. Conf. - 2000 (Cat. No.00CH37036)*, 2000.

[21] T. Esram and P. L. Chapman, "Comparison of Photovoltaic Array Maximum Power Point Tracking Techniques," *IEEE Trans. Energy Convers.*, vol. 22, no. 2, pp. 439–449, 2007.

[22] M. A. Elgendy, B. Zahawi, and D. J. Atkinson, "Assessment of Perturb and Observe MPPT Algorithm Implementation Techniques for PV Pumping Applications," *IEEE Trans. Sustain. Energy*, vol. 3, no. 1, pp. 21–33, 2012.

[23] J. J. Nedumgatt, K. B. Jayakrishnan, S. Umashankar, and D. Vijayakumar, "Perturb and Observe MPPT Algorithm for Solar PV Systems-Modeling and Simulation," *2011 Annu. IEEE India Conf., 2012.*

[24] H. A. Sher, A. F. Murtaza, A. Noman, K. E. Addoweesh, K. Al-haddad, and M. Chiaberge, "A New Sensorless Hybrid MPPT Algorithm Based on Fractional Short-Circuit Current Measurement," *IEEE Trans. Sustain. Energy*, vol. 6, no. 4, pp. 1426–1434, 2015.

[25] A. Sangwongwanich, Y. Yang, D. Sera, and F. Blaabjerg, "Mission Profile-Oriented Control for Reliability and Lifetime of Photovoltaic Inverters," *IEEE Trans. Ind. Appl.*, vol. 56, no. 1, pp. 601–6010, 2020.

[26] Z. Zhang, Y. Yang, M. Ruiqing, and F. Blaabjerg, "Zero-Voltage Ride-Through Capability of Single-Phase Grid-Connected Photovoltaic Systems," *Appl. Sci*, vol. 7, no. March, p. 315, 2017.

[27] M. Odavic, V. Biagini, P. Zanchetta, M. Sumner, and M. Degano, "One-Sample-Period-Ahead Predictive Current Control for High-Performance Active Funt Power Filters," *IET Power Electron.*, vol. 4, no. 4, pp. 414–423, 2011.

Chapter V

Conclusions and Future Work

In recent years, model predictive control shows a trend towards the research and development of the large, it has been successfully used for controlling power converters, including explicit control in an optimization framework via a mathematical model to predict future system behaviour and select appropriate control actions under a rolling horizon scheme. Moreover, the three-level neutral-point clamped (NPC) inverter structure is considered a good solution for high power due to its advantages: reduction of the total harmonic distortion (THD) and the common-mode voltage, and increasing the power level of inverter thanks to a decreased voltage applied to each component. In this thesis, we have investigated different control strategies based on MPC and deadbeat methods with delay compensation for three-level NPC inverter applications. We have demonstrated that the new proposed controllers can achieve better control performance in terms of power quality and dynamic response compared to the conventional MPC method. The main drawbacks of conventional MPC are the computational burden. The computational burden has been reduced by using the selection voltage vectors method. The modulated predictive control (M²PC) was introduced with the aim of improving the performance of conventional MPC and suppressing the variable switching frequency. Finally, the proposed deadbeat predictive controllers and M²PC method was the best solution for decrease the computational burden and improve the quality of currents. The last chapter presents the performance evaluation of proposed control strategies for three-level NPC grid-connected photovoltaic generation system applications for steady state and dynamic performance.

V.1 Summary of contributions

This chapter summarizes the results and outcomes of the research during the Ph.D. study. The major contributions and conclusions of this thesis are summarized as follows:

1. **An improved deadbeat predictive control based on voltage vector selection is presented to control three-level NPC inverter**

In this dissertation, the MPC strategy was employed to track the current while maintaining the voltage balance of DC-link capacitor and reducing the switching frequency for three-level NPC inverter. The principle of the proposed control scheme is to use the discrete time model to predict the behavior of the load current and DC-link capacitor voltages for all possible configurations of voltage vectors, conventional MPC requires evaluating the cost function for all the switching states of the three-level NPC inverter, thus requiring a high computational burden that consumes a lot of the calculations resources. In order to reduce the computational burden A deadbeat predictive controllers with different numbers of effective vectors, namely, 19 vectors-based, 6 vectors-based, and 3 vectors-based DB, are proposed and compared beside the conventional current-based model predictive control (MPC), In addition, the neutral-point voltage is balanced using the redundant voltage vectors. Furthermore, the improved DB predictive controllers can eliminate the weighting factors for balancing the NP voltage and takes full play of utilizing the negative and positive small voltage vectors to balance the NP voltage, which simplifies the control implementation. By using the 3 vectors-based DB predictive controller, it can be seen that the execution time is reduced by nearly 60% compared with the other two algorithms, which significantly reduces the computational resources for implementation.

2. **Modulated model predictive control M²PC for three-level NPC inverter with optimized switching pattern is investigated**

An M²PC formulation for three-level NPC inverter was presented in this thesis. This technique is proposed to overcome the limitations of conventional MPC approach with is typically characterized by a variable switching frequency, large output current ripple, and heavy computational burden. Both M²PC methods have perfect capability in the NP voltage balancing in the steady-state performance and dynamic response, while the proposed nine-segments based M²PC method owns the best value of the output current THD, lowest power losses, and best

efficiency. That means the increase in the number of segments switching led to improve the performance of the system.

3. **Application the proposed MPC strategies for three-level NPC grid-connected PV system**

Recently, the three-level NPC inverter have become an attractive solution for some application such as the grid-connected photovoltaic generation systems to due to low total harmonics distortion (THD), lower switching device stress, the efficiency of three-level NPC inverter is the highest among the two-level inverters. The proposed algorithms are applied for these systems, in order to prove the effectiveness of the new algorithms compared to the conventional MPC methods.

4. **Simulation and experimental studies are performed to verify the system operations**

Simulation studies firstly to verify the system operations in order to confirm the feasibility and effectiveness of all the proposed control strategies, all simulation studies were carried out in MATLAB/Simulink and SimPowerSystems toolbox. The predictive control algorithms are programmed using SFunction Builder Block for easy real time implementation. The simulation times have been revised on a large time-scale in order to show the efficiency independent with the transistorise. Then, we have validated experimentally to build up an understanding and awareness of each algorithm.

V.2 Future work

The future research works can be suggested as follows:

1. **Experimental results of the proposed methods for three-level NPC inverter applications.**

To provide convincing evidence for the proposed control strategy for the three-level NPC inverter applications, experimental test should be carried out and this is representing the main objective in order to bring the current line of research towards a wide acceptance and to validate/adjust the assumptions made along the design procedure as presented in the present manuscript.

2. Model predictive control using artificial neural network for power converters

Designing a new MPC method based on an artificial neural network. The artificial neural network (ANN) has emerged as an excellent solution for input-output mapping problems. The basic concept of ANN-MPC is to set up an ANN to replace the calculation process of the conventional MPC in controlling the actual operation of the power converter in real time. The heavy-duty computation in the conventional MPC is shifted to the off-line training process.

3. Implementation the proposed MPC algorithms on PLECS RT Box

Building all the proposed algorithms through The PLECS RT Box, Where, the RT box is a real-time simulator specially designed for power electronics applications. With numerous analog and digital input/output channels and FPGA embedded CPU cores it is a versatile processing unit for both real-time hardware-in-the-loop (HIL) testing and rapid control prototyping.

Appendices

Appendix A

A.1 Parameters and specifications

Table (A.1): Simulation an experimental configuration parameters

Parameter	Description	Value
V_{dc}	DC-link voltage(V)	80
C	DC-link bus capacitance(μF)	3300
L	Inductive filter(mH)	10
R	Resistance load(Ω)	10
f	Reference frequency(Hz)	50
f_s	Sampling frequency(kHz)	10

Table (A.2): Three-level NPC grid-connected PV system parameters

Parameter	Value
PV subsection electrical parameters	
Maximum power P_{mpp}	175W
Open-circuit voltage V_{oc}	44.4V
Short-circuit current I_{sc}	4.95A
Voltage at P_{mpp}	53.4V
Current at P_{mpp}	4.95
Number of cells connected in parallel Np	1
Number of cells connected in series Ns	36
Boost converter electrical parameters	
Input capacitor C	4700μF
Inductor L	10mH
DC-link capacitors value C	3300μF
Grid electrical parameters	
Grid inductance L	10mH
Grid resistance R	0.5
Grid peak voltage V_g	80 V(rms)
Grid frequency f	50Hz
Simulation parameters	
sampling time T_s	10μs
DC-link PI controller parameters	
Proportional gain K_P	0.45
Integral gain K_i	2.5

Appendix B

B.1 Clarke transformation

The alpha-beta transformation (also known as the Clarke transformation) is a mathematical transformation employed to simplify the analysis of three-phase circuits. The passage of the currents and voltages from the three-phase system *a*,*b*,*c* to the two-phase system *α*,*β* is carried out by the following matrices:

$$\left[f_{\alpha\beta} \right] = \left[T_{\alpha\beta} \right] \left[f_{abc} \right]$$

$$\left[f_{\alpha\beta} \right] = \left[T_{\alpha\beta} \right]^{-1} \left[f_{abc} \right]$$

$$\left[f_{\alpha\beta} \right] = \begin{bmatrix} f_{\alpha} \\ f_{\beta} \end{bmatrix} \qquad \left[f_{abc} \right] = \begin{bmatrix} f_{a} \\ f_{b} \\ f_{c} \end{bmatrix}$$

Similarly, variable *f* may be the currents and voltages, the transformation and its inverse are given by:

$$\left[T_{\alpha\beta} \right] = \frac{2}{3} \begin{bmatrix} 1 & -\frac{1}{2} & -\frac{1}{2} \\ 0 & \frac{\sqrt{3}}{2} & -\frac{\sqrt{3}}{2} \end{bmatrix} \qquad \left[T_{\alpha\beta} \right]^{-1} = \begin{bmatrix} 1 & 0 \\ -\frac{1}{2} & \frac{\sqrt{3}}{2} \\ -\frac{1}{2} & -\frac{\sqrt{3}}{2} \end{bmatrix}$$

B.2 Voltage vectors generation

Considering all possible combinations of the switching states among the three phases of the Three-level NPC inverter, 27 voltage vectors are produced. The inverter output voltage of three-level NPC inverter can be expressed with phase to neutral voltages as:

$$V = \frac{2}{3}\left(V_{an} + a.V_{bn} + a^2.V_{cn}\right)$$

Where V_{an}, V_{bn}, and V_{cn} are the inverter output voltages, and $a=e^{j2\pi/3}$ is the unitary vector.

The phase to neutral voltages V_{an}, V_{bn}, and V_{cn} of 3L-NPC inverter are calculated as a function of the DC-link voltage V_{dc} and switching states S_x.

$$V_{an} = S_a \frac{V_{dc}}{2}; V_{bn} = S_b \frac{V_{dc}}{2}; V_{cn} = S_c \frac{V_{dc}}{2}$$

where S_x represents the state of a leg and has three possible values: (N, O, P) with the index $x \in (a, b, c)$. For example, V_0, V_1, and V_2 can be generated by three different switching states (OOO), (PPP), and (NNN), the three zero voltage vectors can be expressed as:

$$V_0 = \frac{2}{3}\left(0 + a.0 + a^2.0\right) = 0$$

$$V_1 = \frac{2}{3}\left(\frac{V_{dc}}{2} + a.\frac{V_{dc}}{2} + a^2.\frac{V_{dc}}{2}\right) = 0$$

$$V_2 = \frac{2}{3}\left(-\frac{V_{dc}}{2} - a.\frac{V_{dc}}{2} - a^2.\frac{V_{dc}}{2}\right) = 0$$

The small voltage vectors V_3 to V_{14} can be generated by two different switching states, that is, they present redundant switching states, the switching state (POO) generates the small voltage vector V_3.

$$V_3 = \frac{2}{3}\left(\frac{V_{dc}}{2} + a.0 + a^2.0\right) = \frac{V_{dc}}{3}$$

Moreover, switching state (ONN) generates the small voltage vector V_4.

$$V_4 = \frac{2}{3}\left(0 - a.\frac{V_{dc}}{2} - a^2.\frac{V_{dc}}{2}\right) = \frac{V_{dc}}{3}$$

Outer vectors present no redundancies. The switching state (PON) generates the medium vector V_{16}.

$$V_{16} = \frac{2}{3}\left(\frac{V_{dc}}{2} + a.0 - a^2.\frac{V_{dc}}{2}\right) = \frac{V_{dc}}{\sqrt{3}} e^{j\pi/6}$$

The rest of the voltage vectors are calculated following the same procedure.

Appendix C

C.1 Experimental setup

In order to verify the feasibility and advantages of the proposed algorithms, an experimental test bench designed around a dSPACE card, is realized within Power Electronics and Renewable Energy Research Laboratory (PEARL), University of Malaya, Malaysia. The completely experimental setup and its associated measurement facilities are shown in Figure (C.1). Which includes a three-level NPC inverter powered by a DC power supply feeding an R-L load. The DS1104 board built around the TMS320F240 digital processor (DSP) is used to implement the competing MPC controllers. The switching signals of the semiconductor switching devices are generated using twelve digital outputs from the dSPACE. The power analyser WT500 (YOKOGAWA) is used for harmonic spectrum plotting and THD measurement. Figure (C.2) (a) and (b) show hardware design of the three-level NPC inverter and the design of current and voltage sensors which used to measure the dc-link voltages and output currents.

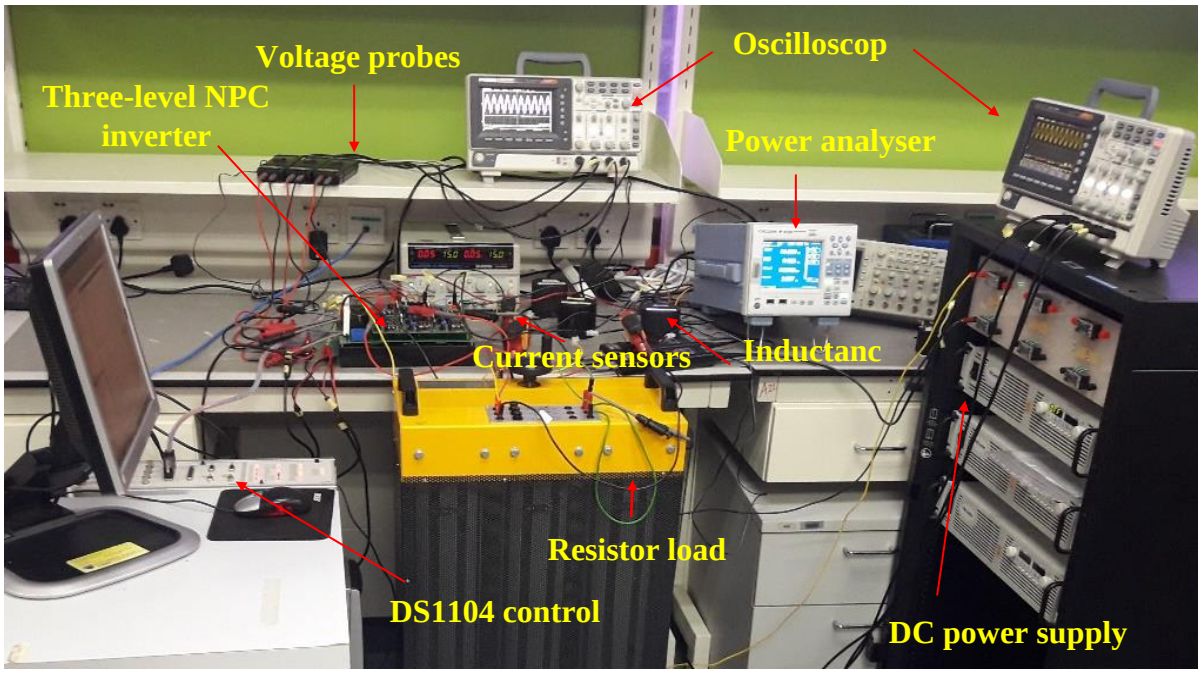

Figure (C.1). Experimental setup used for performance evaluation.

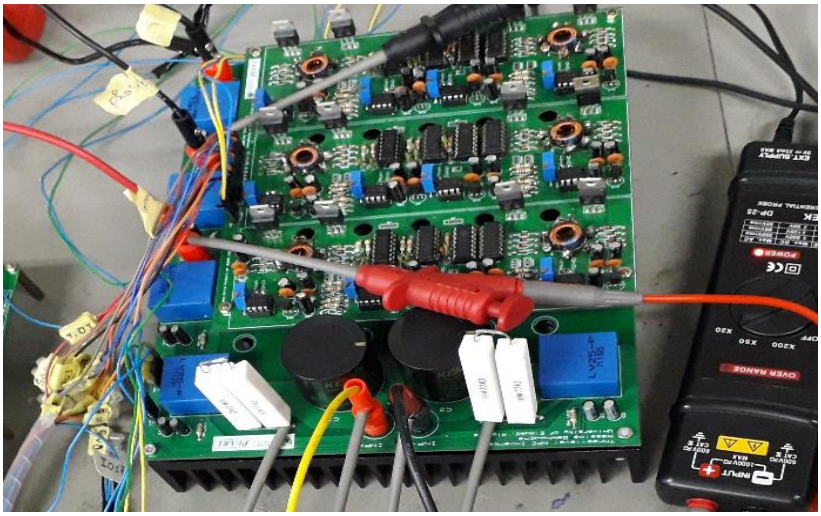

(a)

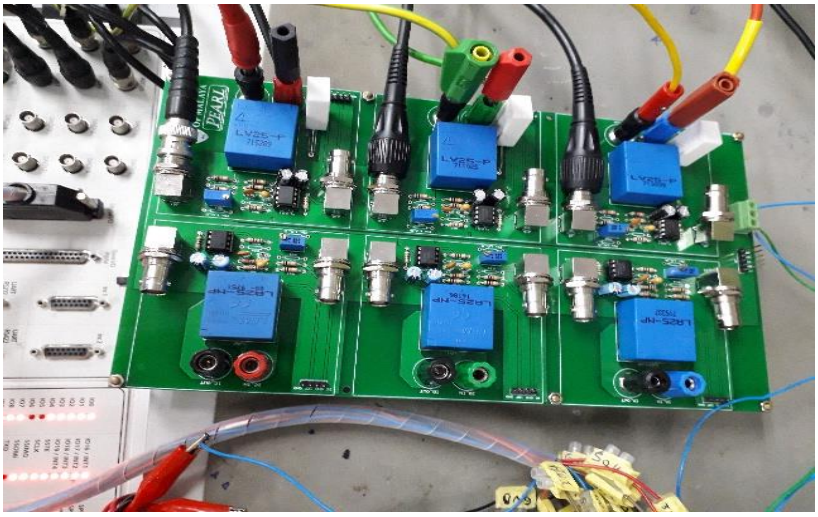

(b)

Figure (C.2). (a) Top view of the three-level NPC inverter with gate driver and heat sink, (b) Current and voltage sensors.

C.2 PCB design using PROTEUS software

PRTEUS is electronic designing-based software that used to make the design of any project and circuit before making it practical. There are numerous options available in this software that helps to design PCB and practical learning of different types of design tools. It is easy to use because of the graphical user interface (GUI) that is very similar to the real prototype board. Moreover, it can be used to design printed circuit board (PCB).

- **PCB design of three-level NPC inverter**

The three-level NPC inverter in this project is designed and tested in PROTEUS. The simulation model is associated to the component and must be available in the library of the software for circuit simulation. The schematic circuit of a three-level NPC inverter circuit with three current sensors and two voltage sensors is shown in Figure (C.3). The inverter is built using twelve SiC C2M0080120D Mosfets, six SiC C4D30120D diodes from CREE Inc, two capacitors, three LEM LA-25P, and two LEM LV-25NP, the sensor signals are sampled using five analog-to-digital-converter (ADC) inputs of the DS1104. The layout of the top and bottom sides of the three-level NPC inverter is shown in Figure (C.4) each layer will represent in different color for example top layer represented in blue color and bottom layer represented in yellow. The PCB hardware board of NPC inverter is shown in Figure (C.5).

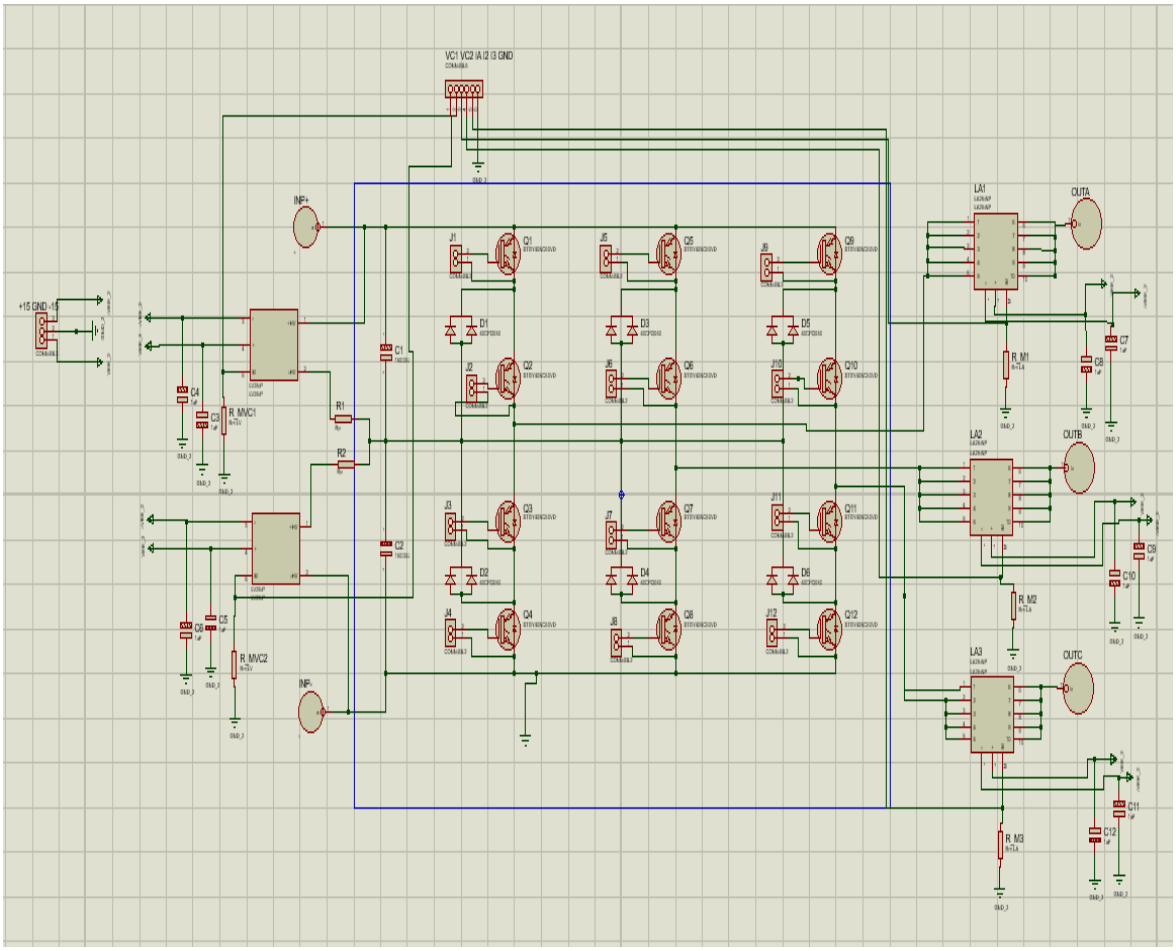

Figure (C.3): Schematic circuit of three-level NPC inverter circuit with three current sensors.

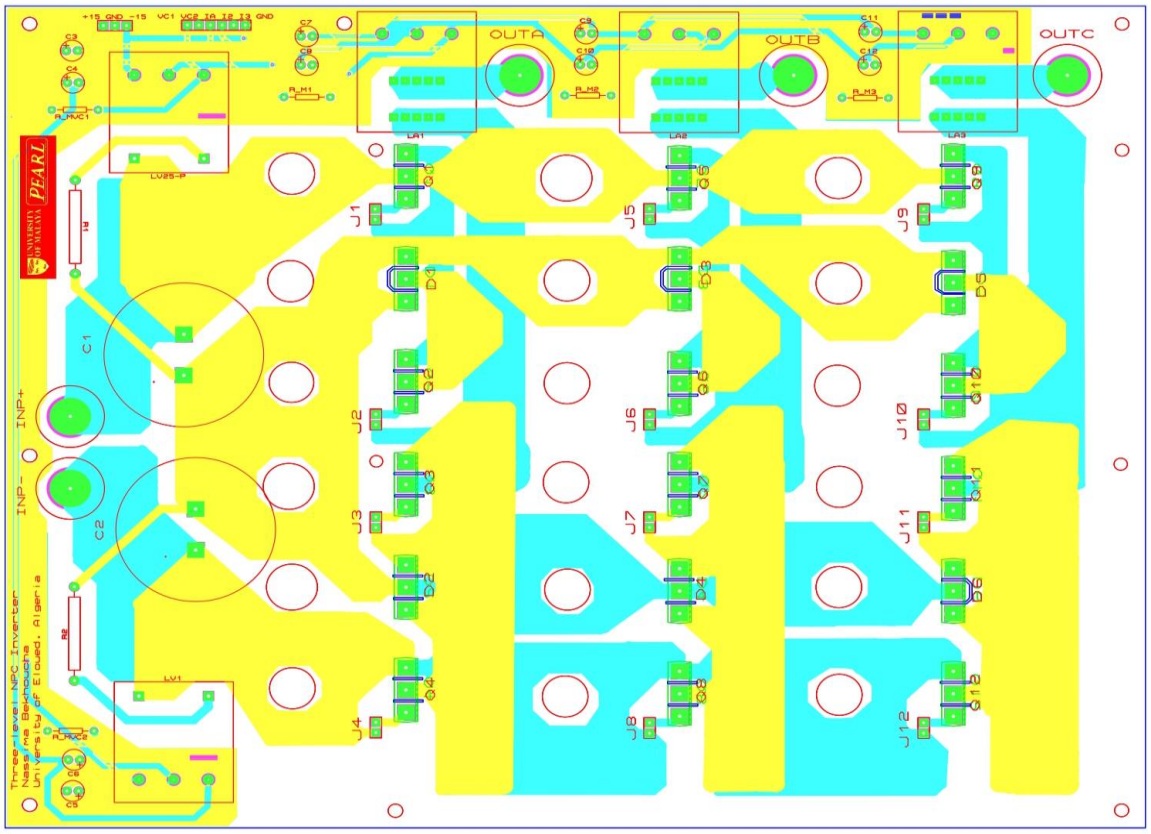

Figure (C.4): Layout of the top and bottom sides of the three-level NPC inverter.

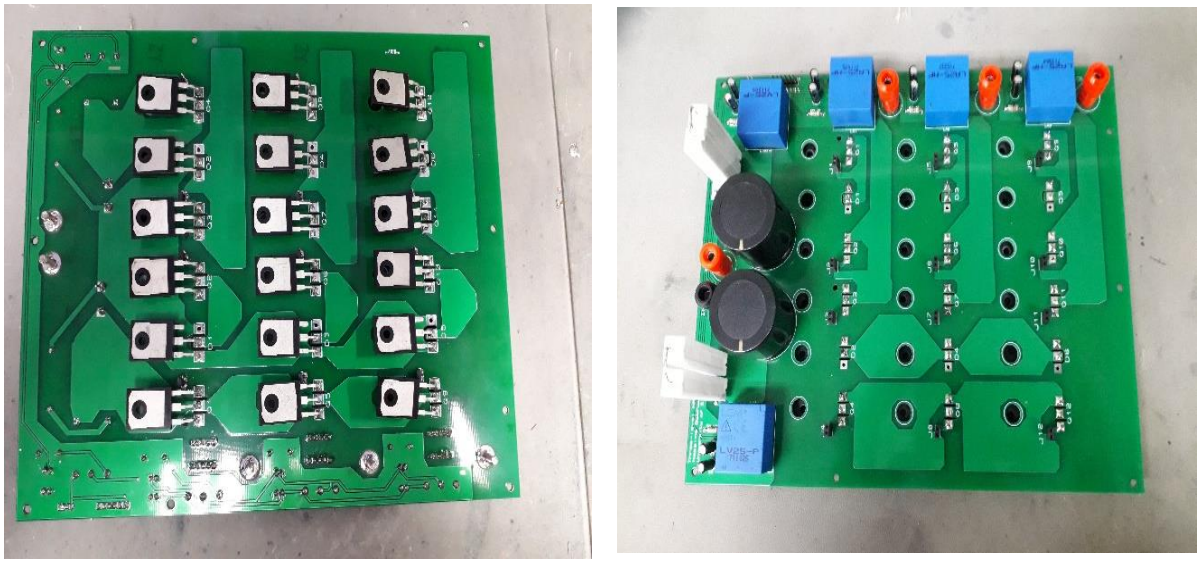

Figure (C.5): PCB hardware design of three-level NPC inverter.

- **PCB design of gate driver**

The three-level NPC inverter employs 12 SIC MOSFETs as shown above which are driven by PWM Signals using gate driver circuits. The PWMs from the microcontroller have been provided at the input of the IC. The Schematic diagram of the proposed driver circuit developed of drive three level NPC inverter is as shown in Figure (C.6). The layout and the hardware design of the top and bottom sides of the gate driver circuit is shown in Figure (C.7) and Figure (C.8), respectively.

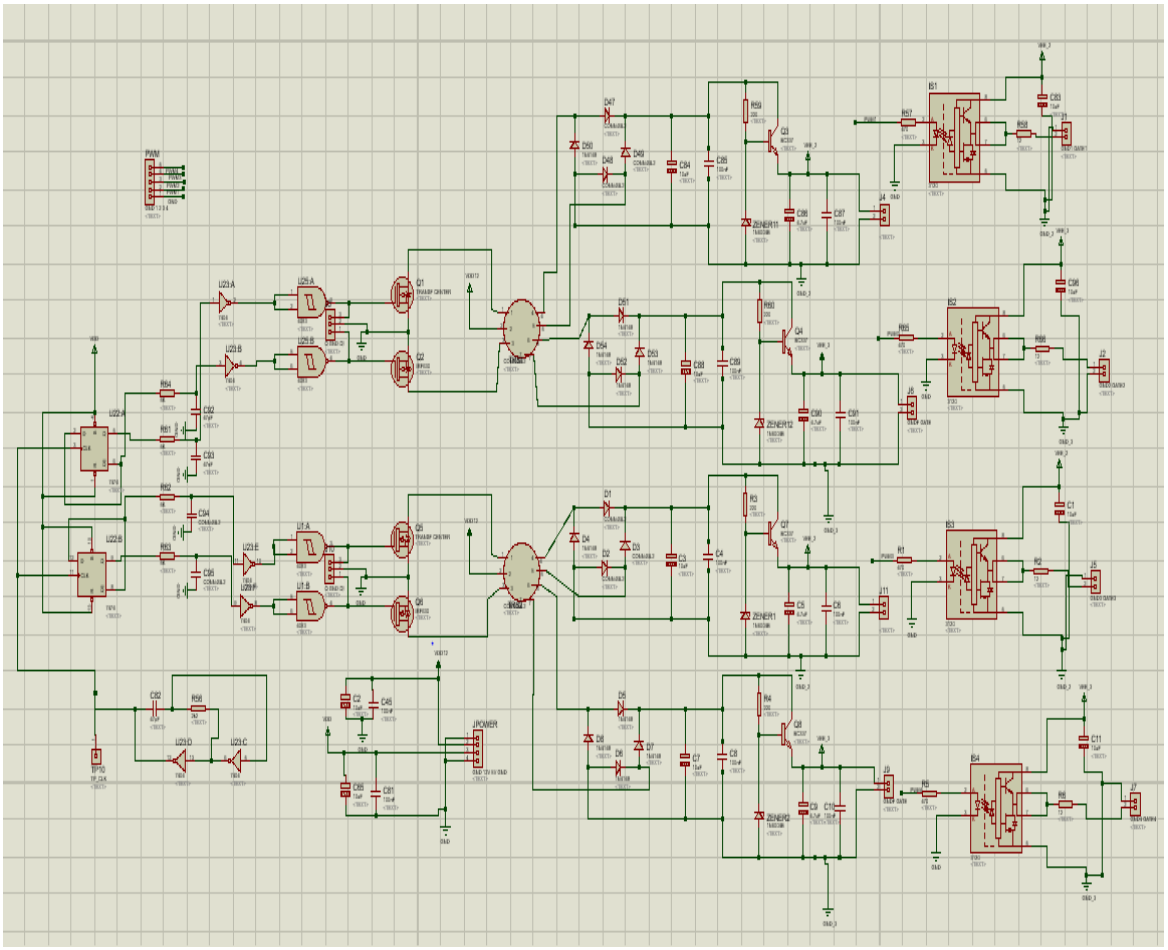

Figure (C.6): Schematic diagram of the gate driver circuit of one cell.

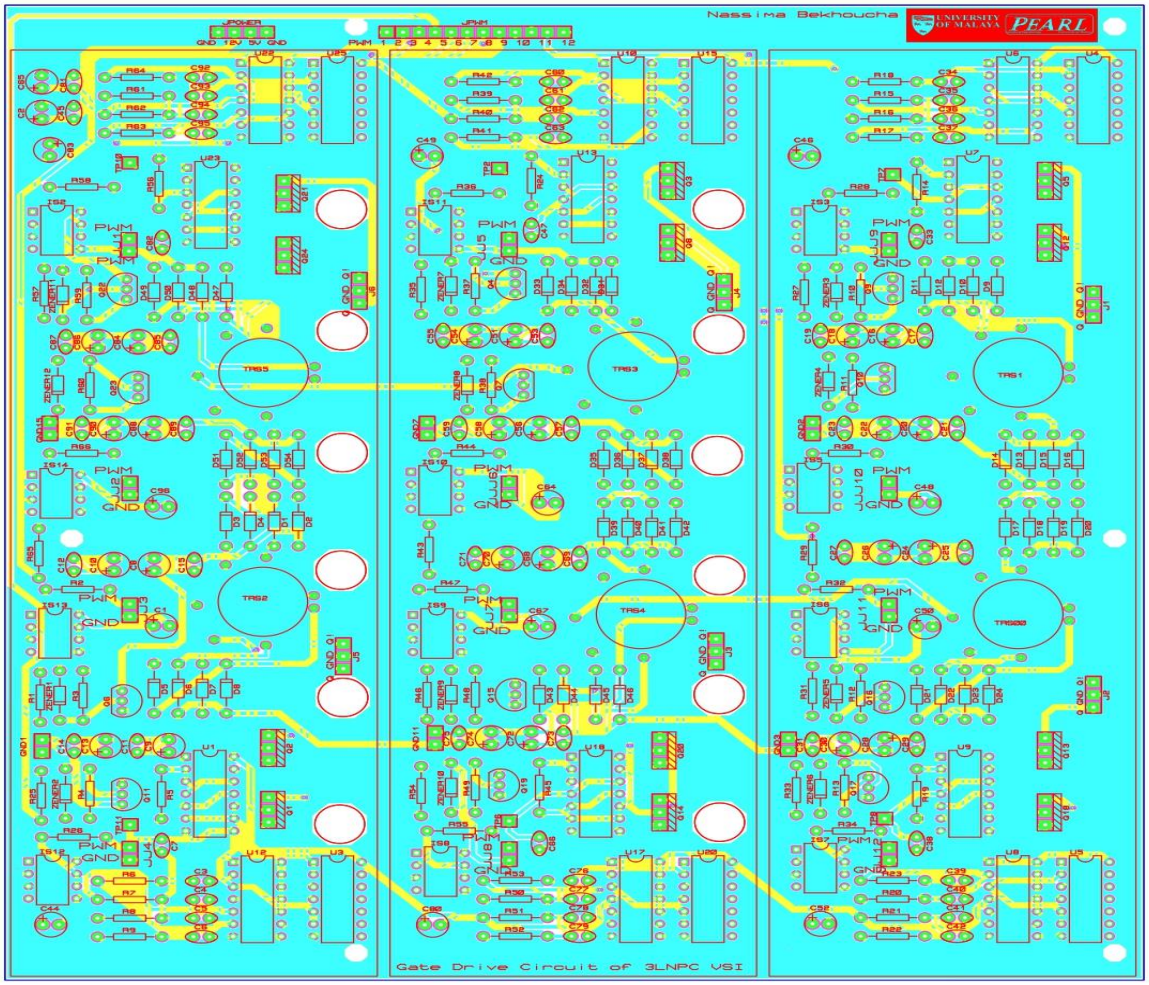

Figure (C.7): Layout of the top and bottom sides of the gate driver.

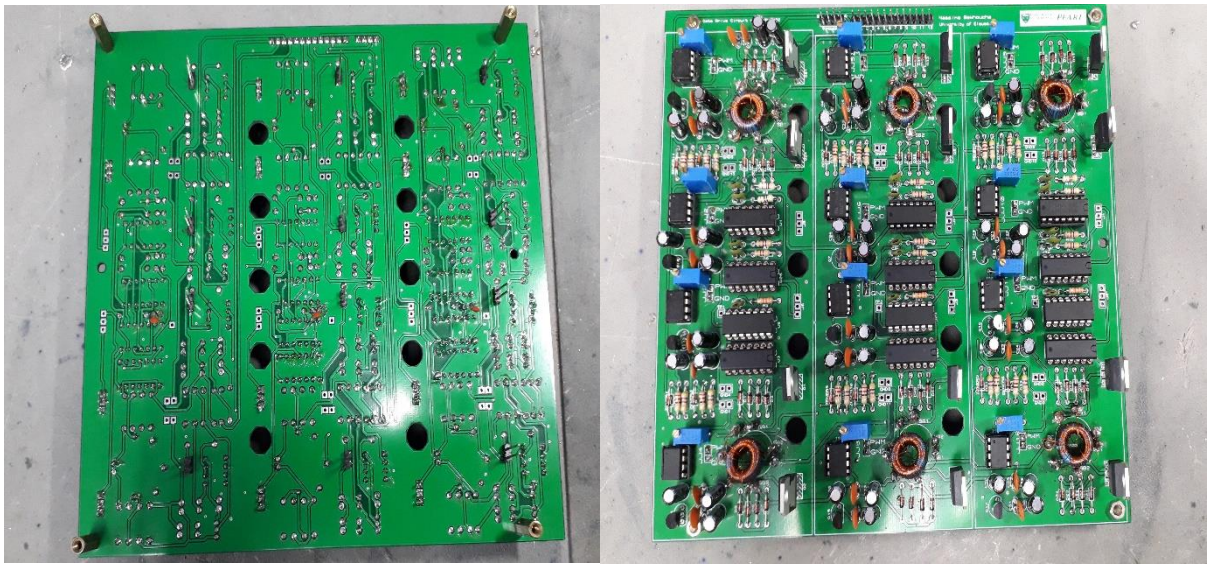

Figure (C.8): PCB hardware design of gate driver.

C.3 Power loss analysis using PLECS software

PLECS (Piecewise Linear Electrical Circuit Simulation) is a software tool for system-level simulations of electrical circuits developed by Plexim. It is especially designed for power electronics but can be used for any electrical network. PLECS includes the possibility to model controls and different physical domains (thermal, magnetic and mechanical) besides the electrical system. Furthermore, it has a domain for modeling thermal structures and accurately calculating switching and conduction losses in switches by means of multi-dimensional lookup tables based on manufacturer information or experimental measurements. The thermal components are found in their own section of the component library, while all semiconductor components have an associated thermal description that can be accessed by double-clicking on them.

Additionally, according to the actual circuit parameters, the PLECS loss simulation model for a three-level NPC inverter is set up as shown in Figure (C.9). This simulation model can simulate the actual operating conditions of the auxiliary inverter system and calculate the loss of each switching device. The thermal models of the SiC MOSFETs and DIODEs used to build the inverter are obtained from the CREE Inc, website.

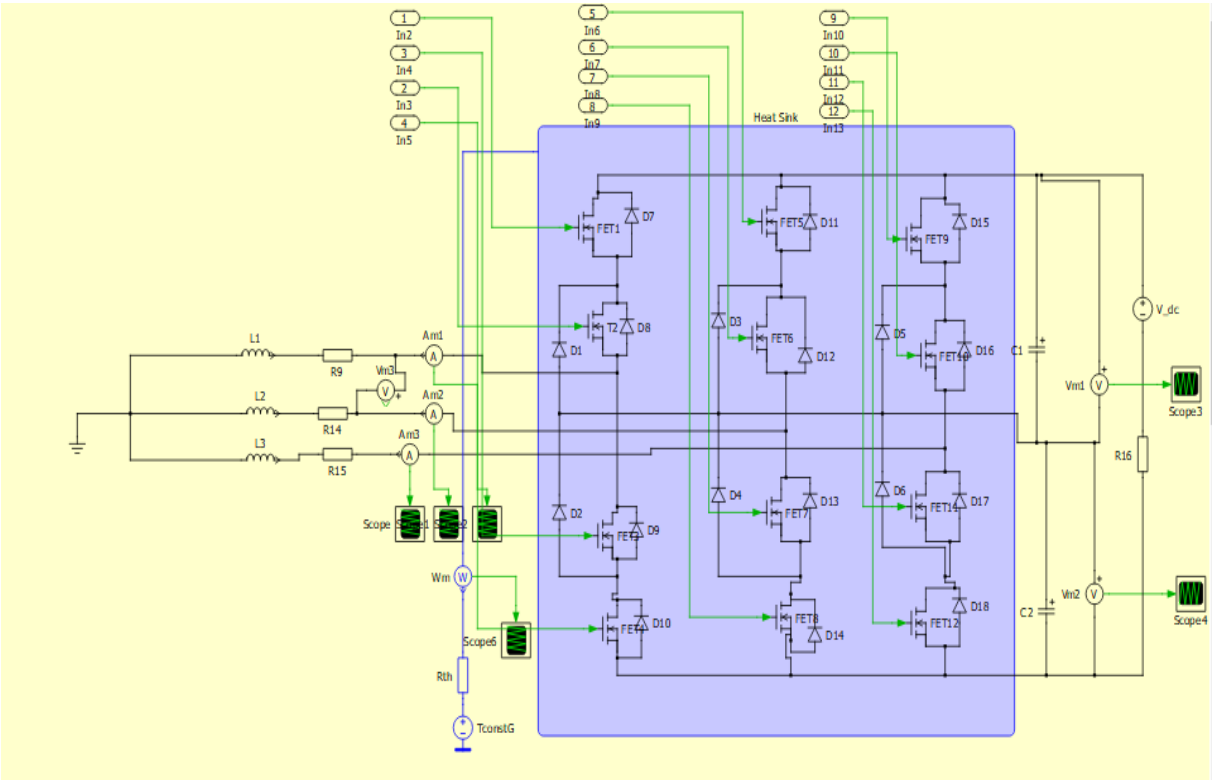

Figure (C.9): Simulation schematic of three-level NPC inverter using PLECS.

Finally, the power losses of these devices are determined by the actual working conditions of the circuit. The average conduction loss and average switching loss of the device can be calculated by the relevant modules in the PLECS module library as shown in Figure (C.10).

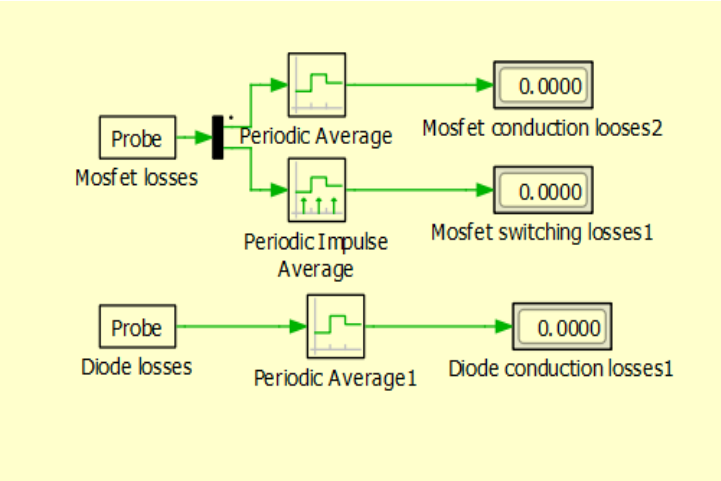

Figure (C.10): The power losses simulation model for each device ‘SIC MOSFET and SIC DIODE’.